Contributions to Quantum Operations with Light

Hao Jeng

A thesis submitted for the degree of
Doctor of Philosophy of
The Australian National University

July, 2022

Declaration

This thesis is an account of research undertaken between March 2017 and July 2022 at the Department of Quantum Science, Research School of Physics, the Australian National University, Canberra, Australia.

Except where acknowledged in the customary manner, the material presented in this thesis is, to the best of my knowledge, original and has not been submitted in whole or part for a degree in any university.

Hao Jeng
July, 2022

Acknowledgements

I wish to express deep gratitude to my supervisor, Assad, for the continual support and encouragement he has given over the past few years. I would also like to thank the panel chair Ping Koy for helping me navigate the difficult path of a PhD; our administrators Amanda White, Lynne Christians, and Siobhan Ryman for assistance with travel to conferences and purchasing of experimental equipment; and Liudmila Mangos at the Research School for looking after us research students, especially during the pandemic.

It is a pleasure to acknowledge the support of fellow members of the research team: Jie (Sophie) Zhao, Lorcan Conlon, Oliver Thearle, Jiri Janousek, and Biveen Shajilal; especially Lorcan, Biveen, and Sophie for equal contributions to the investigations in Chapters 4, 6, and 9. Some of the experiments reported here were performed in close collaboration with Spyros Tserkis and Tim Ralph from the University of Queensland. I thank Assad, Biveen, Lorcan, and Sebastian Kish for reading through the thesis and giving helpful feedback; any errors that remain are that of my own.

During difficult times, the companionship offered by Thibault Michel and Jing Yan Haw has been a source of profound encouragement.

Several visits, of various durations, were made to other laboratories and research groups with financial support from the hosts in part or in full. I would like to thank Professor Tim Ralph and Kaerin Gardner (University of Queensland), Professor Akira Furusawa and Yumiko Yoshikawa (University of Tokyo), Professor Takuya Hirano (Gakushuin University), Takahiro Inagaki and Hiroki Takesue (NTT Basic Research Laboratories), and Chien-Ming Wu and Professor Ray-Kuang Lee (Tsinghua University) for their hospitality.

I acknowledge financial support from the Australian Government Research Training Program (the Australian Postgraduate Award) and the ANU Supplementary Scholarship.

I wish to acknowledge my debt to Professor Craig Savage and Professor Peter Bouwknegt for stimulating my interest in quantum mechanics.

Abstract

Experiments were carried out to examine the basic properties and utility of several quantum states and operations of light. These experiments comprised mostly of the general elements of Gaussian quantum optics but require in addition a pair of special operations known as photon addition and noiseless amplification.

It is shown that a number of important physical quantities are increased by the action of photon addition or noiseless amplification on entangled states, including the distillable entanglement and the rate of distributing secret keys using these entangled states.

It is further shown that noiseless amplification can be embedded in a natural way into feed-forward setups such as quantum teleportation and measurement-based quantum gates, with the valuable effect of suppressing decoherence in these devices.

In some cases, it is observed that multiple quantum operations could merge to produce new quantum effects: the combination of photon addition and coherent displacement leads to strong cubic phase shifts; quantum teleportation combined with noiseless amplification has the remarkable ability to purify displaced thermal states without reducing the displacement.

In the special instance of photon addition on thermal states, a counter-intuitive transformation of the state of light arises which we verified by experiment, and which serves as a test of the validity of quantum mechanics.

The facts established in this thesis have direct implications for quantum technology, including the provision of a route towards universal quantum computation and a new method for removing thermal decoherence without quantum error correction and with a far simpler setup.

Contents

Declaration iii

Acknowledgements v

Abstract vii

1 Introduction 3

2 Quantum optics 5
2.1 Quantisation of the electromagnetic field . . . 5
2.2 Quantum-mechanical properties of light . . . 6
2.3 Photon addition . . . 10
2.4 Noiseless linear amplification . . . 11
2.5 Concluding remarks . . . 13

3 Experimental system 15
3.1 Main components . . . 15
3.2 Optical layout . . . 15
3.3 Measurements and electro-optic control . . . 17
3.4 Interferometer stabilisation . . . 18
3.5 Photon addition and noiseless amplification . . . 19
3.6 Multi-purpose operation . . . 20

4 Strong cubic phase shifts 23
4.1 Quantum computation with light . . . 23
4.2 Universal quantum computation . . . 23
4.3 The cubic phase shift . . . 24
4.4 Experiment . . . 25
4.5 Interaction strength and phase control . . . 26
4.6 Generalisations and limitations . . . 30
4.7 Classical-to-quantum transition . . . 30

5 Non-Gaussian entangled states 33
5.1 Quantum internet . . . 33
5.2 Entanglement distillation . . . 34
5.3 Experimental observations . . . 35
5.4 Kurtosis . . . 37
5.5 Quantum key distribution . . . 39

6 Average number of photons in a beam of light 47
6.1 Tests of quantum mechanics . . . 47
6.2 Adding photons to thermal states . . . 47

6.3 Experimental observations . . . 48
6.4 The difference between addition and subtraction . . . 51
6.5 Phase-space representation . . . 52
6.6 An implicit assumption . . . 53

7 Bounding the distillable entanglement 55
7.1 Quantum entanglement as a physical quantity . . . 55
7.2 The theory of entanglement measures . . . 56
7.3 Noiseless amplification increases distillable entanglement . . . 59
7.4 No-repeater bound for entanglement measures . . . 63
7.5 Implications for quantum communication . . . 63

8 A high fidelity squeezing gate 65
8.1 The squeezing unitary . . . 65
8.2 Measurement-based squeezing gate . . . 66
8.3 Squeezing gate with noiseless amplification . . . 67
8.4 Experimental results . . . 70
8.5 Universality and gates of higher order . . . 71

9 Quantum teleportation with noiseless amplification 73
9.1 When teleportation fails . . . 73
9.2 Quantum teleportation . . . 74
9.3 Experimental device and basic properties . . . 77
9.4 Experiments . . . 80
9.5 Equivalent quantum operation . . . 81
9.6 The fidelity question . . . 83

10 A method for removing thermal decoherence 85
10.1 Applications of quantum teleportation . . . 85
10.2 Methods for suppressing thermal decoherence . . . 86
10.3 Experimental observation . . . 86
10.4 Discussion and comparison . . . 88
10.5 Optical model and basic properties . . . 88
10.6 Prior knowledge of the input state . . . 90
10.7 The question of general input states . . . 91

11 Conclusion 93

A Theory of probabilistic Gaussian quantum optics 95
A.1 Postselection of homodyne measurements . . . 95
A.2 General case . . . 96

Bibliography 99

List of Figures

2.1 **Summary of basic quantum states, operations, and measurements.** 14

3.1 **Optical layout.** . . . 16
3.2 **Measurements of quantum squeezing.** . . . 16
3.3 **Control scheme.** . . . 18

4.1 **Experimental arrangement.** . . . 25
4.2 **Wigner functions of the cubic state.** . . . 27
4.3 **Photon statistics of the cubic state.** . . . 27
4.4 **Controlling the phase of the cubic interaction.** . . . 29

5.1 **Local Wigner functions.** . . . 35
5.2 **Logarithmic negativity.** . . . 36
5.3 **Local kurtosis.** . . . 37
5.4 **Local marginal functions.** . . . 38
5.5 **Non-Gaussian quantum correlations.** . . . 42
5.6 **Evaluation of key rate.** . . . 43
5.7 **Simulations of quantum key distribution.** . . . 45

6.1 **Average number of photons.** . . . 49
6.2 **Raw measurement outcomes and reconstructed Wigner function.** . . 50
6.3 **Photon statistics.** . . . 51

7.1 **Theory of entanglement measures.** . . . 58
7.2 **Distillable entanglement and noiseless amplification.** . . . 60
7.3 **No-repeater bound.** . . . 62

8.1 **Implementation.** . . . 67
8.2 **Experimental results for the squeezing gate.** . . . 71

9.1 **Experimental device.** . . . 77
9.2 **Theoretical fidelity.** . . . 79
9.3 **Noiseless amplification.** . . . 80
9.4 **Quantum teleportation of the vacuum state.** . . . 81
9.5 **Quantum teleportation of coherent states.** . . . 82
9.6 **Equivalent quantum operation.** . . . 83

10.1 **Removal of thermal decoherence using quantum teleportation.** . . . 87
10.2 **Fundamental properties.** . . . 90

Chapter 1

Introduction

The field of quantum optics has flourished since the turn of the century, owing to the acceleration in development of quantum technologies. These new findings are of such brilliance that some researchers have gone as far as to call it the "second quantum revolution", for quantum optics — and quantum mechanics in general — has been transformed from a matter of curiosity to one of application. Yet even with the great amount of knowledge that has been accumulated, realization of a quantum computer breaking the traditional methods of encryption or a quantum internet supporting unconditionally secure communication remains beyond our reach.

To those who have closely followed the developments of quantum technology, the reason for these failures appears to be entirely obvious. Quantum decoherence — the undesired coupling of a quantum system to its environment — prevents the realization of key ingredients for these systems, as well as presenting difficulties in attempts to increase its size and scale. It is responsible for errors in quantum gates, limitations in the physical distance over which quantum key distribution can be established, and restriction of the storage of quantum states to brief durations. Notwithstanding the clarity in our understanding of the problem, just what exactly the solution should be is anybody's guess.

There has been no lack of suggestion that the solution would be based on the principles of engineering rather than that of physics, and by and large that is where most of the current research effort is placed. Take, for example, the use of entirely different physical systems like trapped ions, superconductors, and silicon to implement the exact same quantum system (qubits); different implementations such as measurement-based techniques of the same underlying quantum process; miniaturisation of components that perform the same functions, and the various ways of multiplexing the same physical resource. Although these are all important techniques and may one day prove to be of value, the limitation of these lines of investigation is the lack of new understanding into the fundamental physical processes allowed by quantum mechanics.

It is this circumstance that has led us to consider a different line of attack: we wish to determine what sort of quantum operations are possible with light other than the basic ones that have already been found. Our approach is characterized by the analysis of fundamental properties of quantum operations, the interactions between them, and their connections with contemporary problems in quatum optics. Our main tools are photon addition and noiseless amplification. Our results lead, in every case, to potential solutions for the core problems of quantum technology that include production of key quantum resources and suppression of decoherence.

To clarify, the physical system that we study is light— the whole of it. A great amount of knowledge has already been amassed and organised into a coherent whole regarding the simpler situations of a single photon, or the restricted case of Gaussian quantum optics,

but we make neither assumption. Ample use has been made of both techniques involving single photons as well as non-Gaussian quantum operations. It is in fact true that none of the quantum operations we investigate can be strictly classified as Gaussian, although some can be said to be approximately so.

We deal with a variety of questions in this thesis. For simplicity, I have chosen to divide the thesis into just two parts based on the technique: photon addition (Chapters 4, 5, 6) and noiseless amplification (Chapters 7, 8, 9, 10). Each experiment uses exactly one of the two, and not the pair in conjunction. The subjects we study will therefore be dispersed: quantum computation (Chapters 4 and 8), quantum communication (Chapters 5 and 7), fundamental physics (Chapter 6), and quantum teleportation (Chapters 9 and 10). In Chapter 2, we will describe the basic quantum-mechanical framework within which our experiments are carried out, and Chapter 3 contains a technical summary of our experimental system. A summary of the limitations of the study and an indication of the general direction in which we are heading towards can be found in the conclusion (Chapter 11).

Of the original researches reported in Chapters 4 to 10, the investigations were led or co-led by myself except Chapter 8 (where I partook in data acquisition and paper writing). Chapters 5 and 7 are based on archival data obtained in experiments by Helen Chrzanowski, while all other chapters correspond to experiments carried out on a live setup. Two papers were published prior to submission of this thesis (Chapters 7 and 8).

It must be emphasised that the nature of fundamental research is that it is usually unsuitable for immediate deployment in actual applications. Although I describe possible methods to improve the efficiency and general applicability of these devices, no attempt has been made to optimise. On the other hand, the upside of fundamental research is that it has far-reaching implications— indeed, we shall be able to explore the boundaries of almost every sector in the field of quantum technology, including quantum computation, quantum communication, as well as applications to quantum physics.

Chapter 2

Quantum optics

2.1 Quantisation of the electromagnetic field

The debate between the great minds that took place over a period of more than three hundred years for whether light is a particle or a wave is famous by now. The spectrum of blackbody radiation [1], the photoelectric effect [2, 3], and Compton scattering [4] provided the earliest experimental evidence that electromagnetic waves can be represented by discrete quanta. The experiments that we shall describe in this thesis can be adequately accounted for by this quantum theory of radiation. In this section, a description is given of how the quantum framework arises out of the more widely known equations of Maxwell [5, 6]. Although the derivation itself is not necessary for understanding any of the experiments, it will prove to be important in ensuring logical continuity.

A beam of light propagating in vacuum comprises of oscillating electric and magnetic fields that satisfy Maxwell's equations (in Gaussian units):

$$\boldsymbol{\nabla} \cdot E = 0, \tag{2.1}$$

$$\boldsymbol{\nabla} \cdot B = 0, \tag{2.2}$$

$$\boldsymbol{\nabla} \times E = -\frac{1}{c}\frac{\partial B}{\partial t}, \tag{2.3}$$

$$\boldsymbol{\nabla} \times B = \frac{1}{c}\frac{\partial E}{\partial t}. \tag{2.4}$$

In order to quantise these fields, the easiest way is to first solve for its solution. Divergenceless of B and Faraday's law imply that the electric and magnetic fields can be replaced by the scalar potential ϕ and the vector potential A:

$$B = \boldsymbol{\nabla} \times A,$$
$$E = -\boldsymbol{\nabla}\phi - \frac{1}{c}\frac{\partial A}{\partial t}.$$

Because these relations are invariant under the transformations

$$A' = A + \boldsymbol{\nabla} f,$$
$$\phi' = \phi - \frac{\partial f}{\partial t},$$

for any scalar function f, we can choose f to make A divergenceless: $\boldsymbol{\nabla} \cdot A = 0$. Furthermore, Gauss' law combined with the expression for E in terms of potentials results in the Laplace equation for the scalar potential: $\boldsymbol{\nabla}^2\phi = 0$. We put $\phi = 0$ ignoring the effects of

any electrical charges.

Replacing the electric and magnetic fields in Ampere's law by the vector potential leads to the wave equation

$$\boldsymbol{\nabla}^2 A - \frac{1}{c^2}\frac{\partial^2 A}{\partial t^2} = 0. \tag{2.5}$$

This is readily solved by the method of separation of variables,

$$A = \sum_k \left(a_k u_k(r) e^{-i\omega_k t} + a_k^\dagger \overline{u_k(r)} e^{i\omega_k t} \right), \tag{2.6}$$

where the spatial modes u_k satisfy:

$$\begin{aligned} \text{Eigenvalue equation:} \quad & \left(\boldsymbol{\nabla}^2 + \frac{\omega_k^2}{c^2} \right) u_k(r) = 0, \\ \text{Transversality:} \quad & \boldsymbol{\nabla} \cdot u_k(r) = 0, \\ \text{Orthonormality:} \quad & \int \overline{u_k} u_l dr = \delta_{kl}. \end{aligned}$$

The observable fields E and B can be obtained from the vector potential:

$$E = \sum_k \frac{i\omega_k}{c} \left(a_k u_k(r) e^{-i\omega_k t} + a_k^\dagger \overline{u_k(r)} e^{i\omega_k t} \right), \tag{2.7}$$

$$B = \sum_k \left(a_k \boldsymbol{\nabla} \times u_k(r) e^{-i\omega_k t} + a_k^\dagger \boldsymbol{\nabla} \times \overline{u_k(r)} e^{i\omega_k t} \right), \tag{2.8}$$

and, finally, it suffices to verify that this is indeed a solution to Maxwell's equations in free space.

Quantisation of the electromagnetic field à la Dirac [5] can now be obtained in a single stroke, by promoting each coefficient a_k to an operator $\hat{a}_k$, with its conjugate becoming the Hermitian adjoint $\hat{a}_k^\dagger$. These operators satisfy the commutation relations

$$\begin{aligned} [\hat{a}_k, \hat{a}_l] &= [\hat{a}_k^\dagger, \hat{a}_l^\dagger] = 0, \\ [\hat{a}_k, \hat{a}_l^\dagger] &= \delta_{kl}, \end{aligned}$$

where δ_{kl} denotes the delta function. The rest from here is basic quantum mechanics.

2.2 Quantum-mechanical properties of light

The basic properties of light in the quantum description are set forth below.

1. The particle nature of light follows from the properties of the operators $\hat{a}_k$ and $\hat{a}_k^\dagger$. Dropping the subscript and restricting our attention to a single frequency $\hat{a}$, the commutation relation $[\hat{a}, \hat{a}^\dagger] = 1$ implies that the vector space which these operators act on is a Fock space: it has a basis $\{|0\rangle, |1\rangle, |2\rangle, \dots\}$ with the actions

$$\begin{aligned} \hat{a}^\dagger |n\rangle &= \sqrt{n+1}\, |n+1\rangle, \\ \hat{a} |n\rangle &= \sqrt{n}\, |n-1\rangle, \end{aligned} \tag{2.9}$$

and $\hat{a}|0\rangle = 0$. In physical terms, the quantum states $|n\rangle$ contain a definite number of photons n, being eigenstates of the photon number operator $\hat{n} = \hat{a}^\dagger \hat{a}$. The operator $\hat{a}$

is called the annihilation operator and acts to remove photons from the state, while the operator $\hat{a}^\dagger$ is the creation operator and acts to increase the number of photons in the state.

2. The wave properties of light emerge when the creation and annihilation operators are decomposed into the amplitude and phase quadrature operators $\hat{x}$ and $\hat{p}$:

$$\hat{a} = (\hat{x} + i\hat{p})/2,$$
$$\hat{a}^\dagger = (\hat{x} - i\hat{p})/2.$$

Unlike the creation and annihilation operators, these are Hermitian operators and represent physical observables— the amplitude and phase of the wave.[1] Furthermore, the two observables do not commute so that the Heisenberg uncertainty principle applies:

$$\sigma_x \sigma_p \geq 1, \tag{2.10}$$

where σ_x and σ_p denote the uncertainties associated with a simultaneous measurement of the amplitude and phase quadrature. It is therefore a consequence of quantum mechanics that the amplitude and phase of a wave cannot be simultaneously determined by measurements to arbitrary precision.

3. Wave-like quantum states of light include the states of definite amplitude but unknown phase

$$|x\rangle = \sum_n \psi_n(x) \, |n\rangle \, , \quad \psi_n(x) = \frac{e^{-x^2/4}}{(2\pi)^{1/4}\sqrt{2^n n!}} H_n\left(\frac{x}{\sqrt{2}}\right), \tag{2.11}$$

where H_n is the Hermite function; the states of definite phase but unknown amplitude, $|p\rangle = \sum_n \psi_n(p) i^n \, |n\rangle$; as well as the rest that are "in-between". The set of coherent states $|\alpha\rangle$ is exactly halfway in-between, with an equal uncertainty in amplitude and phase. The photon representation of coherent states is

$$|\alpha\rangle = e^{-|\alpha|^2/2} \sum_n \frac{\alpha^n}{n!} \, |n\rangle \, . \tag{2.12}$$

Coherent states describe accurately the default state of the laser. In the classical picture where the intensity $|\alpha|^2$ is very large, the quantum features can be ignored and only the parameter α kept, which corresponds to the complex amplitude of the wave.

4. The remaining "in-between states" are squeezed states which have less uncertainty in one observable and greater uncertainty in the other. In the photon representation,

$$|r\rangle = \frac{\sinh r}{2\sqrt{\cosh r}} \sum_n \frac{\sqrt{2n!}}{n!} \, |2n\rangle \, , \tag{2.13}$$

where r is the squeezing parameter characterizing the extent of the imbalance of uncertainty. One quadrature has an uncertainty of e^{-2r} while the other has e^{2r}. Squeezed states consist only of Fock states with an even number of photons and are therefore produced by parametric down-conversion from a higher frequency of light: $2\omega \to \omega + \omega$, for conservation of energy ensures that photons at the fundamental frequency ω will always come

[1] To be pedantic, the "in-phase" and "quadrature" components.

in pairs. Squeezed states have recently received much publicity for their role in increasing the sensitvity of gravitational wave detectors [7].

5. Two beams of light exist in a state of quantum entanglement if there are correlations between the photons of each beam which cannot be explained by classical models. In this thesis, our primary source of entanglement is the two-mode-squeezed-vacuum states,

$$|TMSV\rangle = \sqrt{1-\lambda^2}\sum_n \lambda^n |n\rangle_1 |n\rangle_2 , \tag{2.14}$$

where $\lambda = \tanh r$ is the entanglement parameter. This state has correlations in photon number: if a photon number measurement is made on one beam with a result of k photons, then we shall immediately know that the other mode has k photons as well. This state also has wave-like correlations, for the amplitude and phase quadrature operators satisfy the relations

$$\begin{aligned} \hat{x}_1 - \hat{x}_2 &= \hat{x}_0 e^{-r}\sqrt{2}, \\ \hat{p}_1 + \hat{p}_2 &= \hat{p}_0 e^{-r}\sqrt{2}, \end{aligned} \tag{2.15}$$

where $\hat{x}_0$ and $\hat{p_0}$ denote observables of a vacuum state. These relations mean that the amplitude and phase of the two modes are correlated, with the degree of correlation increasing with r. In the limit as r goes to infinity, we obtain the famous entangled state first described by Einstein, Rosen, and Podolsky [8]— although, in fact, it is not a physical state because it would have an infinite number of photons. For arbitrary finite values of r, two-mode-squeezed-vacuum states can be assembled from a pair of squeezed states combined on a balanced beam-splitter, with r corresponding to the squeezing parameter.

6. Quantum decoherence is the unwanted coupling of a quantum system to its surroundings. The general effect of decoherence on a quantum system is to destroy its state of quantum superposition and transform it into a statistical mixture of states. The most prominent and problematic sources of decoherence in quantum optics are optical loss and thermal noise: optical loss refers to the loss of photons, modelled as the coupling of a beam of light to a vacuum mode through a beam splitter, with the reflectivity of the beam splitter determining the extent of the loss; thermal decoherence is the addition of thermal photons to the beam, with the thermal photons described by a mixed quantum state

$$\rho_{th} = (1-\lambda^2)\sum_n \lambda^{2n} |n\rangle \langle n| = \frac{1-\lambda^2}{\pi\lambda^2}\int d\alpha\; e^{-\frac{1-\lambda^2}{\lambda^2}|\alpha|^2} |\alpha\rangle \langle\alpha| . \tag{2.16}$$

Physical reasons for decoherence can vary. Optical loss occurs as a result of imperfections in optical coatings on optics, beam overlap in interferometers, and absorption of photons by photodiodes. Thermal noise can be a consequence of optical loss whereby some photons in the beam are now identified as thermal photons, or it can occur naturally in quantum feedforward setups such as teleportation with the thermal photons injected from an external source. Thermal noise due to background radiation is negligible in our experiments. Phase noise [9] is also present in all our experiments and probably not entirely negligible (it is difficult to pin down the exact values), however it is more appropriately categorized as a technical issue rather than a fundamental source of decoherence.

7. Wigner functions are used to visualise and rapidly identify the various quantum states of light. It is a function of the amplitude and phase quadratures that is completely

determined by the density operator:

$$W(x,p) = \frac{1}{2\pi}\int_{-\infty}^{\infty} dq\, \langle x-q|\,\hat{\rho}\,|x+q\rangle\, e^{ipq}. \tag{2.17}$$

The Wigner function looks almost like a joint-probability distribution of the amplitude and phase quadratures x and p if not for the fact that these observables cannot be determined simultaneously. Indeed, the Wigner function can take negative values so that interpretation as a probability distribution is impossible. The size, depth, and the shape of these regions of negativities reflect the sort of quantum properties the state possesses and plays an important role in the characterization and identification of quantum states. The Wigner functions of some of the states we have mentioned are shown in Fig. 2.1a-d.

8. Gaussian quantum states have Gaussian Wigner functions, by definition. The description of Gaussian states is greatly simplified in the Heisenberg picture, for it is characterized by only the mean vector

$$\mu = [\langle \hat{q}_i \rangle]_i, \tag{2.18}$$

and the covariance matrix

$$\sigma = [\mathrm{cov}(\hat{q}_i, \hat{q}_j)]_{ij} \tag{2.19}$$

of the quadrature operators q_i taken from the set of amplitude and phase quadrature operators $\{x_1, p_1, x_2, p_2, \dots\}$ in that order, with $\mathrm{cov}(\hat{q}_i, \hat{q}_j) = \langle \Delta q_i \Delta q_j + \Delta q_j \Delta q_i \rangle / 2$ and $\Delta q_i = q_i - \langle q_i \rangle$. In this representation, each unitary operator corresponds to a symplectic matrix Σ, and the quantum state transforms by matrix multiplication: $\mu \to \Sigma\mu$, $\sigma \to \Sigma\sigma\Sigma^T$. Coherent states, squeezed states, TMSV states, and thermal states all fall under this category, with mean vectors and covariance matrices given by:

$$\text{Coherent state: } \mu = \begin{bmatrix} 2\mathrm{Re}(\alpha) \\ 2\mathrm{Im}(\alpha) \end{bmatrix},\ \sigma = \begin{bmatrix} 1 & 0 \\ 0 & 1 \end{bmatrix},$$

$$\text{Squeezed state: } \mu = \begin{bmatrix} 0 \\ 0 \end{bmatrix},\ \sigma = \begin{bmatrix} e^{-2r} & 0 \\ 0 & e^{2r} \end{bmatrix},$$

$$\text{Thermal state: } \mu = \begin{bmatrix} 0 \\ 0 \end{bmatrix},\ \sigma = \begin{bmatrix} \frac{1+\lambda^2}{1-\lambda^2} & 0 \\ 0 & \frac{1+\lambda^2}{1-\lambda^2} \end{bmatrix},$$

$$\text{TMSV state: } \mu = \begin{bmatrix} 0 \\ 0 \\ 0 \\ 0 \end{bmatrix},\ \sigma = \begin{bmatrix} \cosh 2r & 0 & \sinh 2r & 0 \\ 0 & \cosh 2r & 0 & -\sinh 2r \\ \sinh 2r & 0 & \cosh 2r & 0 \\ 0 & -\sinh 2r & 0 & \cosh 2r \end{bmatrix}.$$

These examples are given to illustrate how the physical properties of light are captured by the mean and covariance matrix: the complex amplitude of the coherent state corresponds to the mean vector, uncertainty in observables corresponds to the variance (with the thermal state having a larger uncertainty than the limit allowed by the Heisenberg uncertainty principle), and quantum entanglement described by correlations between different beams (the off-diagonal terms).

9. Simple quantum operations can be formed by taking various combinations of the

creation and annihilation operator. The basic unitaries include:

$$\begin{aligned}
\text{Displacement: } D(\alpha) &= \exp\Big(\alpha\hat{a}^\dagger - \overline{\alpha}\hat{a}^\dagger\Big),\\
\text{Squeezing: } S(\zeta) &= \exp\left(\frac{1}{2}(\overline{\zeta}\hat{a}^2 - \zeta(\hat{a}^\dagger)^2)\right),\\
\text{Beam splitter: } BS(\theta) &= \exp\Big(i\theta(\hat{a}_1^\dagger\hat{a}_2 + \hat{a}_1\hat{a}_2^\dagger)\Big),\\
\text{Two-mode-squeezing: } S_2(\zeta) &= \exp\Big(\zeta\hat{a}_1^\dagger\hat{a}_2^\dagger - \overline{\zeta}\hat{a}_1\hat{a}_2\Big),\\
\text{Cubic phase shift: } U(\gamma) &= \exp\Big(i\gamma(\hat{a}+\hat{a}^\dagger)^3\Big).
\end{aligned} \tag{2.20}$$

The effects of these quantum operations can be most clearly seen by their action on vacuum states: displacement, squeezing, and two-mode-squeezing acting on vacuum creates coherent states, squeezed states, and TMSV entangled states respectively. Optical implementations are shown in Fig. 2.1e-g. The cubic phase shift provides an example of a higher-order unitary involving the third power of the creation and annihilation operators, and its action on vacuum states produce "cubic states" which are not Gaussian states. An example of the Wigner function for a cubic state is shown in Fig. 2.1c.

10. Two kinds of quantum measurements are required in our experiments: homodyne detection (Fig. 2.1k) and heterodyne detection (Fig. 2.1l). In a homodyne detector, the input signal beam is mixed with a bright "local oscillator" beam (about 100 times in brightness) on a balanced beam splitter and with both output ports of the beam splitter monitored continuously with photodiodes. The difference between the two photocurrents is

$$\delta i \propto (\hat{a}^\dagger + \overline{\alpha_{lo}})(\hat{a} + \alpha_{lo}) - (\hat{a}^\dagger - \overline{\alpha_{lo}})(\hat{a} - \alpha_{lo}) = 2|\alpha_{LO}|(\hat{x}\cos\theta + \hat{p}\sin\theta), \tag{2.21}$$

with $\alpha_{LO} = |\alpha_{LO}|e^{i\theta}$. Homodyne detection therefore provides a measurement of either the amplitude or phase quadrature, depending on our choice of the phase of the local oscillator θ. Now if the signal beam is instead split first into two beams by a balanced beam splitter and then detected by amplitude and phase homodyne measurements, then the result is a heterodyne detection (coherent state projection):

$$\langle x|_1 \langle p|_2 BS_{1/2} |\psi\rangle |0\rangle = \langle\alpha|\psi\rangle , \tag{2.22}$$

where $\alpha = x + ip$. Heterodyne detection is as close to a simultaneous measurement of amplitude and phase as quantum mechanics would allow, with the vacuum port at the beam splitter introducing quantum fluctuations which enforce the Heisenberg uncertainty principle.

2.3 Photon addition

The photon creation and annihilation operators were the first quantum operations we encountered, featuring in the quantisation of light. However, the interest in these objects is not only fundamental but also practical. Photon annihilation can be implemented by weakly coupling a beam of light to a single photon detector and conditioning on the detection of a single photon (Fig. 2.1h), while photon creation is achieved by weakly coupling a beam of light to a single photon source and conditioning on no photons leaking

out of the system[2] (Fig: 2.1i.). Mathematically,

$$\langle 1|_2 \, BS(\theta) \, |\psi\rangle_1 \, |0\rangle_2 \approx i\theta\hat{a} \, |\psi\rangle \, ,$$
$$\langle 0|_2 \, BS(\theta) \, |\psi\rangle_1 \, |1\rangle_2 \approx i\theta\hat{a}^\dagger \, |\psi\rangle \, ,$$

assuming θ is small. The reflectivity of the beam splitter is $|\sin\theta|$. For obvious reasons, these operations are also known as photon subtraction and photon addition in the quantum optics community, and that is the terminology we will use throughout this thesis.

Unlike the unitary operators discussed in the previous section, photon subtraction and photon addition are probabilistic and are only successful when the detectors register the desired event. The probability of success decreases as θ becomes smaller and as the approximation becomes more accurate.

Between the pair, photon subtraction is the easier operation to implement because it requires only a single photon detector and no single photon sources. Experiments have shown that photon subtraction produces Schrödinger cat states when acting on squeezed states [10] and leads to distillation of entanglement when acting on entangled states [11]. It is the most accessible quantum operation that can transform a Gaussian quantum state into one that is non-Gaussian and is therefore a valuable tool in view of the no-go theorems for Gaussian quantum optics. These theorems state that universal quantum computation, quantum error correction, and entanglement distillation are all impossible using only Gaussian states and Gaussian quantum operations [12, 13, 14, 15].

Incidentally, photon addition has the same effects as that of photon subtraction in the experiments above. Intuitively, this is not too hard to see. When a single photon is subtracted from a squeezed state, the even-number photon states are transformed into states with an odd number of photons— but the same would happen if we were to add a photon instead of subtracting one. Likewise, the subtraction of a single photon from one beam of a two-mode-squeezed-vacuum state will result in an entangled state with a "lopsided" photon number correlation, with one beam always having one less photon than the other. The exact same correlation can be obtained if a single photon had been added to the *other* beam of the two-mode-squeezed vacuum state instead. However, it is nonetheless true that photon addition is in general not the same as photon subtraction, and for a trivial example one recalls the case of raising and lowering of Fock states by these operations.

It is not entirely understood how photon addition acts on non-trivial quantum states, and it is this question that we address in the first half of this thesis. At first sight, this might seem a strange statement to make—for we know very well how to calculate the action of photon addition on *any* given quantum state! Yet it must surely be the case that calculating an answer and understanding what it means are two completely different tasks. Notwithstanding the sound theoretical capabilities of quantum optics, many such avenues remain unexplored.

2.4 Noiseless linear amplification

Amplifiers increase the amplitude or power of a wave and perform key functions in various modern technologies. Take, for example, electrical amplifiers which are used everywhere in analogue electronics, or optical amplifiers which are part of the global communication

[2]For practical reasons it is also implemented by direct coupling to one beam of a parametric down conversion process, conditioned on the other beam having a single photon.

infrastructure ensuring that light packets can traverse the entire length of undersea cables without being lost.

A good amplifier adds a negligible amount of noise to the amplified signal. However, Caves showed that a consequence of quantum mechanics is that (phase-insensitive) quantum amplifiers must always add a certain amount of noise, which depends on the gain factor $G \geq 1$ and is on the order of the zero-point energy [16]:

$$\text{Quantum-limited amplification:} \qquad \hat{a}_{out} = \sqrt{G}\hat{a}_{in} + \sqrt{G-1}\hat{a}_0, \tag{2.23}$$

where $\hat{a}_0$ is an auxiliary mode.[3] It therefore follows that the act of amplification will lead to significant decoherence of quantum states, for if a coherent state is amplified it becomes a displaced thermal state— and if amplified again becomes yet more thermal. Ramifications of this fundamental result include the impossibility of building a quantum analogue of classical optical repeaters based on the same principles.

At first sight, this appears to rule out the possibility of noiseless amplification. However Ralph and Lund have shown otherwise, provided that some requirements are relaxed [18]. The noiseless linear amplifier (NLA) is the quantum operator $g^{\hat{n}}$ which acts on coherent states to give

$$g^{\hat{n}} |\alpha\rangle = e^{(g^2-1)|\alpha|^2/2} |g\alpha\rangle . \tag{2.24}$$

The defining properties of the noiseless linear amplifier are manifest in this expression, which shows that coherent states are amplified in a linear fashion with a gain factor g that is independent of the complex amplitude, and moreover do not decohere under the action of the amplifier.

A closer examination of the operator $g^{\hat{n}}$ reveals that it is also unbounded and probabilistic, unlike normal quantum amplifiers. The former follows from its action on Fock states which leads to a divergent sequence of eigenvalues, while the latter follows from the expression above which is not a normalised quantum state. In physical terms, unboundedness means that the device only works for a small set of coherent states centred around the vacuum state and breaks if the complex amplitude is too large. Probabilistic means that successful amplification is conditioned on certain detection events otherwise the output must be discarded. An optical implementation of noiseless linear amplification is shown in Fig. 2.1j [19, 20, 21].

In addition to amplifying quantum signals, noiseless amplification also has the unique ability to "amplify quantum entanglement":

$$g^{\hat{n}} |TMSV\rangle \propto \sum_k (g\lambda)^n |n\rangle_1 |n\rangle_2 . \tag{2.25}$$

This expression shows the entanglement parameter λ increased by a factor g corresponding to the gain factor of the amplifier. Prevalence of quantum entanglement in quantum technologies implies that noiseless amplification is expected to find use in such devices as quantum repeaters.

Some questions remain regarding the basic properties of noiseless amplification, and much less is known about how it interacts with other quantum operations or its applications in quantum technology. Complementary to the investigation of photon addition, the investigation of noiseless amplification forms the second half of this thesis.

[3] For an example of an optical amplifier operating near this limit, see Josse *et. al.* [17].

2.5 Concluding remarks

It has been assumed that the reader does not possess any prior knowledge of quantum optics but is familiar with quantum mechanics as taught in an introductory undergraduate course. For these reasons, I have given a review of the quantum framework that is used to describe the states of light and their transformations, while suppressing the details of theoretical and practical techniques pertaining to the modelling and execution of experiments which are not essential for understanding the core results. For further information on theoretical models, see Weedbrook *et. al.* [22], Furusawa and van Loock [23], and Appendix A; for experimental techniques, one can consult the thesis of Lam [24] and Stefsky [25] or the classic textbook of Bachor and Ralph [26].

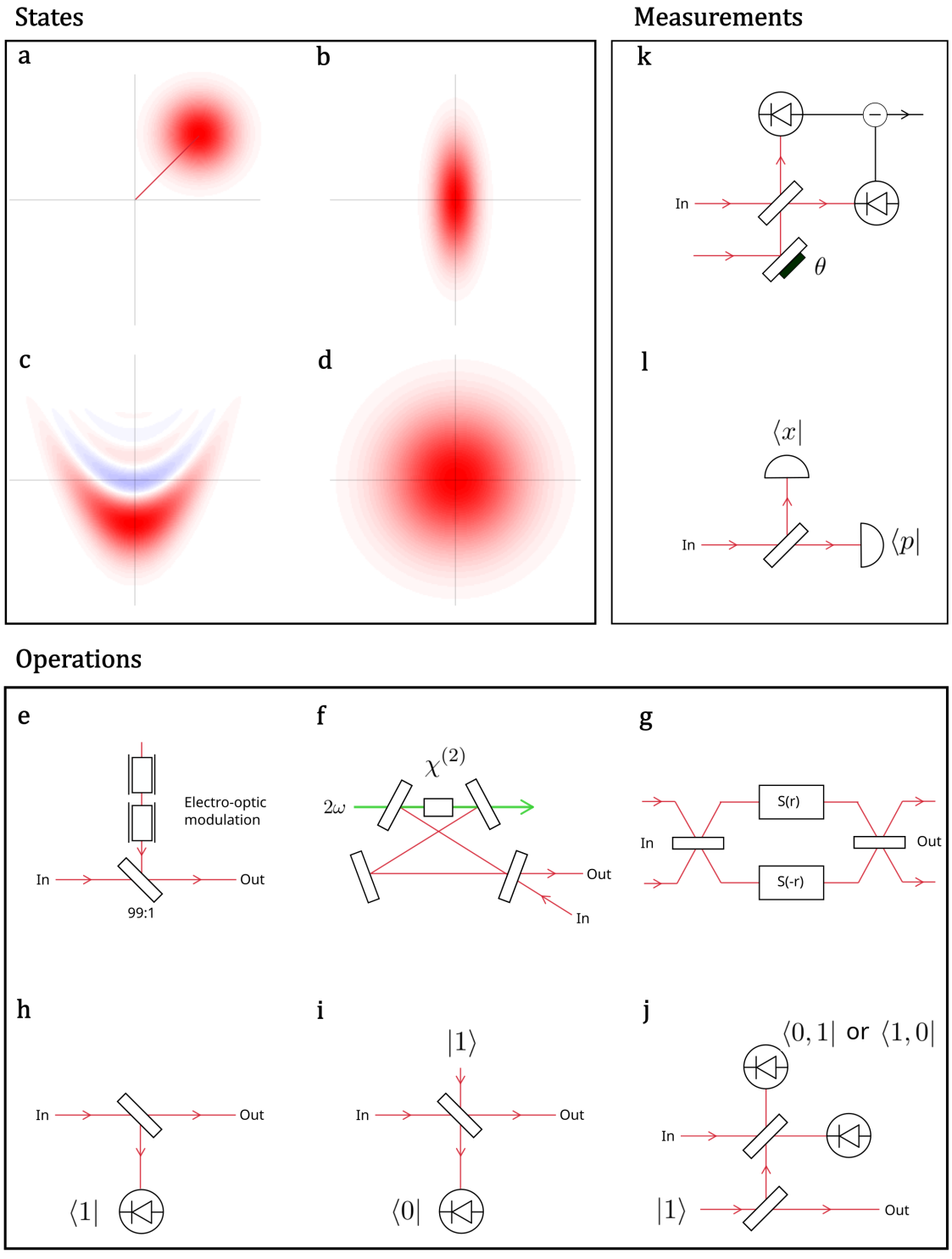


Figure 2.1: Summary of basic quantum states, operations, and measurements. **a-d**: Wigner functions of coherent state, squeezed state, cubic state, and thermal state. **e-j**: basic operations— coherent displacement, squeezing, entanglement, photon subtraction, photon addition, noiseless linear amplification. **k** and **l**: homodyne and heterodyne measurement.

Chapter 3

Experimental system

This Chapter contains a technical summary of the experimental system used in this thesis, in particular the details that are necessary for the operation or replication of experiments.

3.1 Main components

The primary source of light is a continuous-wave laser with emission at the infra-red wavelength (1064 nm), frequency-doubled in part with a built-in converter to green light (532 nm). The laser is equipped with a noise eater with uninterrupted operation.

The quantum state of the laser is defined to be those photons which belong to some range of frequencies in the sidebands of the infra-red carrier, typically with centre frequency located at 3.12 MHz and a bandwidth of 100 kHz. The default quantum state of the laser is the ground state $|0\rangle$, provided the frequency is higher than ≈ 1 MHz (with a mode-cleaner cavity). There is non-negligible intensity noise below this frequency.

The laser feeds into a large optical interferometer that consists of the following main components:

1. A pair of identical optical parametric amplifiers for generating squeezed vaccum states.
2. A "signal" beam with amplitude and phase modulations for generating coherent states.
3. Three sets of homodyne detectors.
4. An analogue electronic feedforward from two of the homodyne detectors to amplitude and phase modulators on a bright auxiliary beam, to implement feedforward displacement unitaries.

The specifications for this apparatus are summarised in Table. 3.2 (located at the end of this chapter), but some more details on this matter would not be amiss.

3.2 Optical layout

A simplified layout of the interferometer is shown in Fig. 3.1. A pair of Faraday isolators are placed at the output ports of the laser to protect it from back-reflection of light. The infra-red beam is then filtered simultaneously to the carrier frequency and the lowest Gaussian spatial mode by a mode cleaner cavity with its length locked to the wavelength of the laser.

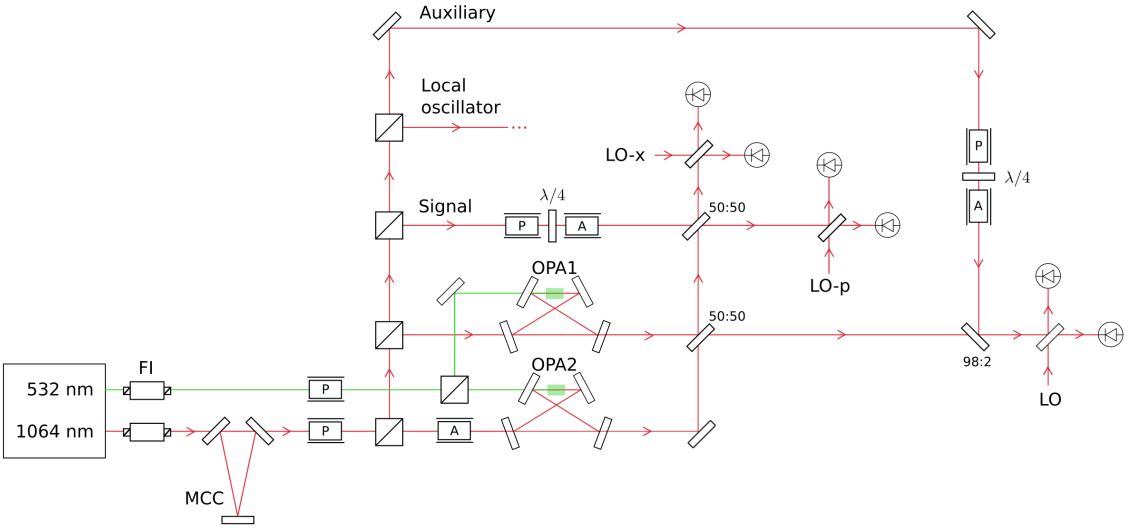


Figure 3.1: Optical layout. FI: Faraday isolator; MCC: mode cleaner cavity; A, P: amplitude and phase modulator; $\lambda/4$: quarter-wave plate; LO: local oscillator.

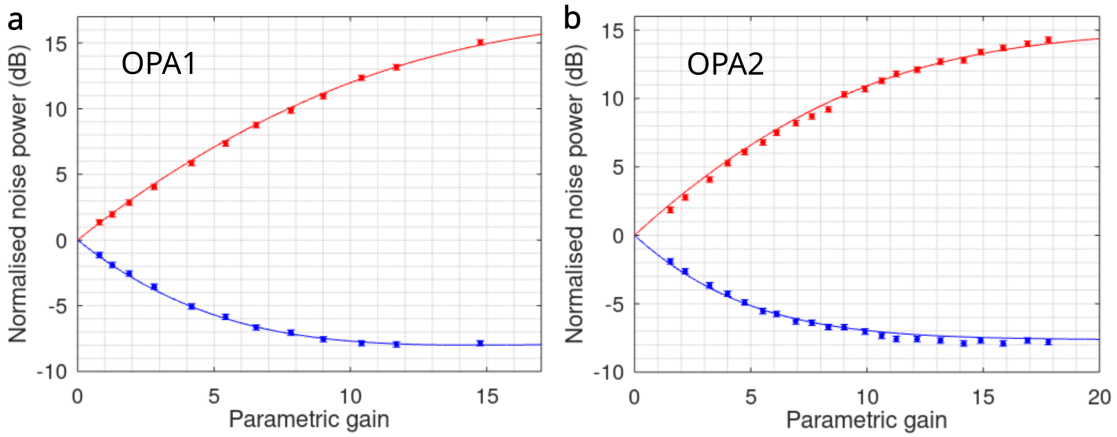


Figure 3.2: Measurements of quantum squeezing. Scanning measurements (at 4 MHz sidebands) with the squeezed beam redirected into a homodyne detector.

The mode cleaner cavity is of a rather standard design. It consists of three mirrors — two flat and one concave of 1m focal length — arranged in a triangular geometry, measuring approximately 50 cm in length and 5 cm in breadth. It can operate with either polarization of light, possessing a finesse of about 8000 for vertical and 1000 with horizontal. We use only the high finesse mode, however, in order to suppress the residual laser intensity noise to a level where it can be neglected. A separate mode cleaner cavity for green light is available but ultimately not used, because it had been found not to make much of a difference for generation of squeezing.

A pair of optical parametric amplifiers [27], driven by green light and seeded with the infra-red, generate the squeezed states used in this thesis. These are bowtie cavities of approximately 30 cm in round-trip length, containing a single PPKTP (periodically-poled potassium titanyl phosphate) crystal which exhibits strong second-order optical nonlinearity. The dimensions of the crystal are 10 mm (length) by 5 mm (breadth) by 1 mm (height) with a poling period of 9 microns. The temperature of the crystal is adjusted

for optimal phase matching. Optical coatings of the cavity mirrors are such that the finesse is about 10 at infra-red wavelength and 30 at green, with an estimated threshold pump power of estimated 140 mW. One mirror has a particularly low reflectivity ($R = 0.87$) to allow out-coupling of squeezed light, with the reflectivity of another mirror also slightly lowered ($R = 0.987$) to allow leakage of light in order to detect and control the cavity length. These devices produce at least 8 dB of squeezing reliably, with highest observed values at around 11 dB. The round-trip loss is estimated to be between 0.5 and 1 percent by multiple independent methods of measurement such as back-seeding [25] and the variation of squeezing and antisqueezing with pump power.

The infra-red source is further split into two additional beams used for creating coherent states and a displacement operation. Coherent states (designated the "signal" beam) are generated with a phase modulator, quarter wave-plate, amplitude modulator in that order, driven by an external function generator at fixed frequency (3.12 MHz); the quarter wave-plate is used to compensate for mismatch between the two crystals in the amplitude modulator. The displacement operation is similar except the modulations are carried out on a bright "auxiliary" beam that is coupled to the system through a 98:2 beam splitter.

For clarity, some optics have been omitted from this figure. These include the alignment mirrors for coupling beams into optical cavities and interfering them on beam splitters; lenses for collimation, mode matching, and focusing onto photodiodes; some polarisers, half and quarter waveplates for precision control of polarization (essentially vertical throughout); and dichroic mirrors which are placed after the parametric amplifiers to remove the green light.

The total optical efficiency of the entire system is estimated to be approximately 70 percent from experiments (see Ch. 9). Some sources of optical loss are known to high accuracy, including the interference visibilities which are measured and optimised daily (Table. 3.2) and the intracavity loss of the optical parametric amplifiers. It is not possible to say with certainty how the rest is distributed amongst the numerous optical components without carrying out a thorough characterisation of each component, although each individual contribution is almost certain to be very small to the extent that direct detection is difficult.

3.3 Measurements and electro-optic control

The optical system is terminated with three sets of homodyne detectors. Two of these (HET-x, HET-p in Fig. 3.1) are of the current-subtraction type with about 20 dB of clearance from the electronic noise floor at 3.12 MHz with 2 mW of LO power [28]. The remaining homodyne is of the voltage-subtraction type with about 14 dB clearance at the same frequencies and LO power.

The outputs of the current-subtraction homodynes are connected to the modulators on the auxiliary beam to implement an electro-optic feedforward displacement operation; the large clearance minimizes electronic noise introduced by the feedforward. The remaining voltage-subtraction homodyne detector is placed at the output of the interferometer for making verification measurements.

To minimise latency, only analogue electronics is used in the feedforward: a suitable combination of amplifiers, bandpass filters, and co-axial cables to adjust the power and the phase of the signal. The group delay of the feedforward was determined to be 160 ns at the signal frequency through measurements with a network analyser. A pair of step-attenuators (with increments of 1 dB and 0.1 dB) are used on each feedforward line for

stable adjustment of the gain factor of the feedforward displacement.

3.4 Interferometer stabilisation

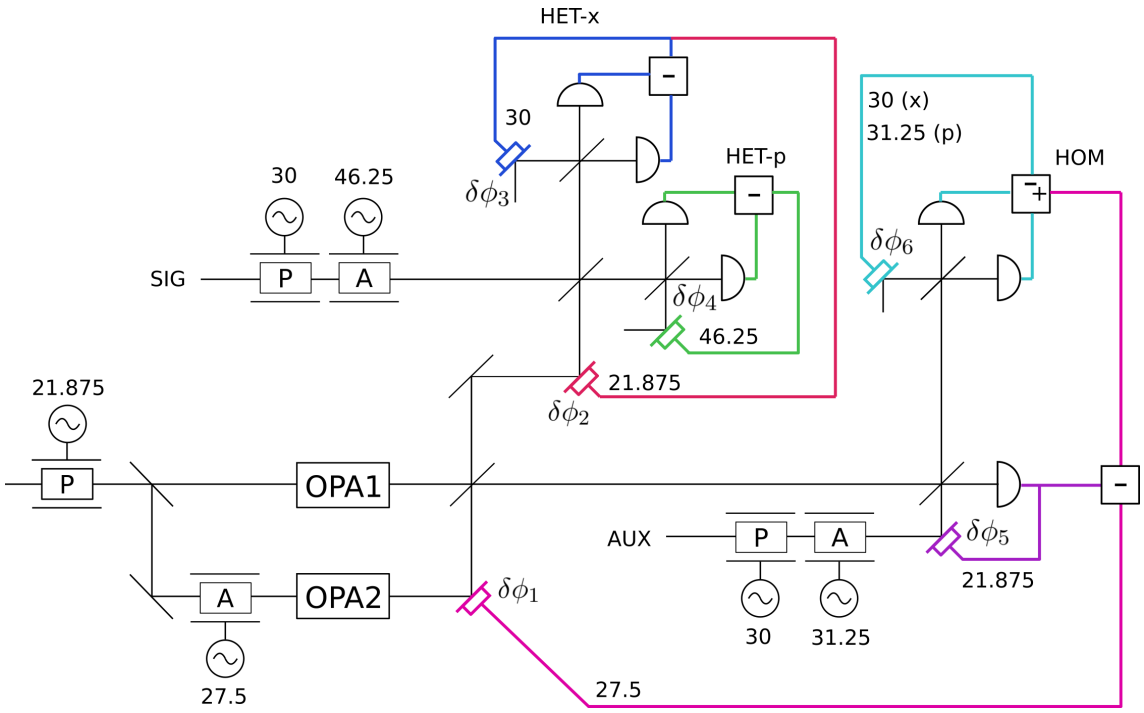


Figure 3.3: Control scheme. Each colour represents a different lock. Numerical values denote the frequency (MHz) of modulation and demodulation. Degrees of freedom corresponding to the six piezoelectric actuators are labelled $\delta\phi_1$, $\delta\phi_2$, ..., $\delta\phi_6$.

Lock	Error signal	Lock point
EPR	$\cos\delta\phi_1$	$\delta\phi_1 = 90°$
Signal	$\cos\left(\frac{\delta\phi_1}{2}\right)\sin\left(\frac{\delta\phi_1}{2}+\delta\phi_2-\delta\phi_3\right)$	$\delta\phi_2 = -45°$
Heterodyne-x	$\sin\delta\phi_3$	$\delta\phi_3 = 0°$
Heterodyne-p	$\cos\delta\phi_4$	$\delta\phi_4 = 90°$
Auxiliary	$\sin(\delta\phi_5-\delta\phi_1)+\sin\delta\phi_5$	$\delta\phi_5 = 45°$
Homodyne	$\sin(\delta\phi_5-\delta\phi_6)$	$\delta\phi_6 = 45°$
	or	or
	$\cos(\delta\phi_5-\delta\phi_6)$	$\delta\phi_6 = -45°$

Table 3.1: Error signal and lock point. The carrier of the entangled state is taken to be the reference point for the locking angles.

We designed a scattering-free control scheme for the interferometer (Fig. 3.3) that does not require any additional photodetectors. This leads to maximum isolation from the environment with no apparent loss of stability. The figure shows six piezo-actuators $(\delta\phi_1, \delta\phi_2..., \delta\phi_6)$ and six feedback locking loops, one for each actuator. Five additional locks for controlling the mode cleaner cavity and the parametric oscillators have been suppressed; the details for these locks can be found in Zhao [27].

All locks use the Pound-Drever-Hall type "AC locking technique" [29, 30]. This means that error signals produced from phase modulation lock interfering beams in phase while those produced from amplitude modulation lock in quadrature. We can read off Fig. 3.3 to find which detectors are used for extracting the error signals, at what frequency this is done, the corresponding source of modulation, and which actuator the error signal controls.

In general, an error signal f depends on multiple degrees of freedom that are coupled by the interferometer

$$f = f(\delta\phi_1, \delta\phi_2, \ldots, \delta\phi_6). \tag{3.1}$$

When feedback control is engaged, the error signal is fixed to the zero-crossing to implement the constraint

$$f(\delta\phi_1, \delta\phi_2, \ldots, \delta\phi_6) = 0. \tag{3.2}$$

The control scheme therefore results in a set of six equations for the six degrees of freedom, and the solution determines the relative phases of the light beams in the interferometer. Table 3.1 shows the error signals and lock points. The error signals can be derived theoretically using the basic principles established by Shaddock [31].

We take the carrier of the entangled state (the EPR carrier) to be the phase reference. The constraints shown in the table therefore translates to: OPA2 locked in quadrature with OPA1; signal beam locked in phase with the EPR carrier; heterodyne-x local oscillator locked in-phase with signal beam; heterodyne-p local oscillator locked in quadrature with the signal beam; the auxiliary beam locked in-phase with entangled state; the homodyne local oscillator locked either in-phase or in quadrature with EPR carrier. The carrier power of OPA1 and OPA2 must be set to equal so that the EPR carrier is at 45° relative to that of each OPA.

Additional electronics such as amplifiers, filters, PID servos for processing the error signal and high-voltage amplifiers (200 V) for driving the piezo-actuator have been suppressed from this discussion— these components are standard by now and the details are not essential. The control scheme is implemented with digital electronics [32].

The main source of error for the control system is phase noise: the locks may not be fixed at the intended point but instead exhibit small variations around that value. Judging from the traces of the error signals and the locks viewed on the oscilloscope (as well as measurements of squeezing, Fig. 3.2), the phase noise appears to be small enough that it can for most purposes be neglected in our experiments.

3.5 Photon addition and noiseless amplification

We implement photon addition and noiseless amplification by postselecting the outcomes of the heterodyne detector [33, 34], which comprises of the homodyne detectors HET-x and HET-p. No additional single photon detectors or single photon sources are required.

To implement noiseless amplification, each outcome α must be kept with probability proportional to a Gaussian function $\exp\bigl((1-1/g^2)|\alpha|^2\bigr)$ and suitably rescaled, viz.

$$\langle\alpha|\,\hat{g}^n\hat{\rho}\hat{g}^n\,|\alpha\rangle = e^{(1-1/g^2)|g\alpha|^2}\,\langle g\alpha|\,\hat{\rho}\,|g\alpha\rangle\,. \tag{3.3}$$

To implement photon addition, the outcomes must instead be kept with probability proportional to a polynomial function $|\alpha|^{2n}$:

$$\langle\alpha|\,(\hat{a}^\dagger)^n\hat{\rho}\hat{a}^n\,|\alpha\rangle = |\alpha|^{2n}\,\langle\alpha|\,\hat{\rho}\,|a\rangle\,. \tag{3.4}$$

The method works regardless of whether the input state $\hat{\rho}$ is mixed or comprises of multiple modes, thus allowing us to study a wide range of situations of interest to quantum technology. The only requirement is that a heterodyne measurement must first be applied.

In both cases, the acceptance probability diverges so that the function must be cut off at some value and normalized to a maximum value of 1 to be interpretable as probability:

$$P(\alpha) \to \begin{cases} P(\alpha)/P_0 & , |\alpha| < \alpha_c, \\ 1 & , |\alpha| \geq \alpha_c. \end{cases}$$

where $P_0 = P(\alpha_c)$ denotes the normalisation and α_c is the cutoff. The cutoff varies with experiments with typical values between 5 and 10. It needs to be large enough so that the cutoff is not visible to most of the data points to ensure that the operation is implemented with good approximation. It cannot be too large because the probability of success falls to zero as the cutoff goes to infinity.

Not every quantum operation can be implemented using this technique. The operation must have the special property that its conjugate maps coherent states to coherent states at the very least, a condition that is true for both photon addition and noiseless amplification. An example — arguably the simplest — of an operation that does not satisfy this requirement is photon subtraction (the annihilation operator) which therefore cannot be accessed in our experiments.

It has been suggested that quantum operations implemented in this manner are "virtual" and not real [33, 35], since the requirement of heterodyne projections would mean that the quantum state must first be destroyed with measurements. In our experiments, we will show that the truth could not have been further. For if postselection is performed as part of a feedforward setup (Ch. 8, 9, 10), then the effects of the operation are inherited by propagating output states which remain physically intact. Nevertheless, we must bear carefully in mind that the method differs in many ways to the standard implementations. The meaning and consequences will vary depending on the context of the experiment and are discussed in each chapter separately.

3.6 Multi-purpose operation

We perform various experiments with this experimental system either with parts of it or by reconfiguring it. For instance, experiments involving a single mode were performed with only the signal beam and heterodyne measurements (Ch. 4, 6). Experiments with entanglement were performed without the signal modulation and with the feedforward displacement switched off (Ch. 5, 7). One of the experiments (the squeezing gate, Ch. 8) was performed by reconfiguring the setup so that only one squeezer is used and bypasses the EPR beam splitter to interact directly with the signal beam. Quantum teleportation experiments were performed with the entire setup (Ch. 9, 10).

	Variable	Value
Interference visibilities	Heterodyne-x	99.2%
	Heterodyne-p	98.5%
	Homodyne	99.5%
	EPR beams	99%
	Signal	99.1%
	Auxiliary	99.5%
Propagation loss	Intra-cavity	1% (round trip)
	Photodiode Q. E. (quoted)	$> 99\%$
	Total efficiency	$\approx 70\%$
Data acquisition	Signal frequency	3.12 MHz
	Bandwidth	100 kHz
	Detector dark noise	≈ 20 dB noise floor clearance
Electro-optic feedforward	Group delay	160 ns at 3.12 MHz

Table 3.2: Typical parameter values for the experiment. The total optical efficiency of the system is inferred from teleportation experiments (Chapter 9).

Chapter 4

Strong cubic phase shifts

Summary:

It is shown that addition of photons to coherent states produces cubic phase shifts, with the cubic strength varying inversely as the magnitude of the displacement.

4.1 Quantum computation with light

It is well-known that quantum operations performed with a system of qubits can correspond to efficient solutions of computational problems that are intractable from a classical perspective [36]. It has turned out that this concept of quantum computation applies also to light, although the situation surrounding optical quantum computers is not entirely understood due to the bosonic nature of photons. One obvious path which has been investigated extensively with experiments is to use the polarisation state of single photons; this system, however, would amount only to qubits in disguise. The fact that photons are bosonic particles allows us to construct more complicated quantum states and transformations which should lead to more possibilities for quantum computation.

Aaronson and Arkhipov produced the first example of such an optical quantum computer [37], a "boson-sampling machine" based on the difficulty of tracking the scattering of light through a large interferometer by classical means of computation. Together with some of its variants [38], boson sampling has been implemented experimentally with sizable interferometers of between 50 and 100 optical modes [39, 40]. Variations of the boson-sampling technique offer solutions to problems of practical interest such as graph problems [41] and quantum chemistry [42].

It has been found by Marandi *et al.* that there is an alternative — and radically different — method of performing optical quantum computation [43]. Networks of interacting optical parametric oscillators are driven continuously such that when the collective system crosses the threshold for oscillation, the phases of the oscillations which result can be identified with the direction of spin of the ground state of the Ising model. This method is also of practical interest as it can be further generalised to solve problems such as combinatorial optimisation [44].

4.2 Universal quantum computation

Examples of the sort above are fixed-purpose quantum computers, designed to implement specific tasks. Here, we are interested in *general purpose quantum computers* which by definition are required to be able to perform any unitary operation, so that it can be

programmed to implement any fixed-purpose algorithm of our choosing. This property is known as universality. The requirement for universality is the existence of a finite set of gates such that any unitary can be implemented through some combination of these gates [45], so that consequently the components of the universal quantum computer need be comprised of only these gates. For example, a universal gate set for qubits is the set of single qubit operations plus the CNOT gate [46].

Universal quantum computation with light is possible at least on paper. Lloyd [47] defines it to be a device which can perform any unitary that is polynomial in the amplitude and phase quadrature operators or generated from these, and the basic example of a universal gate set consists of (1) the Clifford operations, (2) a two-mode gate, and (3) at least one non-linear gate. The Clifford operations consist of displacement and squeezing which are relatively straightforward to implement, while two-mode gates are more complex but nevertheless have also been implemented successfully [48]. However, great difficulty has been encountered in the search for non-linear gates, and no suitable candidate has yet been demonstrated experimentally— a consequence of the weak interaction between light and matter. Nevertheless, it is known that the non-linear gate is necessary, because if it is removed from the set then the remaining system can be simulated efficiently by classical computers [12].

In this Chapter, we report a method for accessing non-linear interactions of the lowest order: the cubic phase shift. We show that addition of photons to coherent states is equivalent to cubic phase shifts on the photon vacuum. We observe that the strength of the interaction to be sufficiently strong to qualify as non-perturbative. As a matter of applied interest, we investigate methods for controlling the strength and phase of the cubic interaction.

4.3 The cubic phase shift

The cubic phase shift is defined to be the unitary operator

$$\hat{U} = e^{i\gamma\hat{x}^3}, \tag{4.1}$$

and represents non-linear interactions of the lowest possible order because it is associated with a Hamiltonian of the third order. Hamiltonians of up to second order correspond to the linear operations of displacement and squeezing (Eq. 2.20). Unlike these operations, the cubic unitary has the effect of bending and distorting the Wigner function of the quantum state it acts on, as well as creating negativities so that it is much more difficult to implement.

Theoretical investigations have lead to several suggested methods for implementing the cubic phase shift. However, all these approaches either assume (1) that the interaction is very weak ($\gamma \ll 1$) so that it can be implemented in a perturbative fashion [49, 50, 51],

$$U = \exp\bigl(i\gamma\hat{x}^3\bigr) \approx 1 + i\gamma\hat{x}^3, \tag{4.2}$$

or (2) that advanced techniques such as photon counting [52, 53] and the Kerr interaction [54] are readily available.

To date, only a single experiment in optics has being successful in generating the cubic interaction.[1] Yukawa *et al.* [56] showed that measurements made on one beam of an

[1] Microwave photons has access to a slightly different unitary [55].

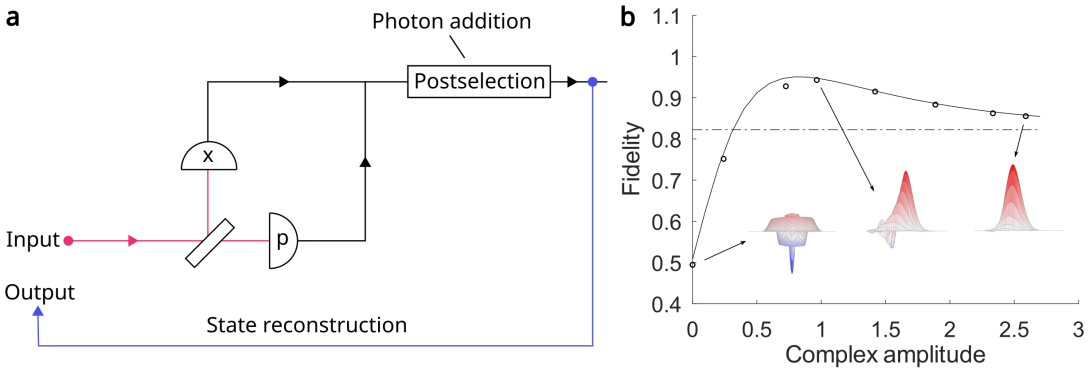


Figure 4.1: Experimental arrangement. a. Experiment schematic. **b.** Fidelity of three-photon added coherent states with a cubic state of fixed interaction strength $\gamma = 0.4$. Insets show Wigner functions of the resulting quantum state. Dashed line gives the maximum fidelity of the cubic state with respect to Gaussian states.

entangled state can collapse the other beam into a controllable superposition of up to three photons:

$$(a_0 \langle 0| + a_1 \langle 1| + a_2 \langle 2| + a_3 \langle 3|) |TMSV\rangle , \tag{4.3}$$

so that with a suitable choice of measurement, the resulting quantum state can be made to match that of the weak cubic state

$$(1 + i\gamma\hat{x}^3) |0\rangle = |0\rangle + 3i\gamma |1\rangle + \sqrt{6}i\gamma |3\rangle . \tag{4.4}$$

The primary limitation of this method is its perturbative nature— trying to control the amplitudes of higher photon numbers requires a substantially more complicated measurement device. The general, non-perturbative cubic phase shift (Eq. 4.1), however, produces non-zero components across hundreds of photons.

4.4 Experiment

In brief, the experimental arrangement we used is the following: coherent states $|\alpha\rangle$ are produced by amplitude and phase modulation at a fixed frequency, and a heterodyne measurement $\langle\beta|$ is made on this state with its outcomes postselected to implement photon addition (Eq. 3.3). This procedure results in the following quantum process:

$$\langle\beta| (\hat{a}^\dagger)^n |\alpha\rangle . \tag{4.5}$$

The complex amplitude of the coherent state can be varied by adjusting the modulation depth.

Because the postselected measurement outcomes do not correspond to a Gaussian state, the effective quantum state is reconstructed by the maximum likelihood method of Lvovsky [57]. Given a sequence of measurement outcomes β_j and an arbitrary density operator $\hat{\rho}$, the projection operator

$$\hat{R} = \sum_j \frac{|\beta_j\rangle \langle\beta_j|}{\langle\beta_j| \hat{\rho} |\beta_j\rangle}, \tag{4.6}$$

has the special property that the fixed point of the map $\hat{\rho} \to \hat{R}\hat{\rho}\hat{R}$ is the most likely density operator corresponding to those observations. The solution is obtained by fixed-point iteration.

Fig. 4.1 shows an experimental run with varying coherent displacements. For a chosen cubic strength there is a corresponding displacement that optimises the fidelity

$$F = \langle \psi_{cubic} | \, \hat{\rho} \, | \psi_{cubic} \rangle \, , \tag{4.7}$$

where the reference cubic state is defined to be

$$|\psi_{cubic}\rangle = \hat{D}\hat{S} \exp\left(i\gamma \hat{x}^3\right) |0\rangle \, . \tag{4.8}$$

In other words, the cubic state is defined only up to arbitrary displacements and squeezing.

We observe fidelities exceeding 90 percent relative to a cubic state with cubic parameter $\gamma = 0.4$ (Fig. 4.1); the choice of this particular interaction strength corresponds roughly to optimal fidelities, based pimarily on comparisons of experimentally reconstructed Wigner functions with simulations at various interaction strengths. The fidelity relative to Gaussian states (optimised across displacement and squeezing by a grid search) is given by the horizontal line which is about 82 percent. Furthermore, we also observe the Wigner function of the state to agree with that expected of an ideal cubic state, with alternating regions of positive and negative parabolic regions (Fig. 4.2).

It is found that the state can still be identified as a cubic state even if the displacement is much larger than what is optimal for the fidelity, however the corresponding cubic interaction is much weaker. The Wigner function has reduced negativity as well as less oscillations (Fig. 4.2). On the other hand, if the displacement is further reduced from the optimum point, then the state deviates significantly from a cubic state, and the fidelity rapidly drops. The reason for this is obvious: in the limit where the displacement goes to zero, the state reduces to the Fock state.

Yukawa *et al.* have suggested that fidelity may not be a very good method for identifying whether the state is cubic or not. Any weak cubic state will be dominated by the vacuum component, making the fidelity of any weak cubic state relative to the vacuum state unbearably high. On the other hand, we find that this is not necessarily true for stronger cubic states which will have higher photon contributions and less from the vacuum state, although the overlap with vacuum remains high because of the dominant "peak" in the Wigner function which represents the first wave of the successive parabolic regions. This peak has considerable overlap with the vacuum state even at strong cubic interactions. In any case, it is difficult to imagine that any measure consisting of only a single number can capture the complicated structure of these quantum states, so it is mainly the Wigner function that is used to identify what the state is and how strong the interaction strength is, with the fidelity playing only a supplementary role.

4.5 Interaction strength and phase control

We examined the photon statistics of the state and determined the interaction strength to be non-perturbative (Fig. 4.3). Perturbative interactions will only produce states with at most three photons (Eq. 4.4), but we observe that the photon statistics have non-zero components not only beyond three photons, but that the general structure of the photon statistics of cubic states up to at least 40 photons is reproduced. Although these

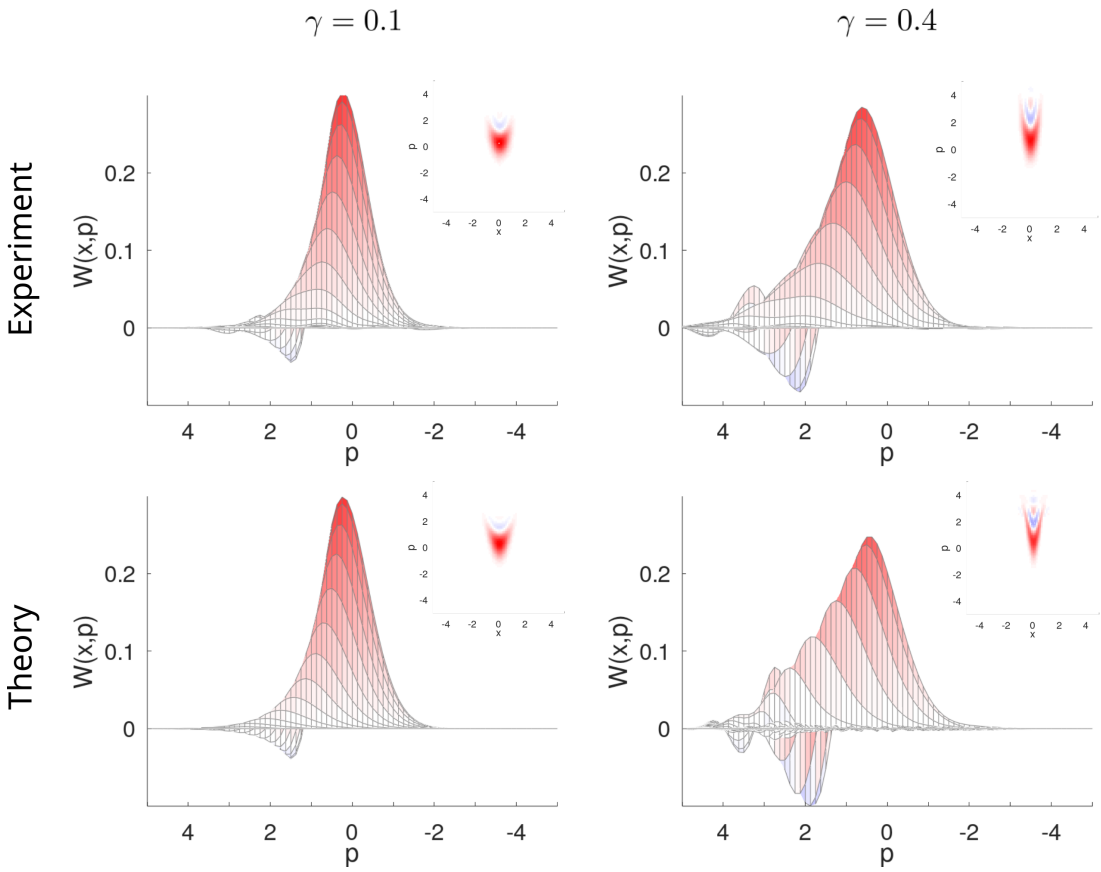


Figure 4.2: Wigner functions of the cubic state. Wigner functions of reconstructed state compared with theoretical model for various viewing angles, for two interaction strengths. Top two figures: experimental reconstruction. Lower two figures: theoretical model.

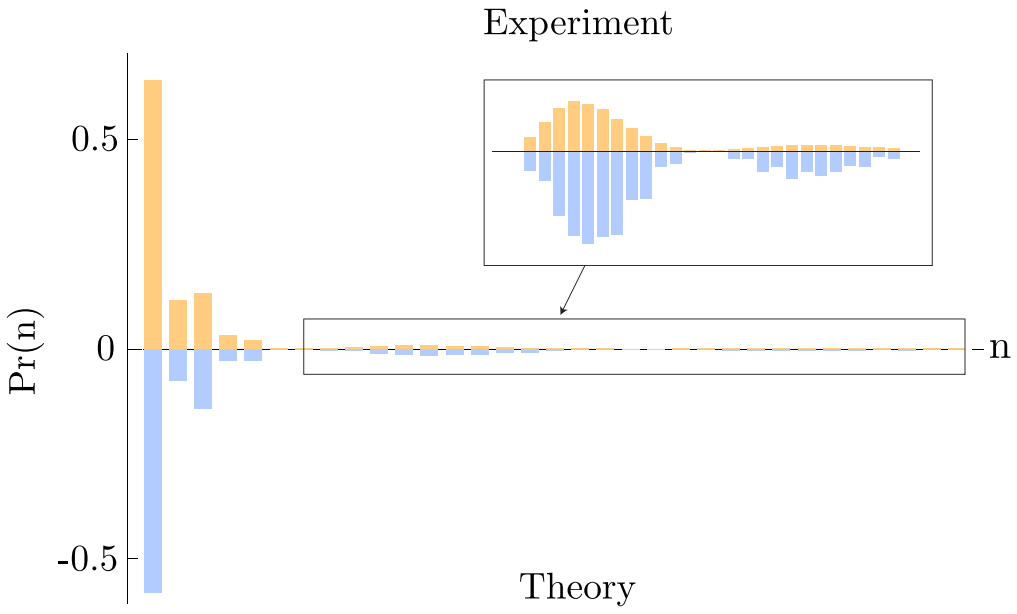


Figure 4.3: Photon statistics of the cubic state. Interaction strength $\gamma = 0.4$. Coherent displacement $\alpha = 1$. Top: experiment. Bottom: theory.

probabilities for higher photons are very small, they are nonetheless visible and reveal the characteristic "island structure" of regions of non-zero probabilities separated by zeroes at certain points. Analogous to how Poissonian statistics characterises coherent states and how the lack of odd photon numbers characterise squeezed states, these island structures are characteristic of the cubic phase shift.

How strong is the interaction strength compared to the observations of Yukawa *et al.*? In short, about one order of magnitude stronger. To arrive at this conclusion, it is first necessary to know how the cubic strength is converted across the various definitions of the cubic unitary, which is dependent on the chosen value of the reduced Planck's constant $\hbar$ through $\hat{x}$. The conversion factor can be found as

$$\hat{x}_{Yukawa} = \frac{a + a^\dagger}{\sqrt{2}} = \frac{\hat{x}}{\sqrt{2}}, \tag{4.9}$$

so that the cubic unitary is

$$\hat{U} = e^{i\gamma\hat{x}^3} = e^{i2\sqrt{2}\gamma\hat{x}^3_{Yukawa}}, \tag{4.10}$$

and hence the interaction strength is related as

$$\gamma_{Yukawa} = 2\sqrt{2}\gamma. \tag{4.11}$$

This means that for our observed value of $\gamma = 0.4$, the equivalent interaction strength is $\gamma_{Yukawa} = 1.13$ which is one order of magnitude greater than their observed value of $\gamma_{Yukawa} = 0.1$.

The greater interaction strength achieved implies that we need not limit our consideration of CV quantum computation to weak cubic protocols. Concretely, this means we could (1) implement one strong cubic interaction in place of many successive weak cubic interactions [58] which is not ideal because of decoherence, and (2) enjoy flexibility in the design of computation schemes, for instance the freedom in choosing the grid spacing in the well-known GKP encoding [52].

Finally, Fig. 4.4 shows that various phases of the cubic interaction can be obtained by varying the phase of the displacement. For instance, displacements of 1, i, $-i$, -1 correspond repsectively to $\exp\big(i\gamma\hat{p}^3\big)$, $\exp\big(-i\gamma\hat{x}^3\big)$, $\exp\big(i\gamma\hat{x}^3\big)$, and $\exp\big(-i\gamma\hat{p}^3\big)$. By extension, any linear combination of x and p, $\hat{U} = \exp\big(i\gamma(\hat{x}\cos\theta + \hat{p}\sin\theta)^3\big)$, can be implemented.

Taking the various observations together, we can summarise the relationship between cubic phase shifts and photon-added coherent states as follows:

1. The strength of the cubic interaction varies inversely with the magnitude of the displacement.

2. The phase is in one-to-one correspondence with the phase of the displacement.

These statements hold provided the displacement is not too small, in which case the state will approach the Fock state. As the transition to Fock states occurs very rapidly (Fig. 4.1), this means that the smallest allowable displacement is approximately the value corresponding to the optimal fidelity.

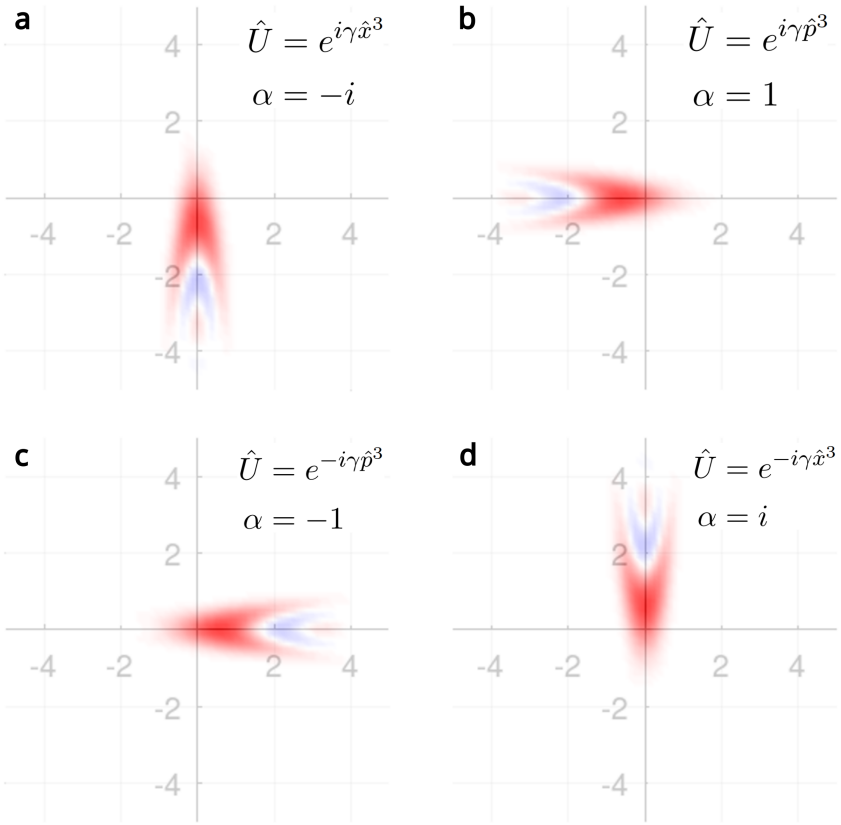


Figure 4.4: Controlling the phase of the cubic interaction. The resulting cubic interaction for coherent displacements with various phases.

4.6 Generalisations and limitations

While it may be too early to say with certainty, there appears to be good reasons to believe that even stronger interactions strength can be obtained with simple modifications of this method. By using displaced squeezed states in place of vacuum states, the elongated shape of the Wigner function of squeezed states allows greater curvatures to be achieved. This would be helpful because in the limit where the cubic strength γ goes to infinity, the cubic states have very narrow and sharply curved regions as well as sustained oscillations across phase space. It is likely that the number of photons added will also have to be increased in order to increase the number of oscillations in phase space.

There is a method which allows the requirement of photon addition to be removed, since the photon-added coherent states can be expressed as

$$(\hat{a}^\dagger)^3 |\alpha\rangle = \langle \overline{\alpha}/\lambda|_1 \, (\hat{a}_2^\dagger)^3 \, |TMSV\rangle \propto \langle \overline{\alpha}/\lambda|_1 \, \hat{a}_1^3 \, |TMSV\rangle \, . \tag{4.12}$$

This would entail the use of three successive photon subtractions on one beam of a two-mode-squeezed-vacuum state and conditioning on a specific coherent state projection on the other. Difficulties associated with this scheme include the impurity of the entangled state which will affect the quantum coherence of the cubic state, as well as the probability of success which approaches zero because of the need to postselect on a single heterodyne outcome. All the same, the equivalence shows that single photon sources are not necessary, at least in principle.

It must be emphasized that there are some limitations to our experiments. First, it is destructive. This is a limitation of the implementation, however, and not a limitation of the method. Provided that proper sources of single photons are used, a freely propagating cubic state can be generated. Second, it is probabilistic. This is a limitation of the method itself. We observed the probability of success for adding a photon to be about 0.1, reducing by one order of magnitude for every photon added. Although the cubic phase shift is unitary and therefore not required by quantum mechanics to be probabilistic, there is at present no sufficiently strong interaction available in the optical domain that will allow the realisation of deterministic cubic phase shifts.

Notwithstanding the multitude of issues to be worked out, the generation of strong cubic states and the easiness by which the interaction strength can be controlled implies that the fruits of the present work is applicable to all continuous variable quantum computing protocols based on the cubic effect, the greater number of which most likely has yet to be discovered.

4.7 Classical-to-quantum transition

The task of adding photons to coherent states was first accomplished by Zavatta *et al.* [59], who noticed that the process can be interpreted as a "classical-to-quantum" transition of the optical state as its complex amplitude decreases. For addition of photons to large coherent states has little effect with the resulting state remaining largely in a coherent state, while photon addition to small coherent states results in states which are highly quantum in nature; Fig. 4.1 provides a visual representation of this process. There has, furthermore, been some interest in the question of tracking the "quantumness" of the evolution quantitatively by some sort of measure [60], although this question has not been resolved in any definite way.

It has not escaped our notice that the observations presented here provide a direct interpretation of the effect described above — the "transition" that Zavatta *et al.* speak of is in fact coherent states turning into cubic states. Consequently, the strength of the cubic interaction provides a measure for the quantumness of the state, increasing as the complex amplitude is reduced.

Chapter 5

Non-Gaussian entangled states

Summary:

Photons are added to two-mode-squeezed-vacuum states, leading to non-Gaussian quantum correlations and an increase in entanglement and keyrate between the two beams.

5.1 Quantum internet

The quantum internet is a hypothetical means for communicating quantum information between distant locations. Although such an entity could serve many purposes, its primary functions are most likely to allow transferal of quantum states between quantum computers in a way similar to the classical internet, and to allow distribution of secret cryptographic keys. The quantum internet is unique in the set of quantum technologies in that it must be based on light as its physical system; while it is probable that local servers might require other kinds of medium to store and process information, photons are the only quantum system we know of which has any hope of surviving, say, the 6000 km journey from London to Washington.

The precise structure of the quantum internet is not at present known. The most plausible suggestion is the model based on distribution of entanglement (i.e., the quantum repeater) [61, 62]. The basic idea is to have multiple repeater nodes between two distant locations and entangled states shared between neighbouring nodes, so that by recursive entanglement swapping we end up with an entangled state between the end nodes. The effects of noise and optical losses are suppressed by purification, and if this results in weakly entangled states then the entanglement could be further concentrated through distillation.

It has been found that a simpler form of quantum networks exists if we are willing to assume that each individual repeater node is secure, resulting in the so-called trusted-node repeater network [63]. This is far easier to build than a fully functional quantum internet, and still provides some of its functions. Field tests have been made, most notably in (from oldest to most recent) America [64], Austria [65], Switzerland [66], Japan [67], and China [68], with quite possibly many more unreported as it may very well be a matter of national security. On the other hand, if the nodes have any chance of coming under attack, then the network would lose its purpose. All the same, trusted-node repeaters do not allow exchange of quantum information but only of classical information (cryptographic keys) using a quantum medium.

It has also been suggested that we can forgo entanglement and instead use quantum

error correction to protect the transmission of light against loss and errors [69]. Quantum error correction therefore serves as the direct analogue of classical optical repeaters that are essential in undersea cable networks. However, the experimental progress of quantum error correction is not at present sufficiently advanced for this to be feasible.

Taking the various evidence together, the question regarding quantum internet then boils down to the simple question of what entangled state to use. There are different candidates. Some have been studied quite extensively, such as those based on single photons [62] as well as those of Gaussian character [70]. Although it is known that non-Gaussian states with a greater degree of entanglement can be produced from Gaussian states [71], the situation surrounding quantum communication with non-Gaussian states is not very well understood. Attempts at tackling this problem [72, 35] make the simplifying assumption of Gaussian extremality [73], which asserts that the keyrate of any non-Gaussian entangled state is lower bounded by the keyrate of the Gaussian state with the same covariance matrix. Yet this can result in paradoxical findings where the maximal distance for QKD is found to decrease despite the use of a more entangled state, so that an analysis that takes into consideration the non-Gaussian properties of the state appears to be necessary.

In this Chapter we examine a class of non-Gaussian entanglement produced by adding photons to the two-mode-squeezed-vacuum state. We present a detailed study of the basic properties of this state, including its correlations in the form of mutual information and without invoking Gaussian extremality. We outline a numerical algorithm for computing Eve's accessible information.

5.2 Entanglement distillation

Given the two-mode-squeezed-vacuum state

$$|\psi\rangle = \sqrt{1-\lambda^2}\sum_{n=0}^{\infty}\lambda^n\,|n\rangle_1\,|n\rangle_2\,, \tag{5.1}$$

if we add one photon to it we obtain

$$|\psi(+1)\rangle = \hat{a}_1^\dagger\,|\psi\rangle = (1-\lambda^2)\sum_{n=0}^{\infty}\lambda^n\sqrt{n+1}\,|n+1\rangle_1\,|n\rangle_2\,. \tag{5.2}$$

This state has stronger correlations because the coefficients are now elevated by a factor of $\sqrt{n+1}$. When multiple photons are added, the correlations become even stronger:

$$|\psi(+k)\rangle = (\hat{a}_1^\dagger)^k\,|\psi\rangle = (1-\lambda^2)^{\frac{k+1}{2}}\sum_{n=0}^{\infty}\lambda^n\sqrt{\binom{n+k}{n}}\,|n+k\rangle_1\,|n\rangle_2 \tag{5.3}$$

although the correlation will in general shift with the number of photons added.

While variations might exist [11, 74, 75], the general principle behind entanglement distillation is very similar to the above. An initial state, quite possibly Gaussian since two-mode-squeezed-vacuum states are some of the most experimentally accessible entangled states, is transformed by some process involving a combination of single photon sources and detectors which increases the entanglement of the state. In general, it is necessary that this transformation takes the state into a non-Gaussian one, because of the no-go theorem on entanglement distillation of Gaussian states with Gaussian operations [14, 15, 76].

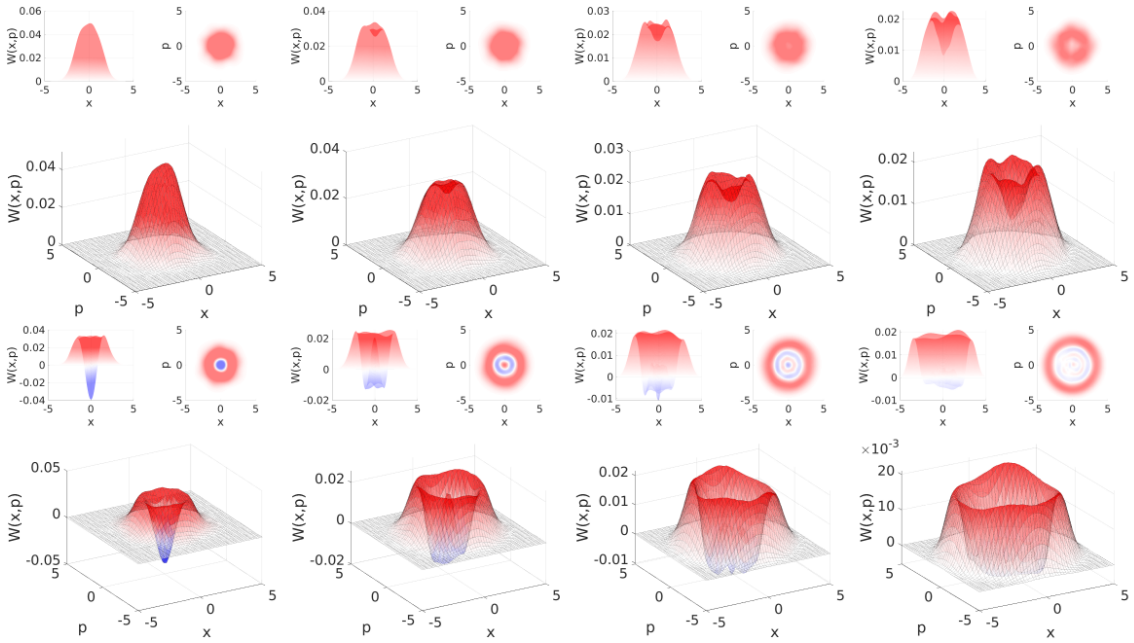


Figure 5.1: Local Wigner functions. Top panel: propagating mode. Bottom panel: photon-added mode. Number of added photons: 1 to 4, from left to right.

5.3 Experimental observations

The problem of adding photons to entangled states was investigated by analysis and re-processing of archival experimental data [34]. The experiment generated two-mode-squeezed-vacuum states with $r \approx 0.4$ and has heterodyne measurement on one beam and homodyne measurements on the other. Although we also have an identical setup on our device, the archived data was found to be sufficient for our purposes.

Photon addition is implemented in a similar way to the previous sections by postselecting on the heterodyne measurements:

$$\langle\alpha|_1 \langle q|_2 (\hat{a}_1^\dagger)^n \hat{\rho}_{12} \hat{a}_1^n |\alpha\rangle_1 |q\rangle_2 = |\alpha|^{2n} \langle\alpha|_1 \langle q|_2 \hat{\rho}_{12} |\alpha\rangle_1 |q\rangle_2 \tag{5.4}$$

but noting that the effect generalises to the case of multiple modes. Both α and q are either kept or discarded. The photon is added to the beam labelled 1 above with the heterodyne. The other beam is left untouched, which we will call the "propagating mode". The local quantum state of the propagating mode is affected however by the conditional transformation.

In order to reconstruct the density matrix of this state, we need to adapt the maximum likelihood algorithm. The density operator of the system is represented in a basis corresponding to an enumeration of the combined states

$$\{|k\rangle \;|\; 0 \leq k \leq N^2 - 1\} \leftrightarrow \{|m,n\rangle \;|\; 0 \leq m,n \leq N\} \tag{5.5}$$

so that the index k runs from 0 to $N^2 - 1$ if both m and n runs from 0 to $N - 1$. The infinite-dimensional density matrix is truncated at the Nth photon. The difference is therefore technical, requiring more computation time since the density matrix of the two-mode state scales as the quartic power of the truncation. The maximum likelihood algorithm is supplied with a set of observation pairs consisting of a heterodyne detection

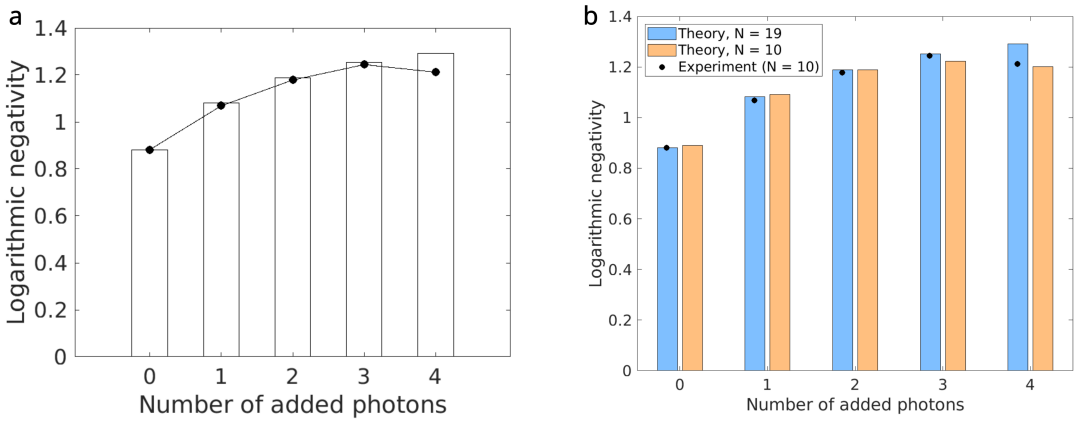


Figure 5.2: Logarithmic negativity. Solid points correspond to experimental data, vertical bars correspond to theory; each data point represents one reconstructed density matrix using the maximum likelihood method. The variable N denotes the photon number truncation for the density matrix representing the state (terms up to $|N-1\rangle$ are kept); **a**, experimental reconstructions with $N = 10$ and theoretical model with $N = 19$, and **b** showing also the theoretical values with $N = 10$.

and a homodyne detection (α, q), with the homodyne detector sampling from both the amplitude and phase quadratures.

We observed strong signatures of non-Gaussianity in the reconstructed states (Fig. 5.1). The photon-added mode exhibits negativity, not necessarily at the origin but rather in alternating annular regions centred around the origin like that of Fock states; the value at the origin oscillates between positive and negative. The negativities are generally less than that observed for Fock states. The propagating mode on the other hand has only a dip in the centre due to the conditioning and no negativities, with the dip deepening with each additional photon added.

We also observed a marked increase in the degree of entanglement as measured by logarithmic negativity (Fig. 5.2). The logarithmic negativity $E_N = \log ||\hat{\rho}^{PT}||$ of the state, where PT is shorthand for partial transpose, provides a measure of how entangled the quantum state is (see Chapter 7). For instance, the logarithmic negativity of a TMSV state is

$$E_N = 2 \tanh^{-1} \lambda, \tag{5.6}$$

which increases with the entanglement parameter λ and is zero if $\lambda = 0$; this expression gives us some intuition for what the number represents. The logarithmic negativity of photon added entangled states is more complicated but can be calculated numerically if the density matrix is known.

The logarithmic negativity was observed to increase with the number of photons added, with the rate of increase slowing down, up to 3 photons. At this point, the size of the density matrix required in order to properly describe the state is too large, and the convergence of the maximum likelihood algorithm too slow to extend the analysis for greater number of photons; this is verified by theoretical calculations shown on the right of Fig. 5.2. No error bars are shown since the maximum likelihood estimation is obtained using the entire data set available; the errors associated with the reconstruction algorithm is minimized by ensuring that the iteration procedure is convergent but not overfitting, as well as by analysing the behavior of the photon number truncation of the density matrix.

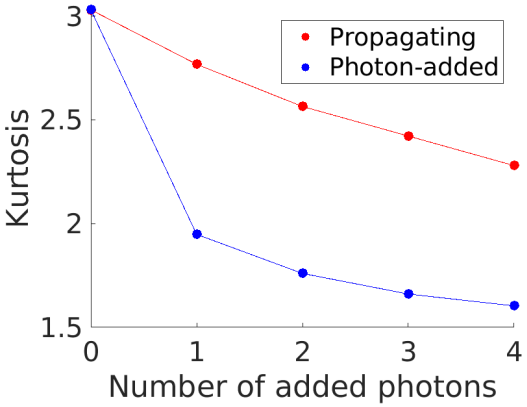


Figure 5.3: **Local kurtosis.**

5.4 Kurtosis

We examined the non-Gaussianity of the state using the kurtosis,

$$K[X] = E\left[\left(\frac{X-\mu}{\sigma}\right)^4\right], \tag{5.7}$$

for a random variable X with mean μ and standard deviation σ, evaluated on the local marginal distributions:

$$f_1(q) = \langle q|_1 \, tr_2\hat{\rho} \, |q\rangle_1 \tag{5.8}$$
$$f_2(q) = \langle q|_2 \, tr_1\hat{\rho} \, |q\rangle_2 \tag{5.9}$$

where q denotes the quadratures. The kurtosis is 3 for a perfect Gaussian distribution, larger than 3 if the distribution has a shortened tail relative to the Gaussian distribution (and looks pointy), and less than 3 if the tail is longer (and looks blunt).

We observe a sharp reduction in the kurtosis of the photon added mode, and a smaller but marked reduction in the propagating mode (Fig: 5.3). The corresponding marginals are shown in Fig. 5.4. The propagating mode has a distribution that broadens slowly and becomes increasingly blunt, but not so crazily far from a Gaussian. On the other hand, the photon-added mode undergoes a dramatic change with increasing number of oscillations and becomes visibly non-Gaussian.

The observations above have interesting implications for the general question of measuring the non-Gaussianity of quantum states. It is supposed that a theory exists that answers this question, similar to that for entanglement measures (see also Chapter 7) but instead attempts to quantify deviations from Gaussian states rather than from separable states. It is expected that the theory will look very similar to the one for entanglement measures, with the existence of multiple measures depending on how the distance to Gaussian states is defined, as well as each measure being associated with a different operational meaning depending on how the specific non-Gaussian characteristic each measure picks up is supposed to be useful in applications. The theory is yet in its infancy and not all is known.

However, it would appear that there is at least one important difference between the two theories. In the case of entanglement, the use of measures is quite necessary. It does

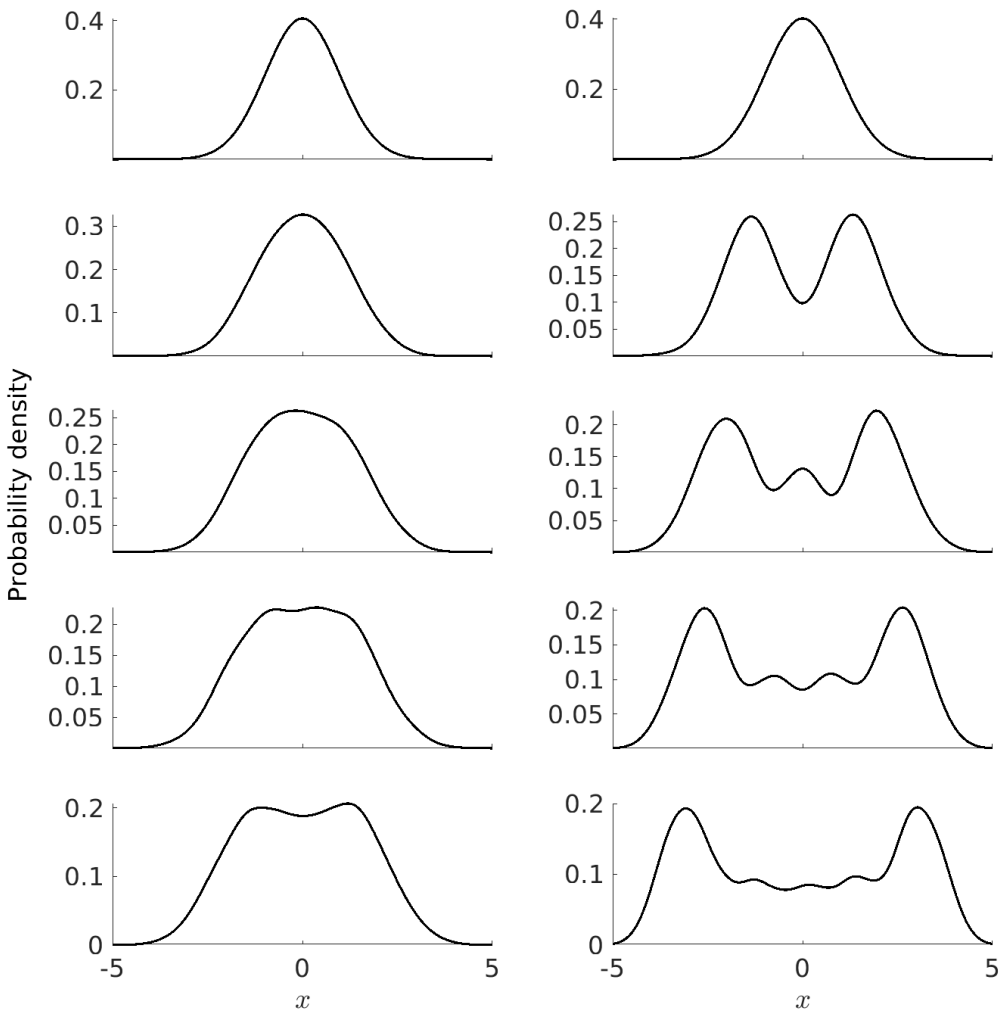


Figure 5.4: Local marginal functions. Left panel: propagating mode. Right panel: photon-added mode. The number of added photons increases from 0 to 4, top to bottom. Measurements of phase quadratures give similar results and have been suppressed.

not matter if we look at the Wigner function or the density matrix or even the covariance matrix, it is impossible to tell whether the state is entangled and much less how entangled the state is. Entanglement measures — inseparability criteria at the very least — provide the only way of determining how entangled the state is.

In contrast, a single glance at the Wigner functions shown in Fig. 5.1 reveals instantly that these states are non-Gaussian, and furthermore, which states are more non-Gaussian and which states less— those states with negativities and oscillating quasi-probability distributions are more non-Gaussian. This therefore suggests that the utility of non-Gaussian measures is not in telling whether a state of Gaussian or not, or to a large extent, how non-Gaussian the state is. Rather, any merit in this theory will lie in its operational definition, linking the degree of non-Gaussianity to specific figure of merits in applications. It is known that non-Gaussian states are often necessary or at least provides some sort of advantage in quantum technologies, however whether such a theory might exist or how much we can get out of it remains an open theoretical problem.

5.5 Quantum key distribution

It is well-known that cryptographic keys can be extracted from measurements performed on entangled states, and that the rate K at which this can be done is given by

$$K = I_{AB} - \chi_E, \tag{5.10}$$

where I_{AB} is the mutual information between the two parties performing the measurement, Alice and Bob, and χ_E is the Holevo bound on Eve's accessible information. Implicit in the expression above is the assumptions of ideal reconciliation efficiency, and the direction of reconcilation (reverse).

If the entangled state used for the protocol is a Gaussian state, then both the mutual information I_{AB} and the Holevo information χ_E can be readily evaluated, depending analytically on only the covariance matrix associated with that entangled state [77]. If the entangled state is non-Gaussian, however, then no closed formula is known in general; the simplest solution in this case is to invoke "Gaussian extremality" which states that the keyrate derived from the Gaussian state with the same covariance matrix provides a lower bound to the true keyrate [72, 35, 73].

The use of Gaussian extremality is inappropriate on at least two counts. First, it might underestimate as a lower bound, so the true keyrate could be much higher. Second, even if a non-Gaussian state is pure, if we look only at the covariance matrix then the state can appear to be mixed— this apparent decoherence will be mistakenly attributed to the eavesdropper, effectively shortening the distance across which quantum key distribution can be established. Indeed, theoretical investigations have found that adding or subtracting more than one photon appears to shorten the QKD distance [35]. Here, we wish to evaluate the mutual information for the photon-added TMSV states without invoking Gaussian extremality, and to outline a similar numerical algorithm for evaluating Eve's information.

To evaluate the mutual information, we first specify the measurements that are to be made. For simplicity we use homodyne measurements on both sides; heterodyne measurements or a combination of homodyne and heterodyne will not require a fundamental alteration of the method. Alice and Bob will therefore share a joint probability distribution

associated with the measurements:

$$P(x,y) = \langle x,y|\,\hat{\rho}\,|x,y\rangle\,, \tag{5.11}$$

with local distributions given by (with an abuse of notation)

$$P(x) = \int dy P(x,y) \tag{5.12}$$

$$P(y) = \int dx P(x,y). \tag{5.13}$$

The mutual information is therefore

$$I_{AB} = \int dxdy\ P(x,y)\log\frac{P(x,y)}{P(x)P(y)}. \tag{5.14}$$

The integral can be evaluated explicitly if the distributions are Gaussian but can nevertheless be computed numerically via Riemann sums if they are not.

Evaluation of Eve's information follows a similar procedure but the numerical method is slightly trickier to carry out, which we will explain below.

Let us first extend the entangled state we have into a larger pure state $\hat{\rho}_{ABE}$ that is held by Alice, Bob, and Eve. This can always be done, for given any density matrix

$$\hat{\rho} = \sum_j p_j\,|j\rangle\,\langle j|\,, \tag{5.15}$$

we can form the pure state

$$|\psi\rangle = \sum_j \sqrt{p_j}\,|j\rangle\,|j\rangle\,, \tag{5.16}$$

which reduces to $\hat{\rho}$ when the second mode is traced out. The specific form of the purification is not important however, because $\hat{\rho}_{ABE}$ is a closed system; we can always rewrite the quantities of interest in terms of only the quantities determined by the quantum states of Alice and Bob.

Applying Holevo's theorem, Eve's accessible information of Bob's measurement outcomes is bounded by

$$I(B:E) \leq \chi_E = S(\hat{\rho}_E) - \int\ dyP(y)S(\hat{\rho}_y), \tag{5.17}$$

where $\hat{\rho}_E = tr_{AB}\rho_{\hat{ABE}}$ is Eve's quantum state, and $\hat{\rho}_y$ is the conditional state of Eve when Bob registers the particular outcome y:

$$\hat{\rho}_y = tr_A(\langle y|\,\hat{\rho}_{ABE}\,|y\rangle). \tag{5.18}$$

The von Neumann entropy of $\hat{\rho}_y$ is

$$\begin{aligned} S(\rho_y) &= S(tr_A(\langle y|\,\hat{\rho}_{ABE}\,|y\rangle)) \\ &= S(tr_E(\langle y|\,\hat{\rho}_{ABE}\,|y\rangle)) \\ &= S(\langle y|\,\hat{\rho}_{AB}\,|y\rangle) \end{aligned}$$

since $\langle y|\,\hat{\rho}_{ABE}\,|y\rangle$ is a pure state. The final expression above is straightforward to evaluate because it depends on just the conditional state of Alice when Bob gets an outcome of

y. The von Neumann entropy of $\hat{\rho}_E$ is also easy to obtain because it is just $S(\hat{\rho}_{AB})$ since $\hat{\rho}_{ABE}$ is a pure state.

Observations of the joint probability distributions of amplitude quadratures are shown in Figure 5.5 and could be seen to be non-Gaussian when at least one photon is added. The joint distributions for phase quadratures are identical except for a clockwise rotation by ninety degrees (i.e. negative correlations instead of positive), and on account of this symmetry will therefore be suppressed from subsequent discussions. These joint distributions are composed of multiple parallel elliptical regions of density, increasing by one in number for each photon added, and most densely concentrated at the two ends. It is clear from the geometrical shape of these distributions that there exists some kind of correlation between the two beams, however it is no longer the same kind as that of EPR states.

The complete knowledge of the joint probability distributions suffice for evaluating the mutual information, with the results shown in Figure 5.6 **a**. We observe a small but marked increase in the mutual information when the Gaussian bound is not used; in other words, the Gaussian bound offers a good but not perfect estimation of the mutual information of photon-added EPR states.

More strikingly, however, is the significant reduction in Eve's accessible information when the Gaussian bound is not used (Fig. 5.6 **b**). The Holevo bound increases only very slightly as photons are added, as opposed to the Gaussian bound which experiences a sudden jump by more than a factor of three when the first photon is added and which continues to increase steadily with more photons added. This result is very interesting: although the over-estimation of Eve's accessible information using the Gaussian bound could be readily anticipated, the observations show that the difference is tremendous. There ought therefore to be substantial difference between the keyrate obtained using the Gaussian bound and the full non-Gaussian method.

Figure 5.6 **c** compares the results for the keyrates obtained by these two methods. The over-estimation of the Holevo bound is found to be sufficient to drive the keyrate negative (i.e. no keys can be distributed securely) after the addition of the first photon; in other words, when the Gaussian bound is used, a positive keyrate could be obtained only for the trivial case of no addition of photons. In contrast, the full non-Gaussian keyrate always increases with each additional photon added, appearing to tend toward a plateau with value approximately equal to twice that of keyrate of the initial Gaussian EPR state (close-up view in Figure 5.6).

The analysis we have given above pertain to those specific quantum states at our disposal, so that we would now like to consider the ramifications of the Gaussian bound in greater generality. We thus performed simulations of the transmission of photon-added entangled states through various levels of optical attenuation (Fig. 5.7 **a**) in order to understand the effect photon addition has on the distribution of secret keys between distant locations. The simulations assume: (1) the initial entangled states are pure, (2) optical attenuation of 0.15 dB per km corresponding to current state-of-the-art research fibres, (3) no additional sources of inefficiencies other than optical attenuation, (4) both parties perform homodyne detection and implement reverse reconciliation, and (5) the probabilistic overhead is neglected (in order to give the intrinsic keyrate of the state).

We found that the keyrate is always positive no matter how many photons were added, increasing with the number of added photons with each value of distance. At long distances the keyrates converge to approximately the same scaling exponent (i.e. the same gradient on a log scale). No significant differences was observed if photon addition was put on the other mode without the optical attenuation loss, however the keyrate would become

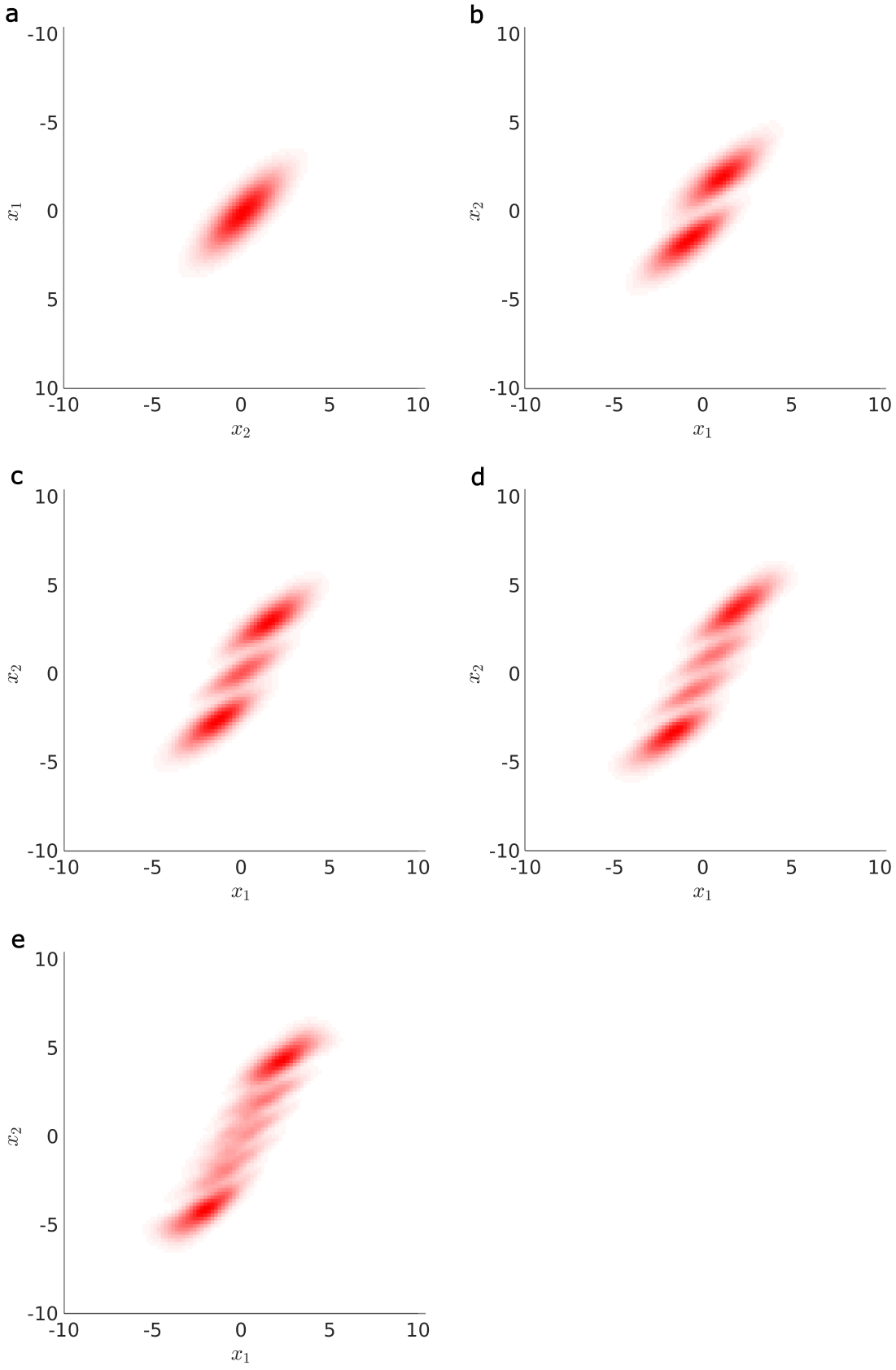


Figure 5.5: Non-Gaussian quantum correlations. Joint distributions of the amplitude quadrature (top view), with between zero and four added photons.

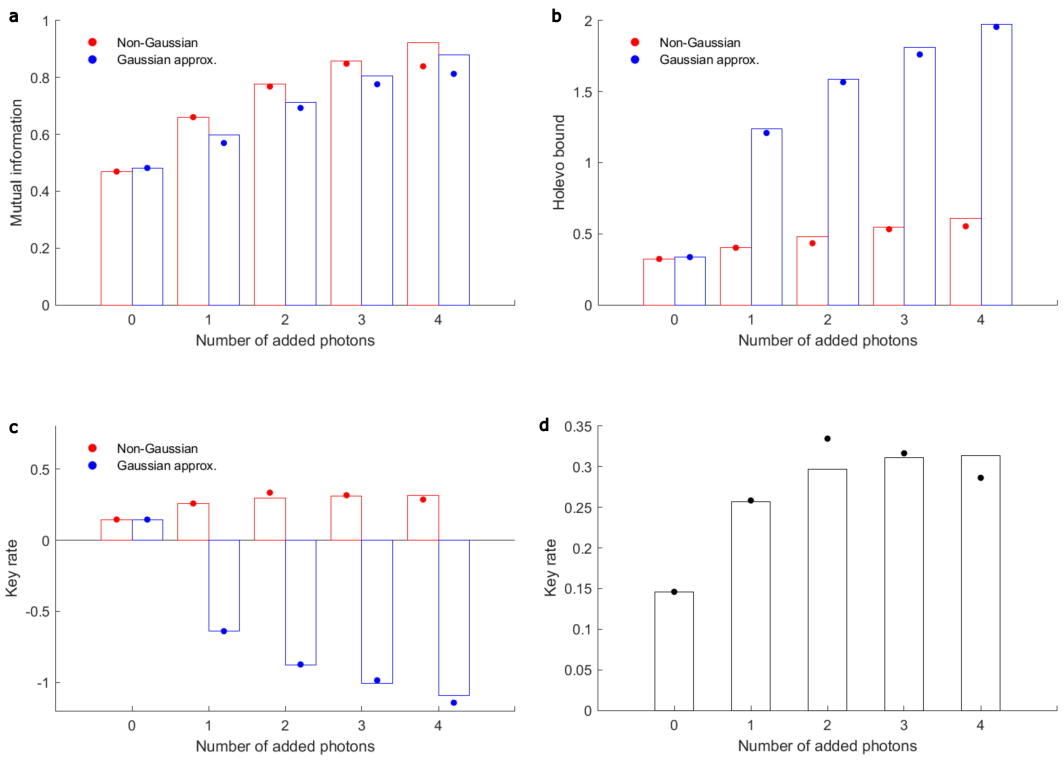


Figure 5.6: Evaluation of key rate. a. Mutual information, **b.** Holevo bound on eavesdropper's information, and **c.** final key rate, with Gaussian bound shown in blue and the full non-Gaussian evaluation shown in red. Solid points represent experimental data, corresponding bars represent theoretical values fitted to the initial Gaussian state (and assuming ideal photon addition). **d.** Close-up view of the final keyrate with an appropriate y-scale.

negative at finite distance if photon addition came before the attenuation (on the same mode). It is not desirable to run these protocols with forward information reconciliation for the same reason as normal Gaussian QKD.

Intriguingly, some keyrates appear to surpass the well-known bound on repeaterless communication. However this is almost certainly an artifact of the unaccounted probability of success. We do not wish to include this factor in our analysis because the probability of success depends greatly on how the photon addition operation is implemented (specifically, the cutoff of our postselection filters and the beamsplitting ratio in physical setups), and therefore greatly complicates the analysis which in our opinion will not do justice to the very simple physical principles involved. As a matter of fact, the probability of success goes to zero in the limit of ideal implementations of photon addition; all known implementations of the photon addition operation are only approximate. At any rate, with the highest probability of success in our experiments being 0.03 for one added photon, there can be no violations of the known theoretical bounds.

We wish to point out, however, that even though a complete analysis that includes the probabilistic effects is lacking, an obvious application does exist. It is possible to use the photon addition procedure as a "compression mechanism" when storing quantum entanglement: for the same number of states we have a greater amount of entanglement as well as a greater value of keyrate obtainable from these states.

To conclude, our results indicate the need to respect the non-Gaussian character of quantum entanglement if we wish to make full use of it in quantum key distribution. The difference between the Gaussian bound and the full non-Gaussian protocol can be an enhanced keyrate and an (apparently) compromised protocol! It must be emphasized that further work is necessary to illuminate the details of classical information processing in these non-Gaussian key distribution protocols, as well as the potential impact of non-Gaussian states on the design considerations of the general quantum communications infrastructure such as quantum memories, entanglement swapping protocols. But, for as far as we can see, the basic physical principles is sound so that the work is complete in itself.

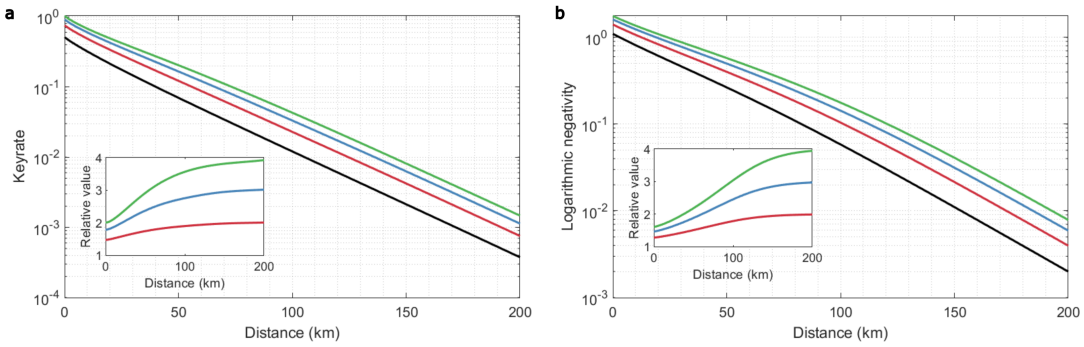


Figure 5.7: Simulations of quantum key distribution. a. Keyrate extracted from the photon-added entangled states varying with distance: none added (black), one added photon (red), two added (blue), and three added (green). Optical attenuation is assumed to be the only source of decoherence and converted into distance assuming 0.15 dB loss per km(see text). **b.** Logarithmic negativity of the corresponding states, displayed with the same choices of colour. Insets in both figures shows the quantities of the photon-added states divided by that of the initial Gaussian state.

Chapter 6

Average number of photons in a beam of light

Summary:

Up to six photons were added to a thermal state, and the counter-intuitive transformation law of the average number of photons is verified.

6.1 Tests of quantum mechanics

The earliest evidence of quantum mechanics came from physical phenomena at variance with classical laws. Take, for example, the quantization of energy in order to explain the spectrum of blackbody radiation [1] and the heat capacity of solids [78], or the observation that electrons in atoms have twice as many states as that expected— a fact later accounted for by the quantum-mechanical spin [79].

Theoreticians have conceived a number of tests with the intention to catch quantum mechanics out, creating scenarios where classical physics gives a different answer to that suggested by quantum mechanics. Nevertheless, quantum mechanics has survived in every instance. Experimental implementations of these schemes are well known by now and include the two-slit experiment which reveals the existence of the wave-function [80] and the Bell test which demonstrates the non-local nature of quantum entanglement [81].

Although quantum mechanics offer a wide range of new physical phenomena which are not always so strikingly counter-intuitive, it is arguably those that run counter to classical intuition which provide the strongest evidence of its correctness.

In this Chapter, we analyse in detail a counter-intuitive transformation law of the average number of photons in a beam of light when photons are added and provide experimental evidence of its validity.

6.2 Adding photons to thermal states

We are interested in the situation where photons are added to a beam of light,

$$\hat{\rho} \to \hat{a}^\dagger \hat{\rho} \hat{a}, \tag{6.1}$$

with $\hat{\rho}$ initially in a thermal state

$$\hat{\rho} = (1-\lambda^2)\sum_n \lambda^{2n} |n\rangle\langle n| . \tag{6.2}$$

It is straightforward — if somewhat tedious — to calculate the effect this has on the average number of photons $\mathrm{tr}(\hat{n}\hat{\rho})$, which will be found to first *double* before increasing by one. Similarly, if we were to subtract a single photon from the thermal state $\hat{\rho} \to \hat{a}\hat{\rho}\hat{a}^\dagger$, it will be found that the average photon number is doubled.

From a classical perspective, this situation appears to be most unusual. For if we had a bank account kept at an average of 1000 dollars (with the precise amount unknown because we are careless), we would not deposit 100 dollars into the account and expect to find 2100 dollars when we check the balance again! And we would most certainly not withdraw 100 dollars from the account and expect to see a balance of 2000 dollars. In other words, the change in photon statistics brought about by the addition and subtraction of photons does not follow the rules of classical probability.

Calculations suggest that this effect is true in general: when k photons are added to or removed from a thermal state, the average number of photons transforms respectively as

$$\begin{aligned} \text{Addition: } & \langle\hat{n}\rangle \to (k+1)\langle\hat{n}\rangle + k, \\ \text{Subtraction: } & \langle\hat{n}\rangle \to (k+1)\langle\hat{n}\rangle . \end{aligned} \tag{6.3}$$

Although this effect has been observed in experiments with subtraction of multiple photons [82], the addition of multiple photons is much harder to carry out so that the effect has been verified only in the simplest case of adding a single photon [83].

6.3 Experimental observations

We prepare thermal states through amplitude and phase modulation of the vacuum state with white noise. Heterodyne measurements $\langle\alpha|$ are made on this state, and the results postselected with the filter $|\alpha|^{2k}$ to add k photons to the state (Eq. 3.3). The measurement outcomes correspond to a non-Gaussian state, so we proceed with the usual maximum likelihood method to reconstruct the quantum state [57].

We observe that the average photon number of the photon-added state has an affine relationship with that of the initial thermal state (Fig. 6.1). For each number of added photons k, we plot the theoretical line of slope $k+1$ and offset k. We find that the experimental observations are in good agreement with these predictions.

This relationship has been verified for up to six added photons before the maximum likelihood reconstruction algorithm becomes too slow to carry out efficiently. This is because the addition of photons shifts the components of the density matrix to higher photon numbers so that a larger truncation is required for the Fock space representation of the density matrix. For the same reason, it is difficult to go much higher with the initial average photon number of the thermal state.

We observe also that the corresponding quantum states are non-Gaussian. Raw outcomes, in the form of histograms, registered by the homodyne detectors and the corresponding tomographically reconstructed Wigner functions are shown in Fig. 6.2. The observed distribution differs from that of a Gaussian state by a dip in the centre that deepens with the number of photons added; the dip originates from the zero of $|\alpha|^{2n}$ at

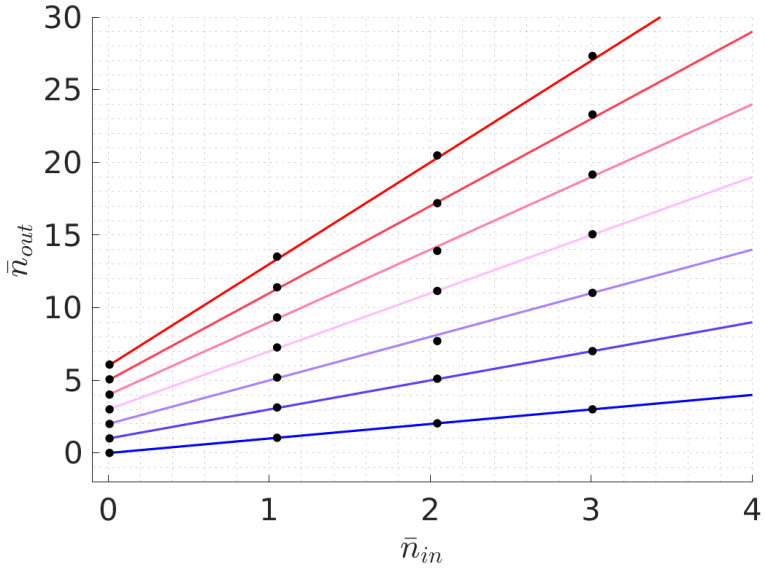


Figure 6.1: Average number of photons. The horizontal axis corresponds to the average number of photons in the initial thermal state, while the vertical axis corresponds to the average number of photons after photon addition. The number of added photons is between 0 and 6, from bottom to top. Solid points are experimental data, solid lines are theoretical.

$\alpha = 0$ and deepens because of the increasing exponent. The reconstructed Wigner functions reveal negativities. The negativity is greatest with one added photon and reduces for higher number of photons, with the number of oscillations in the Wigner function increasing in its place. In the figures shown here, both the heterodyne outcomes and the Wigner function are essentially circularly symmetric around the origin of the phase-space, therefore only the amplitude quadrature is shown with the phase quadrature suppressed.

We examined the photon statistics of these states (the diagonal elements $\langle n|\,\hat{\rho}\,|n\rangle$) and observed that the effect of photon addition is to shift the distribution to the right and instill zeros at the vacated values of n (Fig. 6.3). In other words, conditioned on the addition of k photons to the state, it would be impossible to make a measurement of its photon number to find anything less than k. This is what we would expect even for classical systems.

However, we also find that the distribution is not merely shifted but also weighted. This is a quantum-mechanical feature, accounted for by the fact that the creation operator raises Fock states with a weight (Eq. 2.9):

$$\hat{a}^\dagger\,|n\rangle = \sqrt{n+1}\,|n+1\rangle\,.$$

The probability of successfully adding a photon therefore increases with the number of photons that are initially present, and it is this effect that is responsible for skewing the average photon number to a value larger than classically expected. Similar statements hold for removal of photons: $\hat{a}\,|n\rangle = \sqrt{n}\,|n-1\rangle$, with both effects being a direct consequence of the quantum commutation relations $[a, a^\dagger] = 1$.

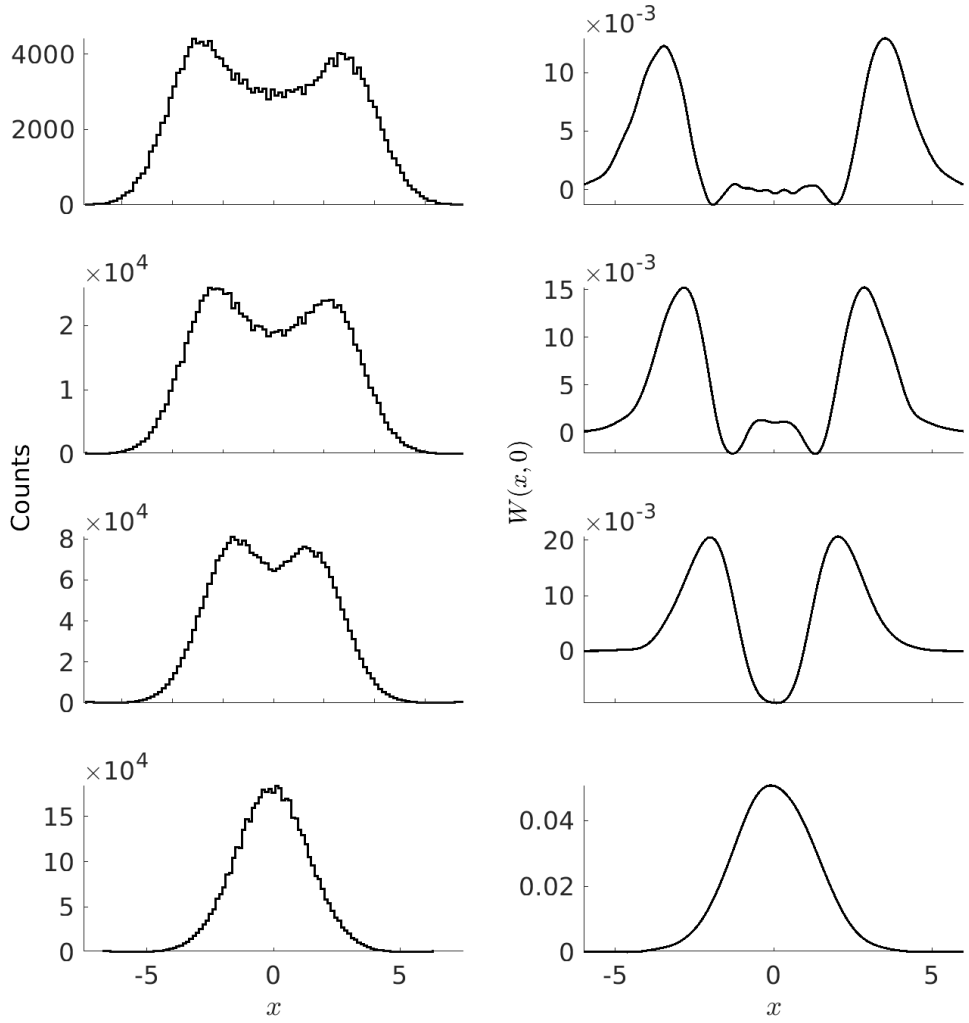


Figure 6.2: Raw measurement outcomes and reconstructed Wigner function. The left panel shows raw measurement outcomes on the amplitude homodyne in the form of histograms, while the right panel shows the x-slice of the reconstructed Wigner function. The number of photons added is 0 to 3, from bottom to top.

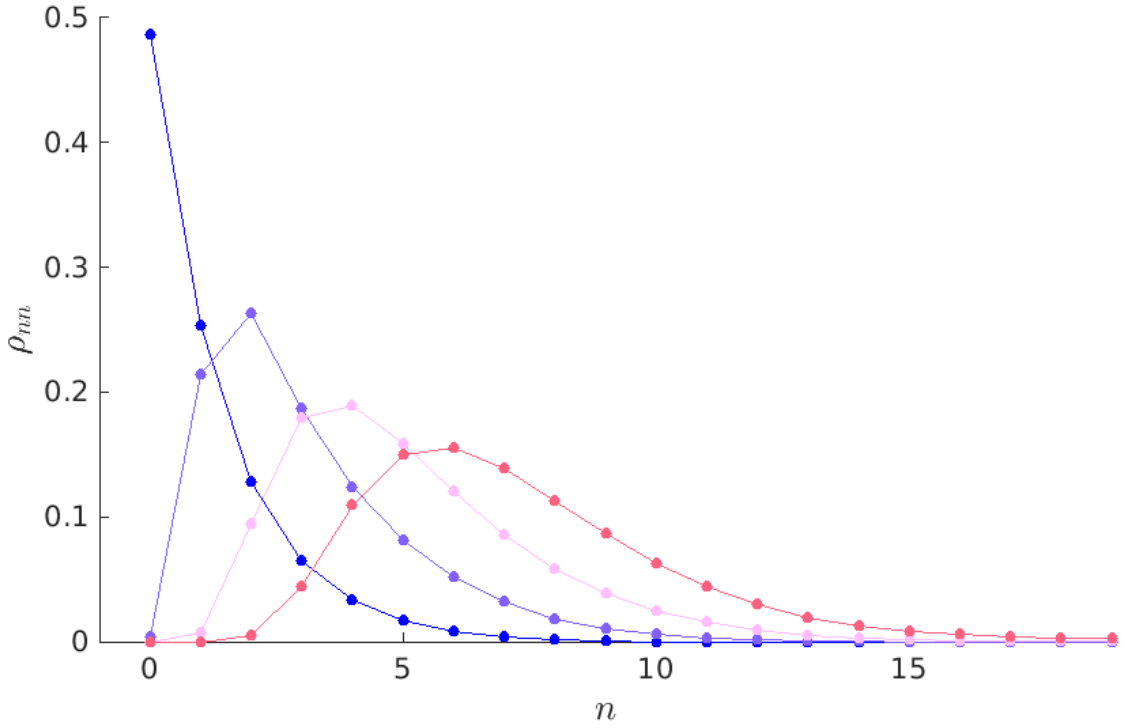


Figure 6.3: Photon statistics. Initial thermal state has a variance of 3 (average photon number of 1). Number of photons added is 0,1,2,3, from left to right.

6.4 The difference between addition and subtraction

The discussion above brings us to the question of whether there are any differences between photon addition and photon subtraction, apart from the difference in sign in Eq. 6.3. The short answer is that there is: unlike photon addition, the effect produced by photon subtraction has a classical analogue.[1]

The argument is the following: Suppose we have a box containing initially either 0 or 10 balls with equal probability, with therefore an average number of exactly 5 balls; when conditioned on the successful removal of a ball from this box, we will find that the remaining average is 9 because the box could not have been empty! Although it must be emphasised that this argument is based not on the general weighting effect of the annihilation operator, it nevertheless provides a striking example of how the doubling of the average by subtraction can also occur in a classical system.

In comparison, the same argument fails in the case of photon addition. If subtraction is replaced by addition in the example above, we would open the box to find an equal chance of getting 1 or 11 balls, resulting in an average of 6. Indeed, if we were to add k balls to a box containing an average of n balls, we would get a new average of $n + k$ without the multiplier, and regardless of the initial distribution.

Taken together, we may say that the effect produced by photon subtraction is more dramatic (multiplication despite removal), whereas that produced by photon addition is more difficult — if not altogether impossible — to reconcile with the classical picture.

[1] Which I first learnt of from Barnett [84].

6.5 Phase-space representation

The observations and interpretations of our experiment have so far been based on the number representation: the quantum state of the system is given by the density operator represented in the Fock basis

$$\hat{\rho} = \sum \rho_{mn} \left|m, n\right\rangle \left\langle m, n\right|, \tag{6.4}$$

with the action of photon addition represented in the usual way and the average photon number given by $\langle \hat{n} \rangle = \sum n \langle n| \hat{\rho} |n\rangle$. If $\hat{\rho}$ is substituted for the density operator of the k-photon-added thermal state, then the transformation rule in Eq. 6.3 may be computed after some standard but tedious calculations.

Our experiment brings to light an alternative interpretation based on the phase-space representation, which appears to provide a simpler description of the system. In this picture, the quantum state is represented by the Fusimi Q-function

$$Q(\alpha) = \langle \alpha| \hat{\rho} |\alpha\rangle, \tag{6.5}$$

so that photon addition transforms the Q-function by weighting it with the same function we used for postselection $|\alpha|^{2k}$, viz.

$$\tilde{Q}(\alpha) \propto \langle \alpha| (\hat{a}^\dagger)^k \hat{\rho} \hat{a}^k |\alpha\rangle = |\alpha|^{2k} Q(\alpha). \tag{6.6}$$

The average number of photons has a straightforward representation, consisting essentially of just the variance of the phase-space distribution:

$$\langle \hat{n} \rangle = \int d\alpha \ |\alpha|^2 Q(\alpha) - 1. \tag{6.7}$$

The extra constant depends on the quasiprobability distribution used, being different if we had instead used the Wigner function or the Glauber-Sudarshan P function. The photon-added state $\tilde{Q}$ has an average photon number of

$$\langle n \rangle_{\tilde{Q}} = \int d\alpha |\alpha|^2 \tilde{Q}(\alpha) - 1 = \frac{\int d\alpha |\alpha|^{2n+2} Q(\alpha)}{\int d\alpha |\alpha|^{2n} Q(\alpha)} - 1 \tag{6.8}$$

where the expression $\int d\alpha |\alpha|^{2n} Q(\alpha)$ is the required normalisation factor after photon addition. If we now let Q be the Q-function of the thermal state, then this expression is characterised by the even moments of the Gaussian distribution which we can read off from publicly available tables of integrals to be

$$\int d\alpha |\alpha|^{2n} Q(\alpha) = (1 - \lambda^2)^{-n} n!. \tag{6.9}$$

It is then straightforward to substitute this into the formula above to give the transformation rule

$$\langle n \rangle_{\tilde{Q}} = (k + 1) \langle n \rangle_Q + k \tag{6.10}$$

as required.

Although the conclusion is the same — as it certainly should be — the phase-space picture appears to give a simpler and more elegant way of handling addition of photons to thermal states as opposed to the brute force method of the number representation; the

transformation rule of Q-functions coincides with our implementation of photon addition.

6.6 An implicit assumption

Throughout this chapter, we have assumed that

$$\langle\alpha|\, a^\dagger = \overline{\alpha}\,\langle\alpha|\,, \tag{6.11}$$

which is required for the equivalence between photon addition and postselection of heterodyne measurement outcomes. We now show that this assumption can be removed on account of the observations in previous experiments.

The argument is quite simple. The expression above amounts to assuming that coherent states $|\alpha\rangle$ are eigenstates of the annihilation operator. This has been shown to be true by Zavatta *et al.* [85] by experiment, who observed that photon subtraction has no effect on coherent states. Furthermore, the eigenvalue can be deduced by considering the expression $(\langle\alpha|\,\hat{a}^\dagger)(\hat{a}\,|a\rangle)$. This is the same expression as the expectation value of the number of photons in a coherent state $\langle\alpha|\,\hat{n}\,|a\rangle$ which must be equal to the intensity $|\alpha|^2$; up to an irrelevant phase factor, the eigenvalue is given by its square-root.

Chapter 7

Bounding the distillable entanglement

Summary:

The distillable entanglement of a two-mode-squeezed-vacuum state is shown to increase under the action of noiseless linear amplification, with its value bounded from above by the relative entropy of entanglement and from below by the reverse coherent information.

7.1 Quantum entanglement as a physical quantity

We have spoken of quantum entanglement as a physical property, referring to how measurements made on one beam allow us to immediately infer the quantum state of the other beam. However, quantum entanglement can also be treated as a physical *quantity*, with a value assigned to each entangled state to indicate its degree of entanglement. A simple, prototypical example of such a number is the entanglement parameter λ of the two-mode-squeezed-vacuum state: the state is not entangled when $\lambda = 0$, becoming increasingly entangled as λ increases. Nevertheless, this particular description has limited utility because entangled states are not in general defined by just one single parameter.

The theory of entanglement measures is the formal way of quantifying entanglement. This theory asserts that a function f defined on the set of entangled states and taking values in the reals is a measure of entanglement provided that (1) it is zero on the set of separable states, and (2) it does not increase under local operations and classical communication. A quantum state ρ is separable if it can be written as a mixture of product states $\hat{\rho} = \sum_n \hat{\rho}_1^{(n)} \otimes \hat{\rho}_2^{(n)}$. For this theory to make any sense, it is necessary for the set of functions f satisfying the properties above to be non-empty. Indeed, the logarithmic negativity we used briefly in Chapter 5 qualifies as a measure of entanglement.

Arguably, the greatest surprise of this theory is that there is more than one measure—in fact, there is at least half a dozen of them. What is more, these measures are not equivalent; in the sense that they often disagree as to whether a given entangled state has more entanglement than another. While there is no good reason to expect beforehand that there should be multiple different measures, it turns out that there is a simple physical meaning which underlies this fact: each measure is associated with a different sort of entanglement. For instance, the *entanglement cost* measures the amount of entanglement that is needed in order to make a given state, while the *distillable entanglement* gives the amount of entanglement that can be extracted from that state. The two measures concern different aspects of entanglement, and thus it is not necessary for them to agree.

The purpose of this chapter is to provide a method for estimating the distillable entanglement [86]. This measure plays a central role in quantifying the efficiency of general quantum communication schemes, yet unlike most other measures, there is no mathematical formula or even numerical method that can be used to determine its value. Our findings indicate that bounds can be placed on the value of the distillable entanglement that are sufficiently stringent to show that it is increased by a certain distillation process (noiseless amplification). Our method exploits upper and lower bounds of the distillable entanglement by other suitably chosen measures that can be more readily evaluated, and for this reason, I should now like to provide some more information regarding the various measures of entanglement as well as their relations.

7.2 The theory of entanglement measures

All entanglement measures reduce to just one quantity on the set of pure states[1] [87], the entanglement entropy

$$E_V(|\psi\rangle) = S(\hat{\rho}_A) = S(\hat{\rho}_B), \tag{7.1}$$

where $S(\hat{\rho}) = -\operatorname{tr}(\hat{\rho}\log\hat{\rho})$ is the von Neumann entropy and $\hat{\rho}_A = \operatorname{tr}_B(|\psi\rangle\langle\psi|)$ and $\hat{\rho}_B = \operatorname{tr}_A(|\psi\rangle\langle\psi|)$ denote the subsystems of the entangled state. For general quantum states, the entanglement entropy is not sufficient; below is a list of the various measures that arise:

- Entanglement cost [88], the lowest conversion rate of Bell states to the given entangled state:

$$E_C(\hat{\rho}) = \inf\{E|\forall\epsilon>0,\delta>0,\exists m,n,\Lambda : |E-\frac{m}{n}| \le \delta \text{ and } D(\Lambda(\Phi_{\text{Bell}}^{\otimes m}),\hat{\rho}^{\otimes n}) \le \epsilon\}, \tag{7.2}$$

  where Λ is any LOCC operation, D is some distance measure between quantum states, and Φ_{Bell} is the Bell state.

- Distillable entanglement [88], the highest rate of extracting Bell states from the given entangled state:

$$E_D(\hat{\rho}) = \sup\{E|\forall\epsilon>0,\delta>0,\exists m,n,\Lambda : |E-\frac{m}{n}| \le \delta \text{ and } D(\Phi_{\text{Bell}}^{\otimes m},\Lambda(\hat{\rho}^{\otimes n})) \le \epsilon\}. \tag{7.3}$$

- Entanglement of formation (EoF) [89],

$$E_F(\hat{\rho}) = \inf\{\sum_j p_j E_v(|\psi_j\rangle)|\hat{\rho} = \sum_j p_j |\psi_j\rangle\langle\psi_j|\}. \tag{7.4}$$

- Logarithmic negativity [90],

$$E_N(\hat{\rho}) = \log||\hat{\rho}^{PT}||, \tag{7.5}$$

  where $||\cdot||$ denotes the trace norm and PT is shorthand for the partial transpose.

[1] Assuming the state has only two partitions. Necessary and sufficient conditions for multipartite entanglement are in general not well established.

- Relative entropy of entanglement [91],

$$E_R(\hat{\rho}) = \inf_{\hat{\sigma}\ \text{separable}} S(\hat{\rho}||\hat{\sigma}), \tag{7.6}$$

  where $S(\hat{\rho}||\hat{\sigma}) = \operatorname{tr}\hat{\rho}(\log\hat{\rho} - \log\hat{\sigma})$ is the quantum relative entropy. If the infimum runs only over Gaussian states, then the corresponding measure is the Gaussian relative entropy of entanglement [92], which upper bounds the proper relative entropy of entanglement since the infimum is evaluated over a smaller domain.

- Squashed entanglement [93],

$$E_{sq}(\hat{\rho}_{AB}) = \frac{1}{2}\inf_{\hat{\rho}_{ABE}} I(A:B|E), \tag{7.7}$$

  where the minimization occurs for the conditional mutual information $I(A:B|E) = S(\hat{\rho}_{AE}) + S(\hat{\rho}_{BE}) - S(\hat{\rho}_E) - S(\hat{\rho}_{ABE})$ over all purifications $\hat{\rho}_{ABE}$ of the bipartite state $\hat{\rho}_{AB}$.

This list is further supplemented by functions that provide necessary and/or sufficient conditions for inseparability but which are not proper entanglement measures because they do not satisfy the two requirements given in the previous section. These are:

- PPT (partial positive transpose) criterion [94]: a Gaussian quantum state is separable if and only if the symplectic eigenvalue of the partial transpose $\tilde{\nu} \geq 1$. It is in a following sense equivalent to the logarithmic negativity:

$$E_N(\hat{\rho}) = \begin{cases} 0 & \text{if } \hat{\rho} \text{ separable,} \\ -\log\tilde{\nu} & \text{otherwise.} \end{cases} \tag{7.8}$$

- EPR steering [95],

$$E_{A>B} = V_{x_B|x_A}V_{p_B|p_A} \geq 1, \tag{7.9}$$
$$E_{B>A} = V_{x_A|x_B}V_{p_A|p_B} \geq 1, \tag{7.10}$$

  with steering occurring when at least one inequality is violated. The V's denote conditional variance of a quadrature operator given the value of another. EPR steering is a sufficient but not necessary condition for inseparability.

- Coherent information [96] and reverse coherent information [97] (sometimes bundled together and simply referred to as just "coherent information"):

$$I_C(\hat{\rho}) = S(\operatorname{tr}_A\hat{\rho}) - S(\hat{\rho}), \tag{7.11}$$
$$I_{RC}(\hat{\rho}) = S(\operatorname{tr}_B\hat{\rho}) - S(\hat{\rho}), \tag{7.12}$$

  providing sufficient conditions for inseparability.

The additional measures in this augmented list are easier to evaluate compared to entanglement measures and provide the simplest method of verifying whether quantum states generated in the laboratory are entangled or not.

In general, it is difficult to calculate the values of entanglement measures for arbitrary quantum states because of the optimisation procedures involved in their definitions.

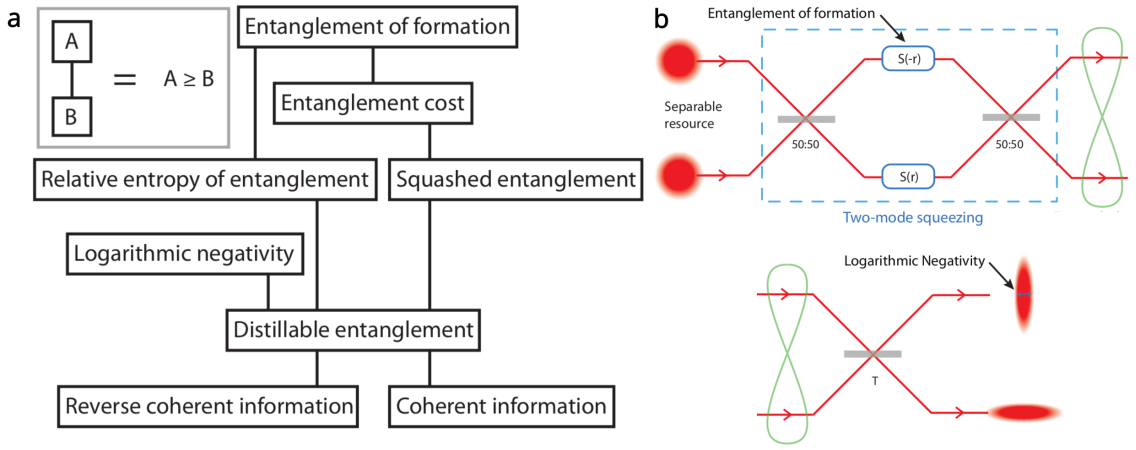


Figure 7.1: Theory of entanglement measures. a. Illustration of the hierarchy of entanglement measures. Each vertical line linking a pair of entanglement measures represents an inequality, with the greater quantity on top. **b.** Illustration of operational interpretation. Top: decomposition of an entangled state by two-mode squeezing. Bottom: extraction of squeezing by interfering the two entangled beams.

This statement has a more precise formulation: the problem of computing entanglement measures is NP-complete for most measures [72]. Analytic expressions exist for restricted cases such as Gaussian states, not even for the entire set but in most cases only for some subset with additional symmetries [98, 99]. Some measures can be evaluated numerically using semi-definite-programs [100], although in the case of (continuous variable) quantum optics where the size of the density matrix scales as N^{2k} (where N is the photon number truncation and k is the number of optical modes), even semi-definite programs are often very slow and memory-consuming. Distillable entanglement is an exception, with simply no known method for its calculation.

The basic structure of the theory of entanglement measures is based on a hierarchy determining which measures are greater than which others. By greater, we mean greater for all quantum states (Fig. 7.1a) [90, 101, 102, 103, 93, 104]. This hierarchical structure arises because the measures have operational interpretations; for instance, the entanglement cost is how much entanglement is necessary to produce a given entangled state while the distillable entanglement measures how much entanglement can be extracted from that state. It therefore follows that the entanglement cost should always be greater or equal to the distillable entanglement because we should not be allowed to extract more than we put in. In general, the operational interpretation of each measure is not always as clear or as intuitive as the examples I gave above, but it can nonetheless be proven mathematically that these inequalities of measures do hold.

One further example that will be of interest to us is the relationship between entanglement of formation and logarithmic negativity. The entanglement of formation is a relative of the entanglement cost and also measures the amount of entanglement needed to form a given quantum state, in terms of the two-mode-squeezing operator (Fig. 7.1b). An analytic

expression is known [98] for two-mode Gaussian states of the form

$$\sigma = \begin{bmatrix} m & 0 & c & 0 \\ 0 & m & 0 & -c \\ c & 0 & n & 0 \\ 0 & -c & 0 & n \end{bmatrix}, \tag{7.13}$$

which has an entanglement of formation of

$$E_F(\sigma) = \cosh^2 r_0 \log \cosh^2 r_0 - \sinh^2 r_0 \log \sinh^2 r_0, \tag{7.14}$$

where r_0 is the squeezing parameter in the two-mode-squeezing operator and is given by

$$r_0 = \frac{1}{4} \log \frac{\kappa - \sqrt{\kappa^2 - \lambda_+ \lambda_-}}{\lambda_-}, \tag{7.15}$$

with $\kappa = 2(\det \sigma + 1) - (m-n)^2$ and $\lambda_\pm = m^2 + n^2 + 2c^2 + 2((mn + c^2) \pm 2c(m+n))$. The requirement that σ be of the form above is actually rather general, for any two-mode Gaussian state can be put into the following form by local unitary operations which will not affect the entanglement [105]:

$$\sigma = \begin{bmatrix} m & 0 & c_1 & 0 \\ 0 & m & 0 & c_2 \\ c_1 & 0 & n & 0 \\ 0 & c_2 & 0 & n \end{bmatrix}. \tag{7.16}$$

On the other hand, the logarithmic negativity corresponds to the squeezing ($\tilde{\nu}$) that can be extracted from the state (Fig. 7.1b) by interfering the two beams on a beam splitter. So, in fact, these two measures are related according to the following inequality:

$$\tilde{\nu} \geq e^{-2r_0} \tag{7.17}$$

which reflects the non-increasing of quantum squeezing under passive operations.

Entanglement measures also have direct applications for quantum communication. It is used to bound the rate of private communication and in some cases coincides with it; consequently, the demonstration and "certification" of a quantum repeater will require one to show that the communication rate is higher than certain measures [106].

7.3 Noiseless amplification increases distillable entanglement

We analyzed the archival data of an entanglement distillation experiment with noiseless amplification [34]. The experimental arrangement is shown in Fig. 7.2a; a two-mode-squeezed-vacuum state is generated from a pair of optical parametric amplifiers and one mode of the entangled state is put through a beam splitter with variable transmissivity to simulate optical loss. Heterodyne measurements are performed on the mode with loss, while homodyne measurements (alternating between amplitude and phase measurements) are performed on the other mode that does not experience loss. Postselection of the heterodyne outcomes by the Gaussian filter (Eq. 3.4) implements noiseless amplification. Since the measurement outcomes of this process correspond to a Gaussian state, the

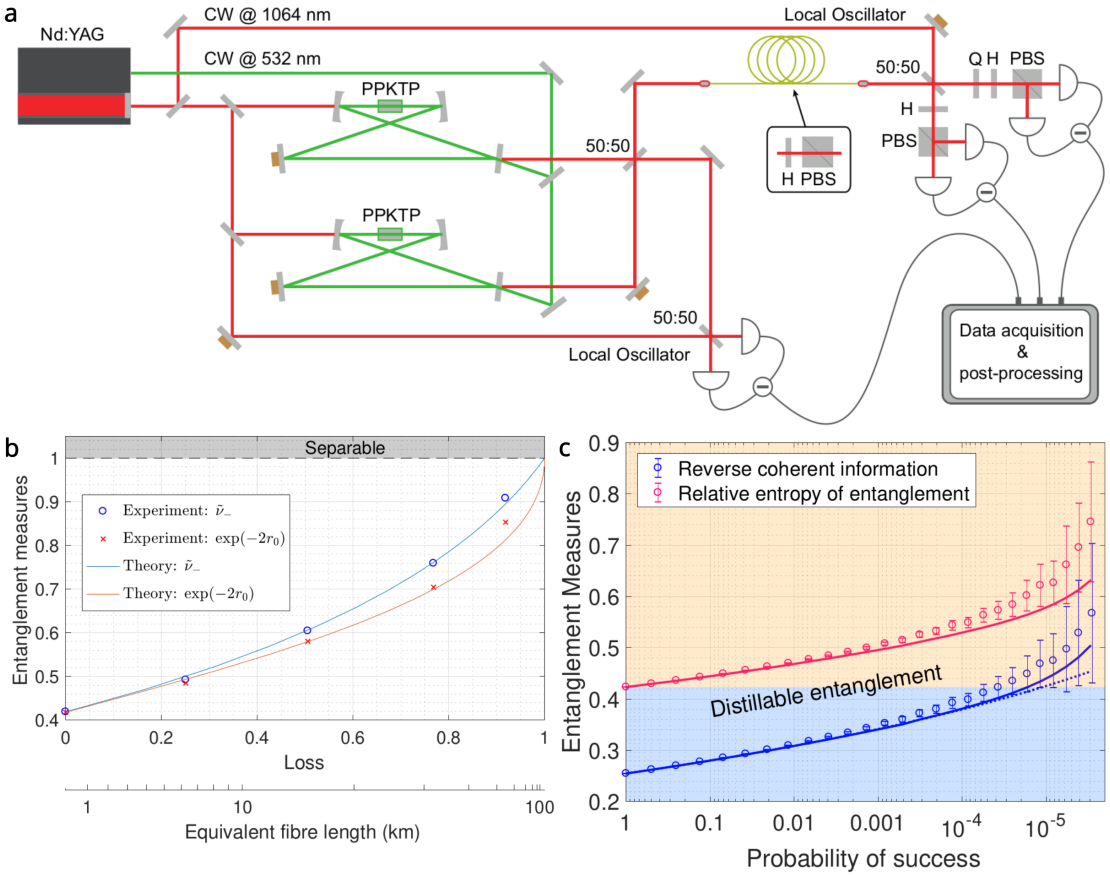


Figure 7.2: Distillable entanglement and noiseless amplification. a. Experiment from the archives. PBS: polarising beam-splitter, H: half-wave plate, Q: quarter-wave plate. **b.** Inseparability as a function of optical loss. Data points are experimental, solid lines are theoretical. Sufficient data exist such that statistical uncertainties are negligible, although fluctuations in the channel transmission appear to be important at low transmissivities. Equivalent fibre length corresponding to each value of optical loss is calculated assuming 0.2 dB attenuation per km (i.e., attenuation of optical fibres at telecommunications wavelength). **c.** Upper and lower bounds for the distillable entanglement. Optical loss setting: 0% loss. Circular points correspond to averaged experimental data, with error bars showing variation over 100 repeated runs. Solid line is theoretical model accounting for cutoff of the postselection filter, dotted line is Gaussian model. Orange shading indicates region where the entanglement measures are greater than the initial relative entropy of entanglement.

heterodyne and homodyne measurements provide sufficient information for a tomographic reconstruction of the effective quantum state.

We observed that entanglement correlations exist at all values of optical loss, except when the beam splitter is fully reflective (Fig. 7.2b). Both the symplectic eigenvalue of the partial transpose $\tilde{\nu}$ and the equivalent EoF squeezing $\exp(-2r_0)$ are below one, indicating that the state is entangled. These quantities have minimum values when there is no loss, and increase monotonically with loss. The symplectic eigenvalue is always larger than the EoF-equivalent squeezing, as required by Eq. 7.17.

We observed the increase of distillable entanglement with noiseless amplification (Fig. 7.2c). The optical loss is set to 0 percent. The distillable entanglement is bounded from above by the relative entropy of entanglement (with the infimum of Eq. 7.6 evaluated only over the set of states with positive partial transpose instead of the set of separable states [107, 100]) and from below by the reverse coherent information. It is found that the value of the reverse coherent information after noiseless amplification is greater than the relative entropy of entanglement before amplification, thus showing that the distillable entanglement must have increased in the process. The following inequality illustrates this reasoning:

$$DE_{after} \geq RCI_{after} > REE_{before} \geq DE_{before}. \tag{7.18}$$

The same method was tried with various other settings of loss between 0 and 100 percent but no increase in distillable entanglement was observed ($RCI_{after} < REE_{before}$). Likewise, all other possible choices of the upper bound (logarithmic negativity, squashed entanglement, entanglement of formation) fail to indicate any increase in the distillable entanglement presumably because they are not sufficiently strong. Only the relative entropy of entanglement worked.

The increase in distillable entanglement is a very important indication that the amount of entanglement that is actually "usable" has increased, so that consequently the distilled state is supposed to be more useful for quantum information tasks. This interpretation is possible only on account of the operational meaning of distillable entanglement and could not have been deduced directly from any increase in the other measures, except perhaps when referring only to some restricted property of entanglement such as EPR steering.

It must be emphasised that a similar technique has been previously attempted by Dong *et al.* [108, 109], although no increase in the distillable entanglement was observed. The experiment involved putting a two-mode-squeezed-vacuum state through a beam splitter with fluctuating transmissivity and distilling entanglement by making a weak homodyne measurement on the state and conditioning on large measurement outcomes.

It is interesting to compare their observations with our findings. First, although the (reverse) coherent information is also used for the lower bound, the logarithmic negativity is used instead for the upper bound. This could explain why the increase could not be observed, since we would expect logarithmic negativity to be weaker than the relative entropy of entanglement. Second, Dong *et al.* found through a theoretical analysis that the technique works better for pure states than it does when there is thermal noise, because the reverse coherent information does not increase very much in the latter case. This may explain why it is more difficult to observe an increase in the distillable entanglement when the optical loss was set to higher values.

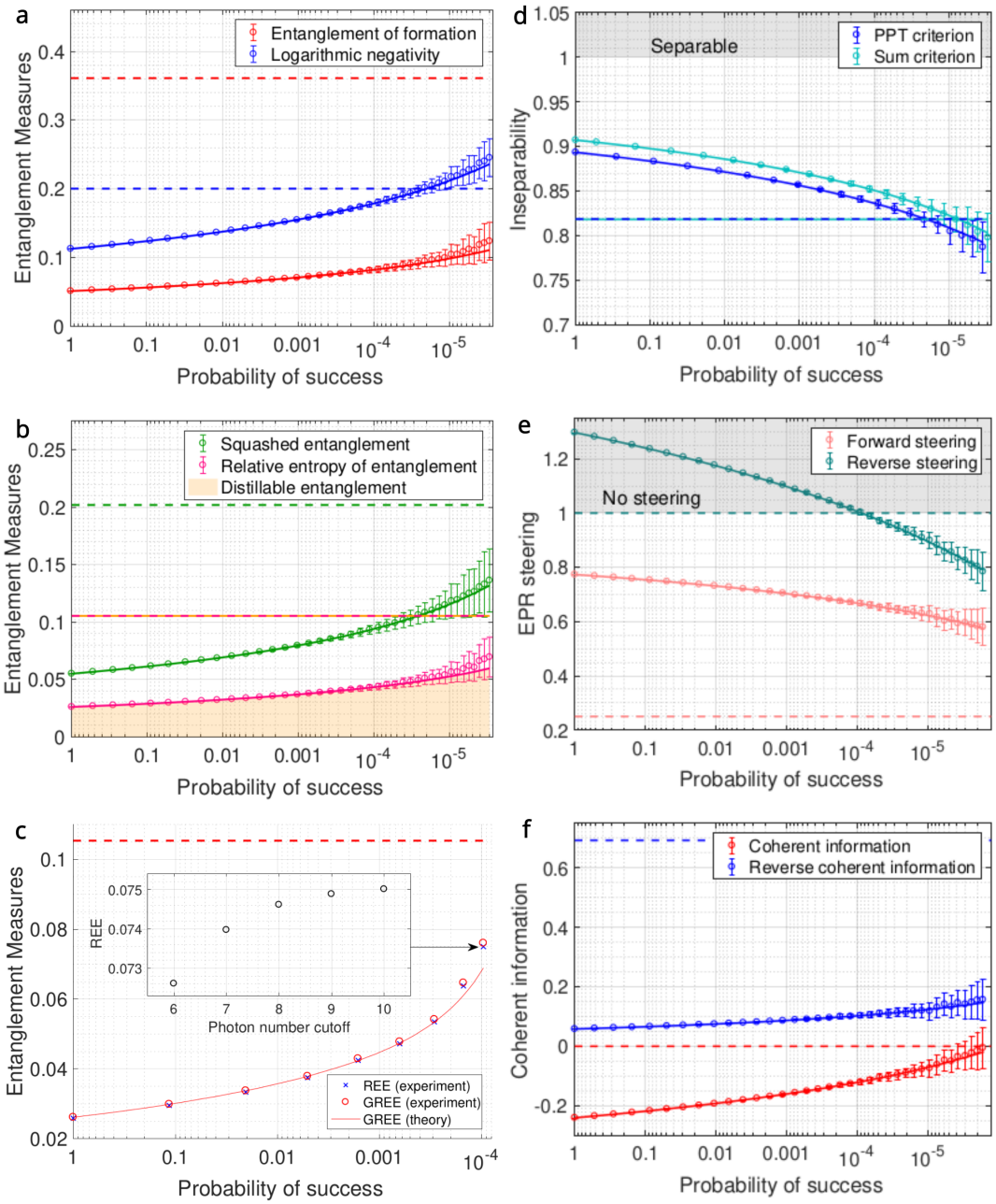


Figure 7.3: No-repeater bound. Data points correspond to averaged experimental results; solid line correspond to theoretical model. Error bars represent individual variations over 100 repeated runs. Dashed line corresponds to the no-repeater bound, with one for each measure. In **b.**, orange shading indicates the region where the value of the relative entropy of entanglement must lie within. The inset in **c.** shows the values of the relative entropy of entanglement as the truncation of the density matrix is varied.

7.4 No-repeater bound for entanglement measures

As a by-product of the analysis in the previous section, we discovered that logarithmic negativity is not sufficient in resolving the question of whether distillable entanglement has increased. That is quite understandable and suggests no fault of the logarithmic negativity. However, in this section we will demonstrate that certain problems arise if logarithmic negativity — as opposed to other entanglement measures — is used to analyse the experiment.

Chrzanowski *et al.* [34] have shown that noiseless amplification increases the logarithmic negativity of the state to the extent that it can become greater than the logarithmic negativity of a maximally entangled state sent through the same optical loss, i.e., that of the following "Choi state":

$$\lim_{\lambda \to 1} BS(T) \left| TMSV(\lambda) \right\rangle \left| 0 \right\rangle , \tag{7.19}$$

where T is the transmissivity of the given optical channel. In the context of quantum repeaters, this is known as the "no-repeater bound" [106], as it represents the maximum entanglement that can be transmitted through the channel in a point-to-point fashion and can only be surpassed by using a quantum repeater.

We observed that logarithmic negativity is the only entanglement measure to cross this bound (Fig. 7.3a, b). Optical loss set to 90 percent. Neither entanglement of formation, relative entropy of entanglement, or squashed entanglement was found to cross the bound. And although inseparability measures and a steering measure do cross it (Fig. 7.3 d, e, f), these are not formal measures of entanglement and carry less importance.

The entanglement measures which do not cross the bound suggest — contrary to the logarithmic negativity — that the limit of point-to-point transmission of entanglement has yet to be reached. The implication of this observation is therefore that analysing the experiment with only logarithmic negativity could potentially result in incorrect interpretations.

Incidentally, the situation above realises what we described earlier as the "disagreement" between entanglement measures; for the logarithmic negativity disagrees with the other measures as to whether the noiselessly amplified entangled state possesses more or less entanglement compared to the corresponding Choi state.

For simplicity, the evaluation of the relative entropy of entanglement in Fig. 7.3b was carried out by approximating it with the Gaussian relative entropy of entanglement. The reason is that the latter can be computed with an analytical formula whereas the former requires a time-consuming numerical method based on semi-definite programming. The approximation is valid in the limit of large optical loss which is the situation here (Fig. 7.3c).

The bounding of the distillable entanglement in the previous section using the relative entropy of entanglement was carried out using the semi-definite program and not the Gaussian approximation.

7.5 Implications for quantum communication

The method of estimating the distillable entanglement using the relative entropy of entanglement and the reverse coherent information has been shown to yield fruitful new insights into the distillation of two-mode-squeezed-vacuum states with noiseless amplification. It

appears possible to generalise this technique to situations of broader interest in quantum communication.

The no-repeater bound on the cryptographic-key rate obtained by Pirandola *et al.* is related to the distillable entanglement, providing a method for certifying quantum repeaters: the bound is equal to the maximum rate of key transfer for point-to-point quantum communication [106]. The bound however is only known analytically for simple cases like the lossy channel, and, for instance, when there is thermal noise in the communication channel then the bound is no longer exact. It can only be estimated by other quantities that provide upper and lower estimates; these quantities are precisely the relative entropy of entanglement and the reverse coherent information.

Chapter 8

A high fidelity squeezing gate

Summary:

A method for implementing noiseless amplification in a squeezing gate is demonstrated, and a marked increase in fidelity of gate operations over previous implementations is observed.

8.1 The squeezing unitary

The overwhelming majority of research work on quantum squeezing concerns the question of producing squeezed vacuum states; this effort is due in large part to the important role which squeezed states play in gravitational-wave detectors [7]. It is important to recall, however, that quantum squeezing is in general a unitary operation $\hat{S}(\zeta)$ that can act on arbitrary quantum states (Eq. 2.20), with the specific case of its action on vacuum states leading to the squeezed vacuum $\hat{S}(\zeta)\,|0\rangle$. The squeeezing operation functions primarily as a fundamental quantum gate in a general-purpose quantum computer [47].

While every physical system that can generate squeezed vacuum states will also act as a squeezing unitary when supplied with non-trivial input states, they are not always designed for this purpose. Optical parametric amplifiers, for instance, requires optical resonators in order to strengthen the non-linear interaction, which results in high optical loss, frequency-filtering effects, as well as difficulties in controlling the relative phases of the operation.

The measurement-based squeezing gate of Yoshikawa *et al.* [110] circumvents these technical difficulties by interacting the input state with an ancillary squeezed vacuum state at an *external* location using only linear optical operations. In this way, the input state will not see all the mess that is happening inside the device used to generate squeezing, whatever that device might be. Nevertheless, there is a drawback with using the measurement-based scheme, which is the creation of a new mechanism of decoherence based on how much squeezing is supplied— an infinitely-squeezed ancillary state is necessary for the ideal operation of the measurement-based squeezing gate.

In this Chapter, we report a method for suppressing this decoherence using noiseless amplification. It is demonstrated by experiment that gate fidelities are enhanced when the device acts on coherent input states.

8.2 Measurement-based squeezing gate

Yoshikawa *et al.* describes the measurement-based squeezing gate as follows: the input state interferes with an ancillary squeezed vacuum state on a variable beam splitter with transmissivity T. One output port is monitored with a homodyne detector and the observed outcomes are used to displace the other beam. This process results in the following transformation of the amplitude and phase quadratures:

$$\begin{aligned} \hat{x}_{out} &= \sqrt{T}\hat{x}_{in} + \sqrt{1-T}\hat{x}_0 e^{-r}, \\ \hat{p}_{out} &= \frac{1}{\sqrt{T}}\hat{p}_{in}, \end{aligned} \tag{8.1}$$

where $e^{-r}\hat{x}_0$ is the amplitude quadrature of the squeezed vacuum state. The transformation has been written, without loss of generality, only for the case when the squeezing occurs in the amplitude quadrature. We can choose which quadrature to squeeze in by simply varying the phases of the beams.

By comparing the equations above with that of the ideal squeezing operation which transforms the input state as:

$$\begin{aligned} \hat{x}_{out} &= \sqrt{T}\hat{x}_{in}, \\ \hat{p}_{out} &= \frac{1}{\sqrt{T}}\hat{p}_{in}, \end{aligned} \tag{8.2}$$

we see an issue with the measurement-based implementation: the two expressions coincide only in the limit when r tends to infinity. In other words, the measurement-based squeezing gate implements an ideal squeezing operation only when the ancillary state is infinitely squeezed.

This leads to two problems. First, Eq. 8.1 implies that there is an upper limit on how much the measurement-based squeezing gate can squeeze— only as much as the ancillary state. For the variance of $\hat{x}_{out}$ is bounded from below by

$$\begin{aligned} v_{out} &= Tv_{in} + (1-T)v_0 e^{-2r} \\ &= T + (1-T)e^{-2r} \\ &= e^{-2r} + T(1-e^{-2r}) \\ &\geq e^{-2r}, \end{aligned}$$

which is the degree of squeezing of the ancillary state. Second, although the output state of an ideal squeezing operation attains equality in Heisenberg's uncertainty principle provided that the input state does, the extra term of Eq. 8.1 spoils this so that the measurement-based squeezing gate will produce an output state that does not reach Heisenberg's limit. In other words, the gate causes the quantum state to decohere and transform into a mixed quantum state.

Both problems could be solved if only r could be made very large. But despite being allowed to go to infinity, the value of r is in general not very large: the best optical squeezing experiments achieved 15 dB of noise suppression below vacuum, corresponding to the value of $r = 1.6$ [111].

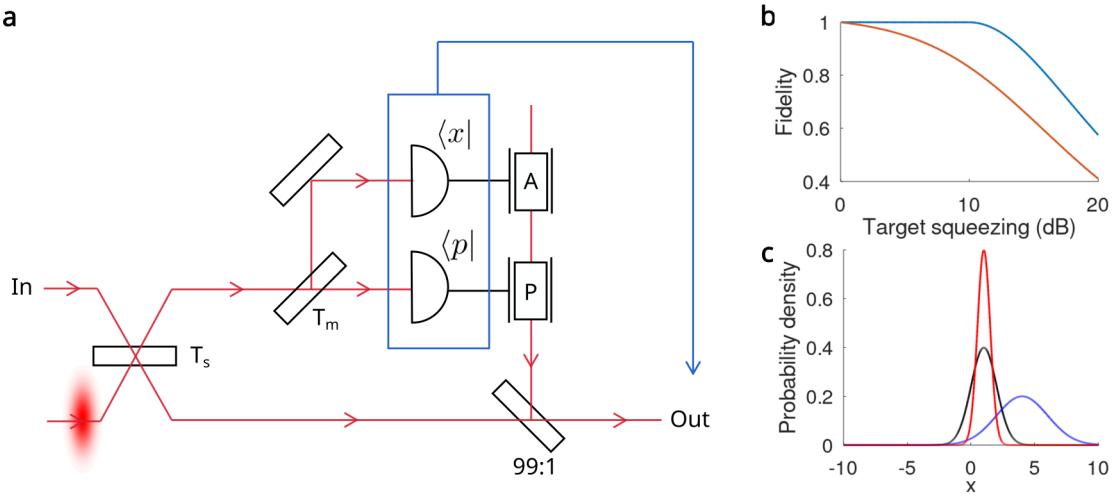


Figure 8.1: Implementation. a. Optical connections for the squeezing gate experiment. Blue box indicates postselection of the output state based on the outcomes of the measurements. T_m,T_S: beam splitter transmittivities. **b.** Fidelity of the output state relative to pure squeezing unitary corresponding to a given target squeezing. Orange line corresponds to the ordinary measurement-based squeezing gate, and the blue line corresponds to squeezing gate with noiseless amplification. It is assumed that the ancillary state has 10 dB of squeezing, with no additional experimental inefficiencies. **c.** Illustration of noiseless amplification by postselection. Black distribution: initial state. Blue distribution: after postselection. Red distribution: after further multiplication by a suitable scalar value.

8.3 Squeezing gate with noiseless amplification

In this section we describe how to implement noiseless amplification within the squeezing gate and its effect. Since all relevant quantum states are Gaussian, they can be characterised by the mean and the covariance matrix, and therefore we seek the ideal squeezing operation:

$$\begin{bmatrix} x_{in} \\ p_{in} \end{bmatrix}, \begin{bmatrix} 1 & 0 \\ 0 & 1 \end{bmatrix} \to \begin{bmatrix} e^{-r} x_{in} \\ e^{r} p_{in} \end{bmatrix}, \begin{bmatrix} e^{-2r} & 0 \\ 0 & e^{2r} \end{bmatrix}. \tag{8.3}$$

The apparatus is shown in Fig. 8.1. In addition to the setup of Yoshikawa *et al.*, we have one additional homodyne detector measuring the amplitude quadrature, and a feedforward also from this detector to the other beam. There are now two beam splitters, with transmissivity T_s which controls the coupling to the squeezed ancilla and with transmissivity T_m which controls the weighting of the measurements. We proceed as follows.

Step 1: Conditional state.

We begin by observing that the measurement will project the propagating mode down to a conditional state that is a displaced squeezed state. The precise state at this point does not matter very much, all that we need to know is that it has a displacement that must depend linearly on the input displacement and the measurement outcome. Furthermore, the covariance matrix of the conditional state must represent a pure squeezed state.

Step 2: Fixing T_m.

For simplicity we put $T_m \approx 1$ (e.g., $T_m = 0.99$). This means that we make only

a weak measurement on the amplitude quadrature and predominantly measure the phase quadrature. This choice for T_m might appear arbitrary and indeed it is— for we could have used any other value and the only thing we will have to do is to adjust T_s accordingly; ultimately, it is T_s which controls the degree of squeezing introduced by the gate.

Step 3: Fixing T_s.

Since the measurement is essentially a homodyne measurement on the phase quadrature, this simplifies the situation for we can compute the conditional variance of the phase quadrature of the propagating state straightforwardly (see Appendix for the general method), which turns out to be

$$v_p = T_s + (1 - T_s)e^{2r}. \tag{8.4}$$

Since the conditional state is pure, the variance of the amplitude quadrature is just the inverse of this quantity:

$$v_x = \frac{1}{T_s + (1 - T_s)e^{2r}}, \tag{8.5}$$

and by adjusting T_s we can make this quantity to be anything between 1 and e^{-2r}. If the target squeezing is less than resource squeezing $r_0 \leq r$, we will choose T_s such that $v_x = e^{-2r_0}$; otherwise, we make it close to 1 so that $v_x \approx e^{-2r}$.

Step 4: Removing the random displacements.

Although the conditional states at this point share the same covariance matrix, its displacement is all over the place because it depends (linearly) on the outcome of the measurements. However, these random displacements are known and therefore easy to remove through the feedforward, with the gain factor ϕ_0 of the feedforward given by the coefficient associated with the linear relationship. We thus arrive at a quantum state at the output of the gate which: (1) does not depend on the measurement outcomes, (2) has the desired covariance matrix, and (3) has a displacement proportional to (but smaller than) the input state.

Step 5: Noiseless amplification.

The final step — and also the most delicate by far — is to amplify the displacement of the quantum state we have above without disturbing its covariance matrix; i.e., noiseless amplification of the output displacement. We now describe how this can be done through postselection and feedforward. Without loss of generality, we consider the amplitude quadrature only; the phase quadrature follows by a symmetrical argument.

We first observe that the measurement outcomes at the homodyne detector are distributed normally with a probability density

$$p(x) = \frac{1}{\sigma\sqrt{2\pi}} \exp\left(\frac{(x-\mu)^2}{\sigma^2}\right), \tag{8.6}$$

where μ and σ^2 denote the mean and variance which can be read off from the diagram

in Fig. 8.1a:

$$\mu = \sqrt{1-T_s}\sqrt{1-T_m}x_{in}, \tag{8.7}$$
$$\sigma^2 = (1-T_m)((1-T_s)+T_s e^{-2r})+T_m. \tag{8.8}$$

This distribution is represented by the black curve in Fig. 8.1c. The specific forms of these expressions are not very important; it is only necessary to observe that the mean is proportional to the input displacement, while the variance is independent of the input state.

Postselecting these measurement outcomes by the Gaussian filter,

$$f(x) = \exp\left(\left(\frac{1}{\sigma^2}-\frac{1}{g^2}\right)x^2\right), \tag{8.9}$$

we transform the distribution as $f(x) \to f(x)p(x)$. But since both functions are Gaussian, their product must still represent a normal distribution which is found to have mean and variance:

$$\tilde{\mu} = \frac{g^2\mu}{\sigma^2}, \tag{8.10}$$
$$\tilde{\sigma}^2 = g^2. \tag{8.11}$$

This distribution is represented by the blue curve in Fig. 8.1c.

If the results above are further multiplied by the number ϵ/g (where ϵ can be any real number), we shall arrive at a distribution with mean $\epsilon g\mu/\sigma^2$ and variance ϵ^2. What is so special about it? By making ϵ very small going to zero, the resulting distribution becomes arbitrarily narrow, and by making g very large to compensate we get a mean that is proportional to the input displacement with arbitrary proportionality constant. To illustrate the striking properties of this situation, we can consider the special example when $g = \sigma^2/\epsilon$ in which case the transformations above produce a distribution with the same mean as what we started out with but having its variance reduced by a factor which scales as $1/g^2$. This is represented by the red curve.

To operate our squeezing gate, we will instead put g such that

$$\frac{\epsilon g}{\sigma^2}\sqrt{1-T_m}\sqrt{1-T_s} = e^{-r}-(1-T_m)(1-T_s), \tag{8.12}$$

which is chosen so that if we feedforward these results, we will find that the displacement of the output state is brought up to the precisely the value $e^{-r}x_{in}$. The displacement is achieved by adjusting the feedforward gain to $\phi = \phi_0 + \epsilon/g$, so that the feedforward comprises of two parts: with the first part ϕ_0 removing the random displacements (in step 4) and the second part ϵ/g attenuating the measurements outcomes (after postselection); Eq. 8.12 shows that ϵ/g scales as ϵ^2 which goes to zero as we let ϵ go to zero.

Since neither the postselection nor the fixed displacement perturbs the covariance matrix, we are therefore done. The output state of the gate at this point is precisely the right-hand-side of Eq. 8.3.

The above analysis is of course more hand-wavy than it is rigorous (not to say lengthy), but it captures the essential physical insights behind how the squeezing gate with noiseless

amplification works. An alternative and more compact mathematical theory of the system has been given in [112], based on the solution of a system of nonlinear equations. Although there is fundamentally nothing wrong with such a mathematical theory, it yields little insight into the physical process which occurs inside the gate.

Why should we care about physical insight if the mathematical theory works? Because we will encounter a similar physical system in Chapter 9 and another in 10, and although the equations describing these systems may change considerably so that they must be re-derived in their entirety, the underlying physical processes are the same so that we shall be able to deduce the basic properties of those systems without carrying out any detailed calculations.

To complete the discussion, we point out the most important result to come out of the analysis above: noiseless amplification makes possible a gate fidelity of F = 1 (on the set of coherent states) for any target squeezing up to the given ancillary resource (blue line in Fig. 8.1b). This contrasts with the deterministic scheme of Yoshikawa *et al.* which will achieve F = 1 only for the trivial case of no squeezing $r_0 = 0$ (orange line in Fig. 8.1b). It must be emphasised that the gate delivers a maximum amount of squeezing determined by the resource squeezing, so that above this point the fidelity will begin to decrease; it will remain nonetheless above that of the deterministic scheme.

8.4 Experimental results

We carried out an implementation of this scheme on our experiment system [112]. One OPA is used, with its optical path re-routed to bypass the entangling beam splitter to interact directly with the signal beam. The variable beam splitter interaction is implemented using a polarising beam splitter, a half-wave plate, and another polarising beam splitter in that order, as in Yoshikawa *et al.* [110].

We observed the system to have higher fidelities than the deterministic scheme (Fig. 8.2a, b). Assuming 6 dB of squeezing ancilla with no experimental imperfections, the orange line gives the fidelity of the deterministic scheme, while the blue line is the upper bound on the fidelity of our device. This is the level of squeezing used in our experiments.

We further observed that the increase in fidelity occurs at any value of target squeezing. For instance, at 2.3 dB we found a small increase from 96 percent to 98.5 percvent, a value very close to the maximum allowable fidelity of 100 percent and suggests an almost perfect squeezing operation. In fact, this value cannot be achieved using the deterministic scheme with the best possible squeezing resource [111] of 15 dB assuming that the same detection losses are present (and no other experimental efficiencies). If the stronger assumption is made that there is no detection loss, then the value of the necessary squeezing is adjusted to 10.5 dB.

The fidelity increases also when the target squeezing is above the ancillary squeezing. With a 10 dB target, we found an increase from 68 percent to 76 percent. This is lower than the numbers above for the 2.3 dB target, on account of the maximum limit the device can squeeze which is still equal to the ancillary squeezing. This we cannot do anything about with noiseless amplification.

We also observed that the system acts in the same way regardless of the magnitude or phase of the coherent state; i.e., it is phase insensitive. Fig. 8.2c illustrates the reconstructions of the Wigner functions of the squeezed output states and the various corresponding input coherent states, overlaid on top of the phase space diagram of the squeezing operation.

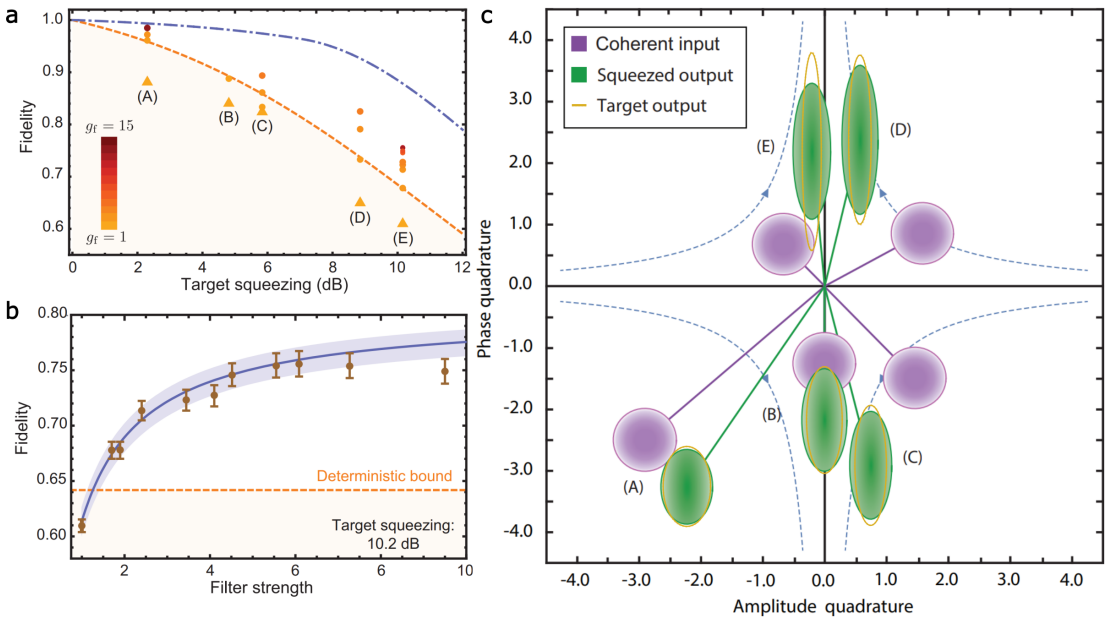


Figure 8.2: Experimental results for the squeezing gate. a. Fidelity of the squeezing gate relative to a target squeezing operation for various noiseless amplification gain factors. Orange line corresponds to the theoretical fidelity of an ordinary measurement-based squeezing gate, blue line corresponds to the maximum obtainable fidelity of our implementation of the squeezing gate; both lines assume no experimental imperfections and only finite squeezing corresponding to our squeezed resource. Each vertical column represents a different input coherent state, labelled (A)-(E), with various gain factors for the noiseless amplification within each column. **b** Fidelity with respect to a target squeezing operation of 10.2 dB. Dashed line corresponds to the upper limit on fidelity of an ordinary measurement-based squeezing gate with 6 dB pure ancillary squeezing and no experimental imperfections. **c.** Wigner functions for the five different coherent input states (A)-(E) coloured in purple. Green elongated Wigner functions correspond to the output state, and the orange lines correspond to the target operation. The broken blue lines indicate the phase space trajectories of a mechanical system when its Hamiltonian is given by the squeezing Hamiltonian.

It must be emphasised that our implementation uses only one homodyne detection (measuring the phase quadrature), which is easier to carry out by a considerable margin. According to theory, this is not the optimal configuration because we lose the opportunity to perform noiseless amplification in the other quadrature. Nevertheless, the loss in the achievable fidelity appears to be sufficiently small (compare Fig. 8.2a with Fig. 8.1b).

8.5 Universality and gates of higher order

We have shown how noiseless amplification increases the fidelity of the measurement-based squeezing gate on the set of coherent input states. However, the question of universality remains open. Blandino *et al.* have analysed a similar situation and concluded that there appears to be hope for generalising the operation to more general input quantum states, although the operation may no longer be the same as what it would appear to be on the set of coherent input states. We will discuss this line of research in further detail in Chapters 9 and 10.

In another direction, it would be interesting to consider how the present setup should

be modified for a higher-order unitary such as the cubic phase gate [113]. This is a particularly important issue because in contrast to the squeezing unitary, higher order unitaries are not known (at least in the case of optics) to have implementations that are free of measurements due to the lack of strong optical non-linear interactions. This question is also non-trivial because the measurement outcomes are no longer distributed normally, and the feedforward is non-linear.

Chapter 9

Quantum teleportation with noiseless amplification

Summary:

Noiseless amplification is embedded into quantum teleportation, leading to a marked increase in fidelity.

9.1 When teleportation fails

In fictional stories, teleportation can often fail with dramatic and unfortunate consequences. While there are no teleporters in real life yet so that there is little to be said about this specific subject, there *are* several interesting things we can say about the analogous technique known as "quantum teleportation", which is a way of transporting quantum states between physical systems.

Now I must be clear: the sort of issues that I would like to discuss are not technical failure, such as when the power to the lab is cut or when there is an earthquake. Instead, I wish to analyse the question that is relevant to physics: is it necessarily the case — in principle at least — that every quantum state can be teleported without suffering some form of undesired alteration in the process? Interestingly, this statement turns out to be false in the most general case.

The condition that determines whether a quantum system can be teleported exactly is very simple. All that is required is that the quantum state of the system can be expressed as a superposition[1] over a finite set of independent quantum states [114],

$$|\psi\rangle = a_0 |0\rangle + a_1 |1\rangle + \cdots a_n |n\rangle . \tag{9.1}$$

For instance, this includes the "qubit" with $n = 1$, such as the polarisation state of photons [115], electronic states of atoms and trapped ions [116, 117, 118], and many more [119, 120, 121]; as well as systems formed by taking the composition of multiple qubits [122, 123] which will have $n > 1$. Although experimental implementations become more difficult as the number of states increases, in principle all these quantum systems can be teleported exactly.

There is, however, one kind of quantum states which does not fit into the description

[1] The case of mixed states is the same in principle.

above. It is *fundamentally impossible* to teleport exactly quantum states of the form,

$$|\psi\rangle = \sum_{k=0}^{\infty} a_k |k\rangle , \tag{9.2}$$

if the sum extends to infinity, so that the states can only be transported in an approximate fashion [124]. Several physical systems are described by such quantum states, and the reader will no doubt be able to guess one of them — a beam of light [125, 126], with the $|k\rangle$'s denoting Fock states. In addition, the collective spin state of atomic ensembles [127, 128], microwave photon states [129], and phonon states in optomechanical oscillators all fall under this category. For ease of reference, this sort of quantum teleportation is colloquially referred to as "continuous-variable" quantum teleportation.

The continuous-variable quantum teleporter produces two kinds of effects on the quantum states that go into it: the quantum state may be (1) partly lost to the surroundings [130], or (2) disfigured by thermal noise [124]. In general, the effect will be a combination of the two, varying with the internal parameters of the teleporter. In any case, quantum teleportation will lead to decoherence of the quantum state, as observed even in the most well-isolated experiments [126].

In this chapter, we report the suppression of decoherence in an optical quantum teleporter using noiseless amplification and observe a marked increase in fidelity when teleporting coherent states of light. The method generalises that used in experiments with the measurement-based squeezing gate. It has been the purpose of this section to indicate only the motivation for the upcoming experiments, so I should now like to explain in greater detail how exactly quantum teleportation works and in what ways noiseless amplification is found to modify its basic properties.

9.2 Quantum teleportation

Bennett *et al.* [114] gave the method for quantum teleportation of qubits as follows. Let there be a qubit,

$$|\psi\rangle = a |0\rangle + b |1\rangle , \tag{9.3}$$

and an entangled state,

$$|\phi_0\rangle = \frac{1}{\sqrt{2}}(|00\rangle + |11\rangle); \tag{9.4}$$

then the composition of the two systems is made up of three modes,

$$|\psi\rangle \otimes |\phi_0\rangle = (a |0\rangle + b |1\rangle) \otimes \frac{1}{\sqrt{2}}(|00\rangle + |11\rangle), \tag{9.5}$$

with the qubit located in the first mode. The quantum state of this system can be rewritten as

$$\begin{aligned}|\psi\rangle \otimes |\phi_0\rangle = &\frac{1}{4\sqrt{2}}(|00\rangle + |11\rangle) \otimes (a\,|0\rangle + b\,|1\rangle) \\ &+ \frac{1}{4\sqrt{2}}(|00\rangle - |11\rangle) \otimes (a\,|0\rangle - b\,|1\rangle) \\ &+ \frac{1}{4\sqrt{2}}(|01\rangle + |10\rangle) \otimes (a\,|1\rangle + b\,|0\rangle) \\ &+ \frac{1}{4\sqrt{2}}(|01\rangle - |10\rangle) \otimes (a\,|1\rangle - b\,|0\rangle),\end{aligned}$$

with the first two modes in entangled states corresponding to the four "Bell states" and the third mode looking almost like the input qubit but differing by some unitary transformation in each case. When a Bell-state measurement is performed on the first two modes, the system is thereafter projected into precisely one of the four cases above, so that it suffices to adjust the third mode with the corresponding unitary transformation that either modifies the relative phases of the $|0\rangle$ and $|1\rangle$ states or swaps them around. In this way, the quantum state $|\psi\rangle$ is transported from mode 1 to mode 3 with its components preserved.

Likewise, a similar process can be carried out if the input state is a superposition of any finite number of states (Eq. 9.1), although we require, in this instance, an entangled state of the form $\sum_{k=0}^{n} |k\rangle\,|k\rangle$ as well as a suitable generalisation of the Bell-state measurements. All the same, the fundamental principles which we have described above remain unaltered.

When the same method is turned to light, however, it breaks down. Generalising the argument above, we now require an entangled state of the form $\sum_{k=0}^{\infty} |k\rangle\,|k\rangle$ which does not exist! This is the well-known "EPR state" [8] and is not a physical state because the expression cannot be normalised. Braunstein and Kimble [124] have shown that a modification of the teleportation procedure would work using finite-energy approximations of the EPR state (the two-mode-squeezed-vacuum states, Eq. 2.14) as the entanglement resource instead; however, the amplitudes of TMSV states decay exponentially so that they correspond to the EPR state only in the limit when the entanglement parameter λ approaches 1 — a limit that cannot be reached physically. This is the basis for the assertion that quantum states of the form Eq. 9.2 cannot be teleported exactly.

To obtain a quantitative analysis of the quantum teleporter, we begin by letting $\hat{a}_{in} = \hat{x}_{in} + i\hat{p}_{in}$ and $\hat{a}_{out} = \hat{x}_{out} + i\hat{p}_{out}$ denote the input and output quantum states of the continuous-variable quantum teleporter. Suppose that the teleporter is supplied with a TMSV state represented by the pair of quadratures $(\hat{x}_A, \hat{p}_A)$ and $(\hat{x}_B, \hat{p}_B)$ satisfying the relations (Eq. 2.15),

$$\hat{x}_A - \hat{x}_B = \hat{x}_0 e^{-r}\sqrt{2}, \tag{9.6}$$

$$\hat{p}_A + \hat{p}_B = \hat{p}_0 e^{-r}\sqrt{2}, \tag{9.7}$$

where $\hat{x}_0$ and $\hat{p}_0$ are quadrature operators of vacuum modes, and r related to the entanglement parameter by $\lambda = \tanh r$. We further let joint measurements (analogous to the

Bell-state measurements for qubits) be made by homodyning the following observables:

$$\hat{x}_M = \frac{1}{\sqrt{2}}(\hat{x}_{in} - \hat{x}_A),$$
$$\hat{p}_M = \frac{1}{\sqrt{2}}(\hat{p}_{in} + \hat{p}_A), \tag{9.8}$$

which can be accomplished by interfering the input beam with one mode of the entangled state on a balanced beam splitter and monitoring the output ports with homodyne detectors. We thus arrive at the general transformation effected on the input state by the quantum teleporter, with the output state obtained by acting displacement operations on the other mode of the entangled state based on the outcomes of the joint measurements:

$$\hat{x}_{out} = \hat{x}_B + \phi\hat{x}_M, \tag{9.9}$$
$$\hat{p}_{out} = \hat{p}_B + \phi\hat{p}_M, \tag{9.10}$$

where ϕ is a real number called the "feedforward gain".

It may be seen from the description above that much of the procedure is analogous — though not the same — to that for qubits, except for the appearance of two additional parameters internal to the quantum teleporter: the feedforward gain ϕ and the entanglement parameter λ. These parameters are very important because they completely determine the behavior of the teleporter.

Two special cases illustrate this point: (1) When $\phi = \sqrt{2}$, the quantum teleporter implements a transformation corresponding to "additive thermal noise" [124]:

$$\hat{x}_{out} = \hat{x}_{in} - \hat{x}_0 e^{-r}\sqrt{2}, \tag{9.11}$$
$$\hat{p}_{out} = \hat{p}_{out} + \hat{p}_0 e^{-r}\sqrt{2}, \tag{9.12}$$

where $\hat{x}_0$ and $\hat{p}_0$ denote quadrature operators of the vacuum, and (2) when $\phi = \lambda\sqrt{2}$, the quantum teleporter is equivalent to a beam splitter (i.e., optical loss) [130]:

$$\hat{a}_{out} = \sqrt{\lambda}\hat{a}_{in} + \sqrt{1-\lambda^2}\hat{a}_0, \tag{9.13}$$

where $\hat{a}_0$ denotes an auxiliary vacuum mode. In other words, the effect of the quantum teleporter is to inject a fixed number of thermal photons to the state in the first case, while in the second case it throws away a fraction (equal to $1 - \lambda^2$) of the photons in the input state. In either case, the result is decoherence; only in the limit $\lambda \to 1$ do the two expressions reduce to the ideal transformation $\hat{a}_{out} = \hat{a}_{in}$.

The behavior of the teleporter, in general, can be divided into two regimes: if $\phi > \sqrt{2}$, then the output state has a greater displacement compared to the input state so that the teleporter is *amplifying*; and if $\phi < \sqrt{2}$ then the output has a smaller displacement than the input so that the teleporter is *attenuating*. The point of operation $\phi = \sqrt{2}$ is called "unity-gain", with the output state possessing the same displacement as the input; the point $\phi = \lambda\sqrt{2}$ is sometimes called "gain-tuning" and represents a special case where the teleporter passively attenuates without injecting any thermal photons.

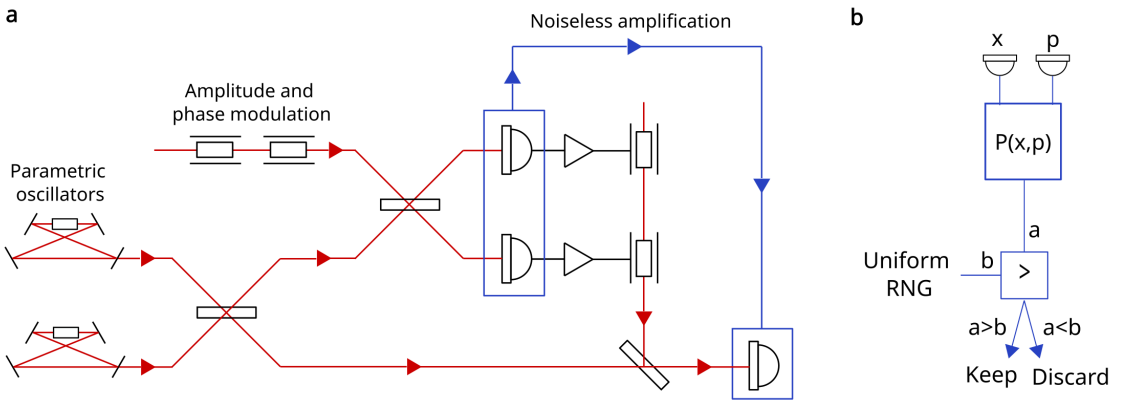


Figure 9.1: Experimental device. a. Schematic of the optical quantum teleporter. Noiseless amplification is implemented by postselecting the output of the teleporter based on the outcomes of the joint measurement. **b.** Postselection algorithm. The function P is the inverted Gaussian function in Eq. 3.4. The random number generator (RNG) outputs a real number that is uniformly distributed between 0 and 1.

9.3 Experimental device and basic properties

Fig. 9.1 a shows a schematic of our experimental setup with an optical quantum teleporter modified by postselection. In brief: the setup consists of a source of two-mode-squeezed-vaccuum states with one mode coupled to a coherent input state through joint measurements, and the other mode displaced by an electro-optic feedforward based on the outcomes of the joint measurements; the output state is postselected (Fig. 9.1b) based on the outcomes of the joint measurements with acceptance probabilities proportional to the Gaussian filter (Eq. 3.4).

As usual, the postselection procedure is parameterised by a single parameter g which we will refer to as the "noiseless gain". It will become clear later that this parameter is responsible for noiseless amplification in the quantum teleporter, but for now we will simply treat it as a third internal parameter of the teleporter, whatever its physical meaning might be.

If the input state is a Gaussian state, then the output state must also be Gaussian since the postselection filter is Gaussian. Supposing that the input is a coherent state with complex amplitude of α_{in}, then the corresponding output state may be found — using the method outlined in Appendix A — to possess a complex amplitude and variance of the form,

$$\begin{aligned} \alpha_{out} &= \alpha_{in} f(\lambda, \phi, g), \\ v_{out} &= h(\lambda, \phi, g), \end{aligned} \tag{9.14}$$

where f and h are functions of the internal parameters of the teleporter. The specific form of these functions is not important; however, it is important to observe that α_{out} depends linearly on α_{in}. The variance v_{out} is identical for both quadratures.

We now proceed to fix the free parameters of this system. We begin by letting λ be fixed, positive, but otherwise arbitrary— in other words, we allow any level of entanglement. We next impose the well-known "unity-gain condition" [124, 125]:

$$\alpha_{out} = \alpha_{in}, \tag{9.15}$$

which is equivalent to the constraint $f(\lambda, \phi, g) = 1$ and can be expressed explicitly in terms of the parameters as:

$$\phi = \sqrt{2}e^{-r}(\sinh r + \frac{1}{g^2}\cosh r). \tag{9.16}$$

In this scheme, therefore, the feedforward gain ϕ varies with g. However, the unity-gain condition remains independent of the input coherent state, so that consequently we do not need to know what the input state is in order to configure the quantum teleporter. This is an important property of the ordinary quantum teleporter that is inherited by our system.

This leaves us with the parameter g. In order to get noiseless amplification, we know that g must be greater than 1 (Eq. 3.4). On the other hand, we also find from Eq. 9.14 that the output state does not correspond to any physically sensible state when g is above a certain value g_{max}; this occurs when $v_{out} < 1$ (for both quadratures) and corresponds to the expression:

$$g_{max} = \sqrt{\frac{c_{11}}{c_{11} - 1}}, \tag{9.17}$$

where c_{11} is the variance of the homodyne measurements. In the absence of experimental imperfections, this expression reduces to just $g_{max} = 1/\lambda$.

With the teleporter configured as above, the output state has a fixed complex amplitude $\alpha_{out} = \alpha_{in}$ and a variance that depends only on g, with g taking values between 1 and g_{max}. When $g = 1$, we see from Eq. 3.4 that there is effectively no postselection so that the system reduces to ordinary quantum teleportation.

Fig. 9.2 shows the dependence of the output state on the parameter g. As g approaches g_{max}, the variance of the output state approaches the quantum limit $v_{out} = 1$ and therefore a coherent state; furtheremore, the output state has the same displacement as the input state since the unity-gain condition is always satisfied. The fidelity of the teleportation,

$$F = \langle \alpha_{in} | \, \hat{\rho}_{out} \, | \alpha_{in} \rangle = \frac{2}{1 + v_{out}}, \tag{9.18}$$

therefore approaches 1.

It may be observed that according to Eq. 9.16, the feedforward gain reduces from $\sqrt{2}$ to $\lambda\sqrt{2}$ as g goes from 1 to g_{max}. In other words, the feedforward gain ϕ should now be set to the gain-tuning point instead of the normal unity-gain point of $\phi = \sqrt{2}$, in contrast to that of ordinary quantum teleportation. Noiseless amplification will compensate for the attenuation without introducing extra thermal noise.

There is a simple way to see that variation of the parameter g leads to noiseless amplification of the output state. Suppose instead of varying ϕ along with g, we now have it fixed at a value just above $\lambda\sqrt{2}$. When $g = 1$, this corresponds to ordinary quantum teleportation at the gain-tuning point, with the output state given by an attenuated state $|\lambda\alpha\rangle$. However, as g increases to approach g_{max} (while keeping ϕ fixed), we must now end up with the state $|\alpha\rangle$, so that we arrive at the transformation

$$|\lambda\alpha\rangle \rightarrow |\alpha\rangle \tag{9.19}$$

effected by the variation of g. This is precisely noiseless amplification of coherent states (Eq. 2.24).

What physical process in the teleporter brings about this transformation? To answer this question, we observe that the output state $|\psi_{out}\rangle$ for *each run* of the teleporter can

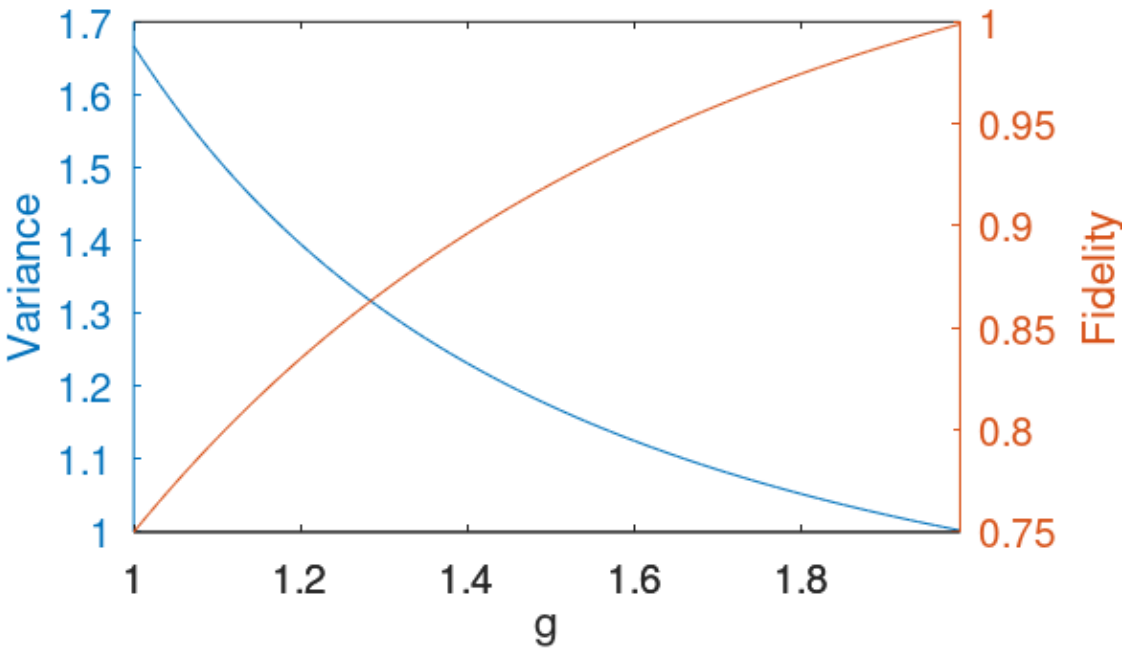


Figure 9.2: Theoretical fidelity. The variance of the output state is given along the left axis and the corresponding fidelity on the right axis. The feedforward gain ϕ varies along with g according to the unity-gain condition (Eq. 9.16). Without loss of generality, the entanglement parameter is set to $\lambda = 0.5$.

be written as:

$$|\psi_{out}\rangle = D(\delta\phi\alpha_M)\,|\lambda\alpha_{in}\rangle\,, \tag{9.20}$$

where $\alpha_M = x_M + ip_M$ is the outcome of the joint measurements (Eq. 9.8) and $\delta\phi = \phi - \lambda\sqrt{2}$ is the differential gain that determines how far above the gain-tuning point we are operating. In ordinary teleportation, the displacements will be random because α_M is not fixed but normally distributed, so that the collective output state is a thermal state; as we saw for the squeezing gate, the effect of postselection is to transform α_M into a distribution increasingly narrow centred at some fixed point (Fig. 8.1c). As a result, the random displacements are transformed by postselection into a fixed displacement that is proportional to that of the input state, since the mean of α_M is proportional to that of the input state, leading to noiseless amplification.

It must be emphasized that quantum teleportation with postselection has been tried before, most notably with the experiments of Bouwmeester *et al.* [115] and that of Fuwa *et al.* [131]. However, these experiments employ the method of postselecting on a specific predetermined outcome, and consequently do not exhibit noiseless amplification.

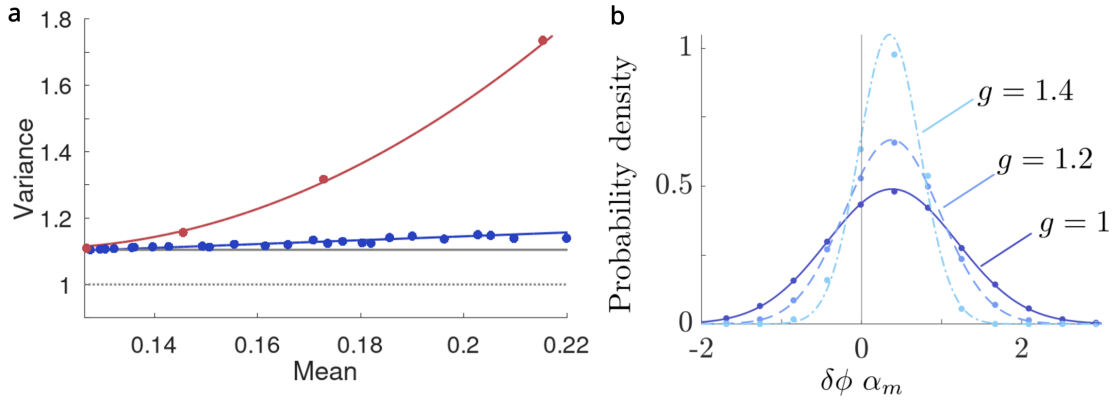


Figure 9.3: Noiseless amplification. a. Measurements of the output state with noiseless amplification (blue trace) and without (red); its mean value and variance (of the amplitude quadrature) are plotted along the horizontal and vertical axes respectively. Input coherent state has a fixed displacement of $\alpha = 0.11$, with the feedforward gain ϕ varied in the red trace and the noiseless gain g varied in the blue trace. **b.** The distribution of feedforward displacements (Eq. 9.20) measured for several values of g.

9.4 Experiments

We observed noiseless amplification of the output state of the teleporter, as shown in Fig. 9.3a. The input state is a fixed coherent state with complex amplitude of about $\alpha = 0.11$. When ϕ is fixed to be just above the gain-tuning point ($\phi = 0.92$, with $\lambda \approx 0.6$), variation of g results in amplification of the mean with barely noticeable change in the variance. If instead we put $g = 1$ (i.e., no postselection) so that the feedforward gain ϕ is varied instead, the same amplification of the mean could be observed but with significantly more thermal noise. We also observed (Fig. 9.3b) that $\delta\phi\alpha_M$ of Eq. 9.20 is a Gaussian distribution that varies with g, with a fixed mean value equal to $(1-\lambda)\alpha_{in}$ and a variance that decreases with increasing g as required.

We observed suppression of thermal decoherence when teleporting the vacuum state with noiseless amplification (Fig. 9.4a-d). The variance of the output state was found to reduce from 1.73 to 1.16 as g increased from 1 to 1.57. The fidelity relative to the input coherent has a simple inverse relationship with the variance (Eq. 9.18), with the results above translating to $F = 0.73$ in absence of noiseless amplification and up to $F = 0.92$ at the highest gain factor (Fig. 9.4e). It is not possible to continue increasing g any further, for the quantum teleporter quickly reaches the point where it breaks, with $g_{max} \approx 1.68$.

We can state with relative confidence that the fidelities with noiseless amplification are greater than that without, for at least two reasons. First, it is necessary for each optical parametric oscillator to deliver about 10 dB of quantum squeezing in order to reach $F = 0.92$ without noiseless amplification, even if we were to assume that no experimental imperfections are present. Inclusion of imperfections will only raise this value further. In contrast, our experiments use only a modest level of about 5 dB. Second, the maximum fidelity of the quantum teleporter without noiseless amplification could be determined by separate deterministic teleportation runs with varying degrees of squeezing which turned out to be approximately $F = 0.8$, markedly lower than the fidelities with noiseless amplification.

Using the same procedure, we also observed suppression of thermal decoherence when

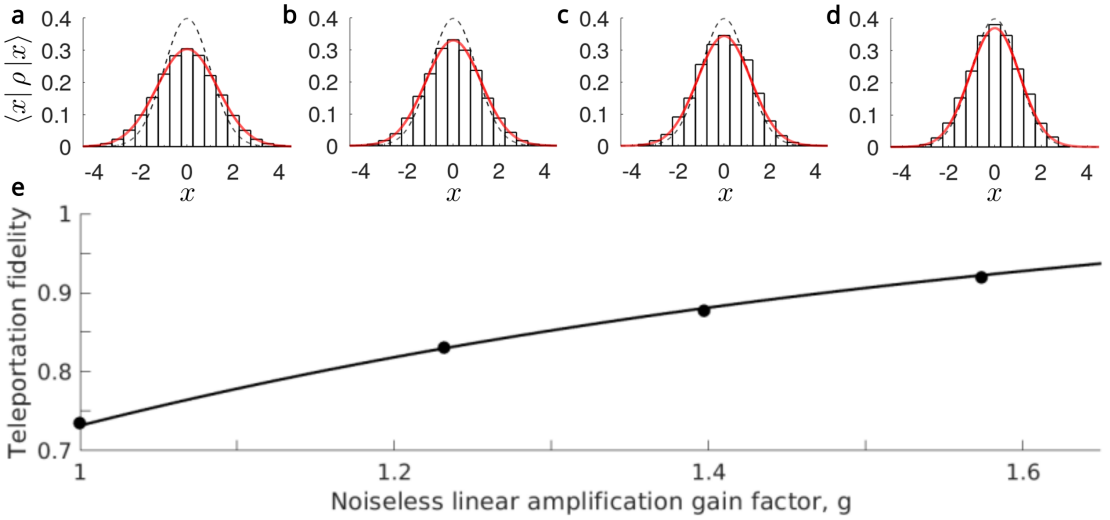


Figure 9.4: Quantum teleportation of the vacuum state. a.-d. Histograms of amplitude homodyne measurements on the teleported state for varying noiseless gain g. Measurements of the phase quadrature give essentially identical results and have been suppressed. Gaussian fits to the data are given by the red curves, while the quantum limit (i.e., vacuum state) is given by the dashed black curves. **e.** Corresponding teleportation fidelities.

teleporting non-trivial coherent states (Fig. 9.5). The input states are chosen to include both displacements in the amplitude and phase quadrature to demonstrate that the process is phase insensitive. Similar fidelities were observed, with a slight decrease ($\approx 5\%$) towards greater displacements on account of the use of a smaller noiseless gain, $g = 1.42$, which is to ensure that noiseless amplification behaves linearly. It is ideally expected that the results should be completely independent of the input coherent state, however noiseless amplification is known to have a finite dynamical range [132].

It must be emphasized that noiseless amplification is probabilistic, which is an unavoidable consequence of the fundamental theorem of quantum amplifiers [16]. This implies that the quantum teleporter is also probabilistic, succeeding only when noiseless amplification does. The probability of success varies with the noiseless gain but is generally between 10^{-5} to 10^{-6} at the highest fidelities. In addition, bounds on the fidelity such as the "classical limit"[125] or the "no-cloning limit"[133] are absent, for its values must now depend also on the probability of success. Evaluation of these quantities remains an open theoretical problem.

9.5 Equivalent quantum operation

We owe very much to Blandino *et. al.* for a theoretical analysis of the effect postselection has on the optical quantum teleporter [134]. Their calculations suggest that the system is equivalent to (Fig. 9.6 inset) a physical noiseless linear amplifier (in the original sense of Lund and Ralph [18]) concatenated with a beam splitter that is coupled to a thermal reservoir.

A prediction of this theory is that postselection with the Gaussian filter can transform the thermal reservoir in this model to a vacuum state, so that, consequently, coherent states can be teleported with less thermal decoherence. Our experimental observations

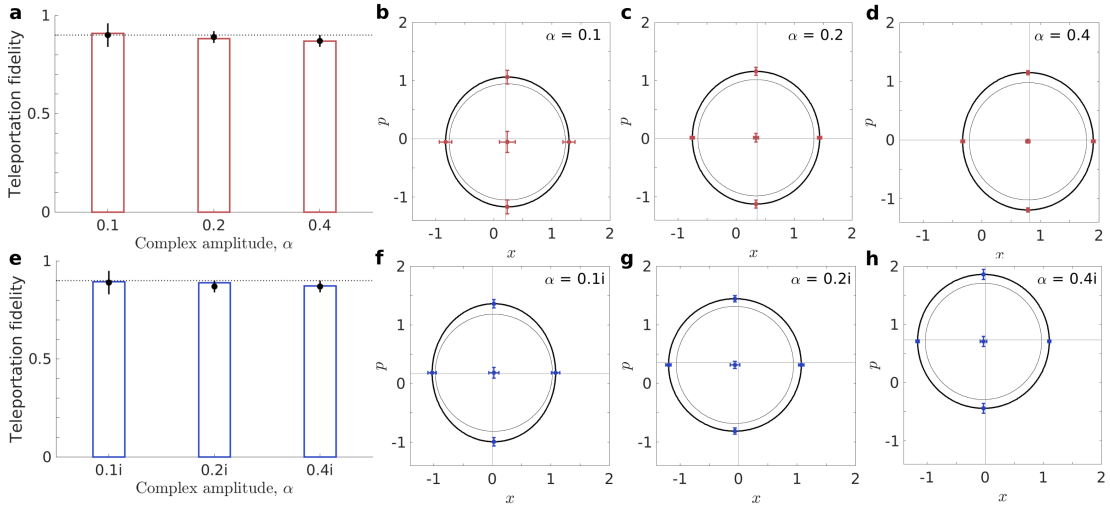


Figure 9.5: Quantum teleportation of coherent states. a. Recorded fidelities for coherent states that are displaced in the amplitude quadrature. Error bars are three standard errors (for visibility) to either side, estimated with 20 samples. The horizontal dotted line is intended as a guide for the eye and corresponds to 90 percent fidelity. **b.-d.** Corresponding Wigner functions represented by the one-standard-deviation contour. The inner circle corresponds to the vacuum state, while the outer circle corresponds to the teleported state. Errors for measurements of the mean and variance are indicated by coloured markers, obtained and displayed in the same way as above. Cross hairs locate the displacement of the input state. **e.-h.** Likewise for coherent states that are displaced in the phase quadrature.

support this proposition. The parameters of the equivalent quantum operation are: the gain factor g_{eff} of the effective noiseless linear amplifier, the transmissivity T of the beam splitter, and the additive noise v_0; the dependence of these parameters on postselection can be determined experimentally from the results for quantum teleportation of the vacuum state (Fig. 9.4). When there is no postselection, $g_{eff} = 1$ (no NLA), $T = 1$ (unity gain), so that only additive thermal noise is present (0.7 units). The effective gain g_{eff} increases with postselection with the maximum (power) gain obtained to be about 10, while both the beam splitter transmissivity and the additive thermal noise falls: the former reduces to one-tenth of its initial value and the latter to about one-third. These observations allow us to gain a more concrete understanding of the constituents of the equivalent operation.

An important corollary that follows from this discussion is the fact that the device provides an implementation of the physical noiseless linear amplifier. This is surprising! For no single photon detectors or sources were employed at any point in this experiment. In other words, the device required only Gaussian states, Gaussian operations, and Gaussian measurements— in stark contrast to the known implementations of the physical noiseless linear amplifier [19, 20, 21]. But since it is well known that the NLA can distill entanglement, it is necessary that the NLA must not exist on its own in this setup in order to avoid violating the no-go theorems for entanglement distillation with Gaussian elements [13, 14, 15, 76]. Thus there is an additional beam splitter dangling on its end, with non-trivial transmissivities (Fig. 9.6). When viewed from a different perspective, however, this appears to be all that is needed in order to circumvent those no-go theorems.

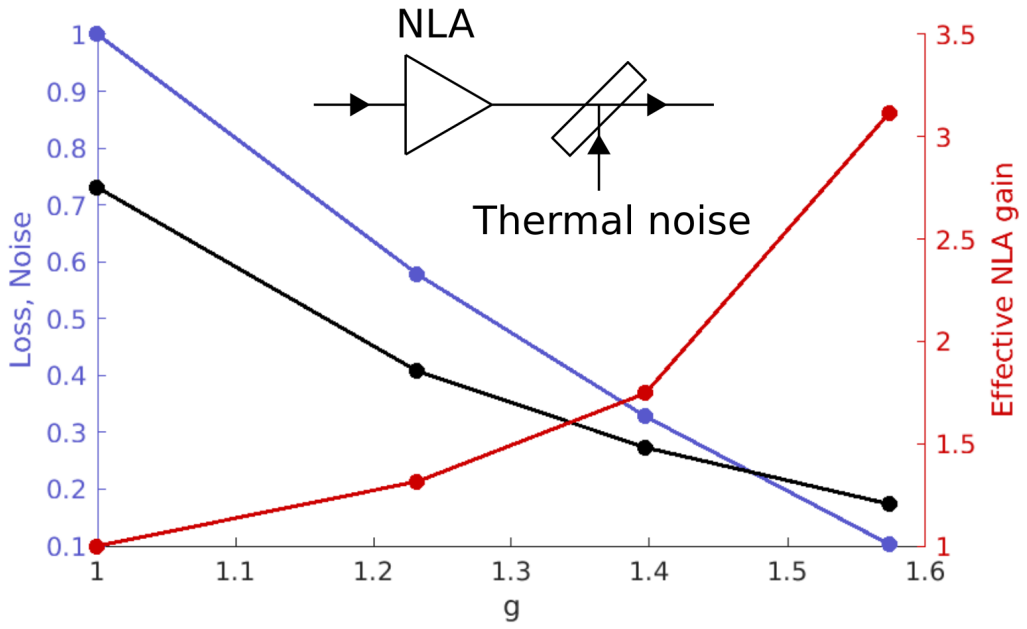


Figure 9.6: Equivalent quantum operation. Inset shows an equivalent description of our apparatus using a physical noiseless linear amplifier, optical loss, and thermal noise. Corresponding parameter values are extracted from the vacuum teleportation results in Fig. 9.4. Blue and black traces correspond to the beam splitter (power) transmissivity and additive thermal noise respectively, with values bound to the left axis. The red trace shows the (amplitude) gain factor of the effective noiseless linear amplifier, with values bound to the right vertical axis. Data points are connected by straight lines as guides for the eye.

9.6 The fidelity question

In this chapter, we have shown that use of noiseless amplification leads to higher fidelities when teleporting coherent states. However, I would like to conclude by pointing out the difficulties associated with the interpretation of this result. As the fidelity depends only on the input and output states of the quantum teleporter and is completely ignorant of everything that occurred in between, it is not possible to say very much when the input states are more general than coherent states. All we can say at this point is that the teleporter with noiseless amplification will behave quite differently to how we might expect an ordinary quantum teleporter to behave, as evidenced by the equivalent quantum operation of Blandino *et al.*

Although some alternative measures have been suggested to me, including the so-called "T-V diagram" [135, 136] and the method of channel characterisation [137], I can see no simple resolution along this line of thought; for both methods suffer from the same limitations as that of fidelity which I have described above. It is my belief that the question lies not so much in choosing the right measure, but rather in how to do away with measures altogether.

In the next chapter, I purpose the attack of this problem from a different angle with a simpler and more direct method. We will investigate the question of the action of the teleporter on *displaced thermal states* and discover that the situation is yet more interesting and surprising than that of coherent states. The behaviour of the device will be found to deviate greatly from that expected of an ordinary teleporter, allowing us to implement a unique quantum transformation with the device. Noiseless amplification will prove to be essential for this to occur.

Chapter 10

A method for removing thermal decoherence

Summary:

It is shown that quantum teleportation combined with noiseless amplification increases the purity of a displaced thermal state without reducing its displacement.

10.1 Applications of quantum teleportation

In the previous chapter, we showed that coherent states could be teleported with higher fidelities using a noiseless amplifier embedded in the quantum teleporter. That is an interesting observation in its own right, for we would much prefer the quantum state to make its way through the teleporter in one piece! Nevertheless, there is interest in quantum teleportation not only for the sake of teleportation, but also for the various important applications that it brings to the field of quantum technology.

Two examples come immediately to mind: quantum teleportation of entanglement (i.e., entanglement swapping) is essential for quantum repeaters [61], and quantum teleportation with cluster states functions as quantum gates in one-way quantum computers [138]. Yet some simple consideration shows that these are not suitable applications for our teleporter, because of the difficulties encountered when working with more general input states than just coherent states. It would of course have been a very different story if the higher fidelities we observed were due to an increase in quantum squeezing supplied to the teleporter, but, alas, that is not the same as how noiseless amplification works.

Knill [139, 140] and Luo *et al.* [141] have previously put forth the interesting suggestion that quantum teleportation could also be used to suppress decoherence. It is required, however, that the quantum teleporter be modified in such a way that the setup amounts to quantum error correction in essence, so that the heavy lifting is achieved by quantum error correction with the act of quantum teleportation playing little role in the reduction of decoherence. Indeed, there appears to be little reason to expect otherwise, for quantum states emerging from an ordinary quantum teleporter will be identical to the input state at best and be decohered if the teleporter contains imperfections.

In this chapter, we report the surprising observation that quantum teleportation with noiseless amplification has the effect of increasing the purity of displaced thermal states without reducing its displacement. This observation is a generalisation of our previous results with coherent states and suggests a method for removing thermal decoherence using quantum teleportation. Although strictly speaking the observed removal of decoherence

is partial, complete removal is theoretically possible, the conditions of which are given in section six. We investigate also the general properties of this device and compare it with the known methods for removing thermal decoherence.

10.2 Methods for suppressing thermal decoherence

It has been known for some time that the problem of removing thermal decoherence is a difficult one. Intuitively, this is due to the difficulty of telling apart which photons represent thermal noise and which ones bear quantum information.

Noh, Girvin, and Jiang [142] have suggested that the methods of quantum error correction can be applied to suppress thermal decoherence. An input quantum state $|\psi\rangle$ (which can in general be arbitrary) is encoded into a two-mode entangled state through two-mode-squeezing operations with an ancillary "Gottesman-Kitaev-Preskill (GKP) state" [52],

$$|GKP\rangle = \sum_j |x_0 + j\delta x\rangle \,. \tag{10.1}$$

Both modes of this entangled state are passed through a channel with additive thermal noise, with measurements then performed on the ancillary mode and fedforward to the data mode; the resulting quantum state is approximately equal to the input state $|\psi\rangle$, with some left-over thermal noise that is less than that added by the channel. The main problem with this procedure lies in the synthesis of the GKP state— there are limited ways, none of which are optical [143, 144].

Andersen *et al.* [145] gave a simpler, but more restrictive method based on the concept of "purification", by reducing several identical quantum states into a single copy that has greater purity. The technique is based on a statistical trick: if x_1, x_2, ..., x_n are n uncorrelated random variables with the same distribution (i.e., "i.i.d." random variables in stats talk), then their average,

$$X = \frac{1}{n}\sum_{k=1}^{n} x_k, \tag{10.2}$$

will have a variance smaller than each variable by a factor of n but the same mean notwithstanding. Andersen *et al.* pointed out that if the x_k's represent the quadrature operators of some collection of optical modes, then their averaging can be achieved by combining the corresponding modes on beam splitters with suitably chosen transmissivities, and thus the thermal noise on each mode x_k can be suppressed. Although this method is relatively straightforward, it assumes that we have available n copies of the same state; this is not a reasonable assumption in general because of the no-cloning theorem [146, 147].

10.3 Experimental observation

We carried out experiments with quantum teleportation of displaced thermal states. White noise generators are connected to the electro-optic modulators at the teleporter input to generate thermal noise, in addition to the fixed-frequency modulations which produce coherent displacements. The motivation for choosing displaced thermal states is to explore the situation where coherent states have decohered through additive thermal noise.

We observed that the thermal decoherence of the output state could be suppressed,

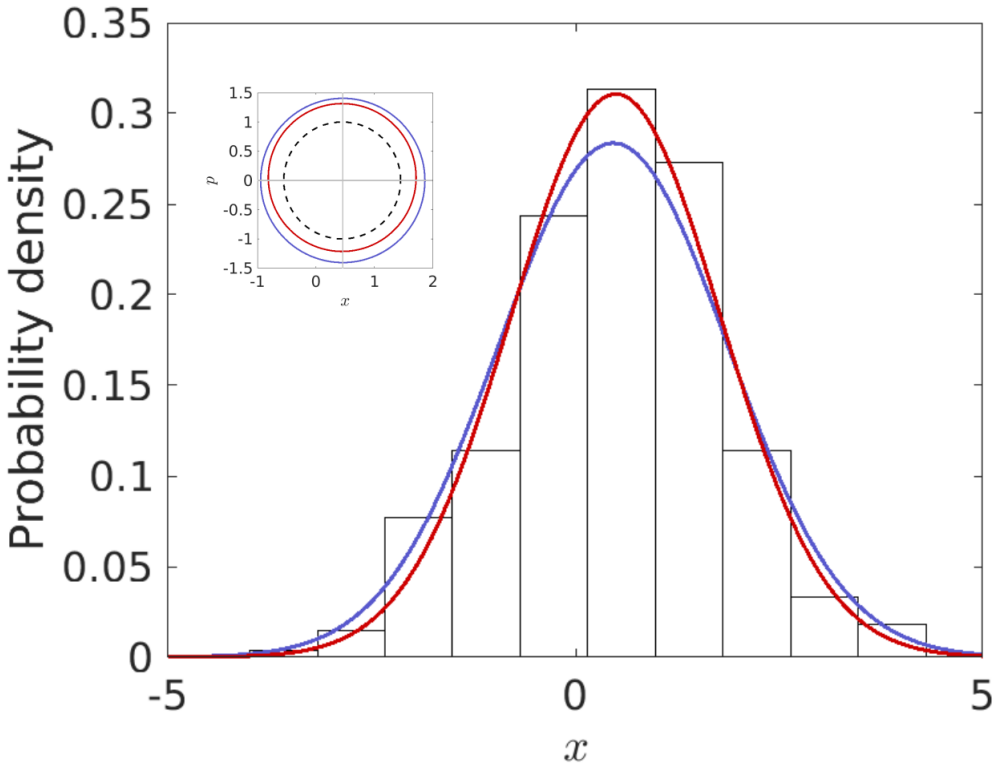


Figure 10.1: Removal of thermal decoherence using quantum teleportation. Characterisation of the output state: histogram shows experimental observations with homodyne measurements of the amplitude quadrature of the output state, overlayed with a Gaussian fit (red curve). The input state is given by the blue curve. Inset shows contours of the corresponding Wigner functions at one standard deviation. Dashed circle corresponds to vacuum state.

but now to a level *below* that of the input state (Fig. 10.1). For an input displacement 0.46 along the amplitude quadrature and variance 1.98, we recorded a teleported state with displacement 0.45 and a markedly smaller variance 1.6 ± 0.1. The one-standard-deviation contour of the reconstructed Wigner functions are shown in the inset of Fig. 10.1.

Although further experiments are necessary in order to fully characterise this effect, its interpretation is clear: the quantum teleporter has taken a mixed quantum state and transformed it into a state of higher purity. Furthermore, there can be no question as to whether the process might be throwing away the coherent signal along with the thermal noise, since the displacement has remained the same. This observation deviates wildly from the expected behavior of ordinary quantum teleportation, which cannot remove thermal noise from the quantum state without also shrinking the displacement.

10.4 Discussion and comparison

In the previous chapter, we have described how the quantum teleporter with noiseless amplification is equivalent to a physical noiseless amplifier concatenated with a beam splitter coupled to a thermal reservoir. This model provides a straightforward way of explaining the observations above: the physical noiseless amplifier *increases*, while the beam splitter *reduces*, the displacement and thermal noise in such a way that we win out overall.

However, this conclusion is very surprising. Although the noiseless amplifier is known for its ability to amplify coherent states noiselessly (Eq. 2.24) as well as to distill quantum entanglement (Eq. 2.25), it is not known to also be capable of purifying quantum states. Furthermore, we can show by a straightforward calculation that the same cannot be true if the noiseless amplifier is replaced by an ordinary phase-insensitive quantum amplifier because of extra thermal noise introduced (Eq. 2.23). Noiseless amplification is probably necessary in order to observe this effect.

It must be emphasised that the situation above bears considerable similarities with the observations of Usuga *et al.* [148, 49], who reported an increase in "signal-to-noise ratio" of a displaced thermal state following noiseless amplification. Nevertheless, no increase in purity was observed in their experiments— both the displacement and the noise were increased. Although it is not immediately clear that a higher purity at fixed signal could be observed had an additional optical attenuator been included in their experiment (which will reduce the signal-to-noise ratio due to the coupling to a vacuum ancilla), it should, in all likelihoods, be the case.

Compared with the quantum error correction procedure of Noh *et al.*, the end effect of our experiment appears similar although there are significant differences: our method is probabilistic and probably has additional restrictions on the input state, but in return requires a setup that is simpler by far. Compared with the purification method of Andersen *et al.*, teleportation of displaced thermal states occurs independently for each input quantum state, so that, consequently, our method does not require the assumption of having in our possession multiple copies of the state.

10.5 Optical model and basic properties

While the equivalent operation of Blandino *et al.* provides a simple way of analysing the device, the parameters of this model have a complicated relationship with the experimental

elements in reality so that it is not the most intuitive way for describing the experiment. In this section, I will provide a description based directly on the optical and electrical elements and apply it to derive the basic properties of the device as a filter for thermal noise.

In order to see how the suppression of thermal noise can occur, we first recall that the quantum teleporter is equivalent to a beam splitter at the gain-tuning point. At this point, the output state has both reduced displacement and thermal noise compared to the input displaced thermal state. Now if we had been teleporting coherent states then the gain-tuning point is also the place where no correlations between the joint-measurement outcomes and the output state could be found, however when the input state is thermal then the beam splitter will remove only part of the thermal noise so that some correlations will remain.

The left-over correlation can be completely removed by further reducing the feedforward gain, for it is given by:

$$cov(x_m, x_{out}) = \sinh 2r - \frac{\phi}{\sqrt{2}}(v_{in} + \cosh 2r), \tag{10.3}$$

which is equal to $\sinh 2r$ when $\phi = 0$, and $-v_{in} - e^{-2r}$ when $\phi = \sqrt{2}$; by the intermediate value theorem there exists some ϕ_0 between these two points where the correlation is exactly zero. We put the feedforward gain to ϕ_0.

Finally, it suffices to repeat what we did with the squeezing gate and teleportation of coherent states: we postselect the outcomes of the joint measurements with the Gaussian filter (which does not affect the state above because the output is no longer correlated with the measurements) and feedforward these results with an attenuation $\epsilon \ll 1$ (equivalent to using the perturbed feedforward gain $\phi = \phi_0 + \epsilon$) to implement noiseless amplification. The net result is an output state chosen to have the same displacement as the input state but possessing less thermal noise.

To examine how the output state varies with the input, we fix the feedforward gain ϕ and enforce the unity-gain condition (thereby fixing the noiseless gain g). We find that the system behaves linearly: the variance of the output state has an *affine* relationship with that of the input state (Fig. 10.2a). This shows that the device can be characterised by just two parameters: the *slope* of this line which measures how much noise is filtered out, and the *offset* of the line which measures how much noise it adds. For example, a slope of 1/2 means that half of the thermal noise on the input state is thrown away, and an offset of 0.1 means that the device adds an additional 0.1 units of thermal noise to the state.

The strongest filtering effects are obtained when both the slope and offset are simultaneously minimised; simulations suggest that this occurs when the feedforward gain ϕ and entanglement parameter λ approach zero. This makes sense because we want the transmissivity of the beam splitter in Blandino *et al.*'s model to go to zero in order to throw out as much noise as we can, which is realised when the entanglement goes to zero and the feedforward also to match. It must be emphasised, however, that this analysis assumes that the input state is a displaced thermal state, so that this regime may not always be the best thing to do depending on what the input state is. The precise action of the filter on general quantum states remains to be worked out.

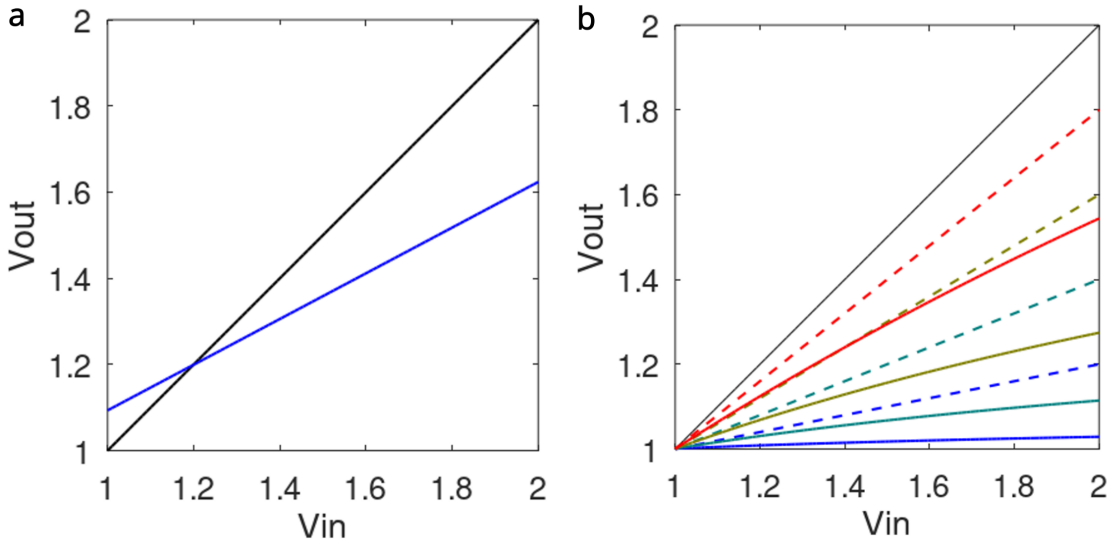


Figure 10.2: Fundamental properties. a. The blue line shows a simulation of the output variance of the device as a function of the input variance. The black line corresponds to $y = x$ and is simply a guide for the eye. **b.** Simulations of the output variance as a function of the input variance, with the latter assumed to be unknown (dashed lines) and known (solid lines), respectively, when choosing the parameters λ and ϕ. Black line corresponds to $y = x$. In each case, the four lines from bottom to top correspond to entanglement parameters of $\lambda = 0.2$, 0.4, 0.6, and 0.8.

10.6 Prior knowledge of the input state

We have explained how quantum teleportation of coherent states with noiseless amplification does not require us to know what the input displacement is, for the unity-gain condition does not depend on the input displacement. The same is true when teleporting displaced thermal states, so that knowledge of the input displacement is also not required. However, knowledge of the *variance* of the input state does have considerable sway over the performance of the system. Let us divide this problem up into three cases.

First, let us assume that the variance of the input state is known before we configure the three parameters of the device (entanglement parameter λ, feedforward gain ϕ, and noiseless gain g). This assumption amounts to knowing precisely the degree of additive thermal noise applied to the input quantum state. In this case it is possible to obtain the optimum solution where the correlation between the joint measurements and the output state is put to zero (see previous section for details); with the feedforward gain given by

$$\phi_0 = \frac{\sqrt{2}\sinh 2r}{v_{in} + \cosh 2r}, \tag{10.4}$$

which can be seen to depend on the variance of the input state v_{in}. Operating with the feedforward gain at an epsilon above this value and implementing noiseless amplification to enforce unity gain, the output states of the device are given by the solid lines in Fig. 10.2b. All possess a variance that is smaller than the input state, with the excess thermal noise approaching zero when λ approaches zero.

Now it is also possible that the variance is not known when deciding the parameters of the system but can be inferred afterwards so that only g is allowed to depend on the

variance. In this case, the feedforward gain can no longer depend on v_{in}, and the best results are obtained when $\phi_0 = \sqrt{2}\tanh r$. Any value smaller than this will lead to a sign-change of correlations, and result in unphysical states for some values of the input variance, so this is the best we can do. With this set of parameters, the behavior of the device is linear with slope $m = \tanh r$ and no excess noise (Fig. 10.2 dotted lines).

It is not possible to relax the assumption any further and run the system assuming that all three parameters are independent of v_{in}, for it will no longer be possible to enforce the unity-gain condition (which in turn is because the gain factor depends nonlinearly on v_{in}). In this case, there exists only one trivial solution $g = 1$ and $\phi = \sqrt{2}$, which corresponds to ordinary quantum teleportation without noiseless amplification.

The last of the three cases above corresponds to the hypothetical situation where the thermal noise on the input state is rapidly fluctuating so that it is meaningless to infer its value at any one point in time because the value will already have changed by the next moment. Our experiments resemble most closely that of the first case because we can freely choose how much thermal noise to put on the input state but can also correspond to the second case if we decide to forget what value we chose.

It must be emphasised that the theoretical analysis presented here makes very optimistic assumptions, including the possibility of approaching as close to the gain-tuning point as we wish. It has already been seen with the teleportation experiment that this is not possible in general. In reality, the operating parameter regimes can only be determined by further experiments.

10.7 The question of general input states

The question remains as to whether we can expect similar effects for more general input states. This question is strongly connected to quantum technology which frequently requires quantum states that are more complicated than those studied here. Although we can immediately rule out the application of this apparatus to distillation of Gaussian entangled states since that entails the violation of a well-known no-go theorem [14, 15, 76], it is not possible to straightaway say the same for non-Gaussian states in general.

All the same, the purification of displaced thermal states is already a non-trivial result regardless of whether the effect is found to generalise. When stated in the broadest terms, these results show that not only can the decoherence of quantum teleporters be suppressed, but that the problem could be turned on its head with the teleporter itself used as a method for removing decoherence.

Chapter 11

Conclusion

I have given a description, in the foregoing pages, of the basic properties and applications of a number of quantum operations. These operations are implemented with light and are based on photon addition and noiseless amplification. Just as the understanding of the basic principles of quantum optics has fuelled the rapid development of quantum technology, I believe that insights gained into these more sophisticated quantum operations may yet lead to quantum technologies that could be more powerful, efficient, and reliable. The observations of strong cubic phase shifts and removal of thermal decoherence with quantum teleportation represent some of the most important results that have emerged from this line of research.

It is important, however, to emphasise some of the limitations and difficulties encountered in this study. First, the experiments on photon addition have been carried out in a destructive manner which prevented us from observing physically propagating output states; this is a limitation of our choice of the implementation however, and not fundamentally of the method itself. Second, our experiments with noiseless amplification re-affirm the known fact that it is an inefficient process, with probability of success on the orders of 10^{-5} and 10^{-6}. Consequently, I do not think that it will be easy to make use of the noise suppression characteristics of noiseless amplification in quantum information tasks such as quantum computation or quantum communication.

Several new questions emerge from our investigations, which I think will lead to fruitful avenues for exploration. For instance, it is not at present known how the probabilistic teleporter will act on states more general than that of coherent states and displaced thermal states; furthermore, it is also not known whether Blandino's equivalent operation can be generalised to the case of non-Gaussian postselection procedures, which must no doubt also be a non-Gaussian operation if it exists. By answering these questions, we gain deeper understanding into the fundamental quantum processes allowed in quantum optics.

There appears also to be plenty of room for improving the probability of success, an issue that has for the most part been dusted under the carpet. Recourse is required to the use of light-matter interactions instead of restricting to optical techniques, applying both to photon addition and noiseless linear amplification.[1] Very little has yet been established so far, but it is hoped that this line of inquiry will lead to improved methods for experiment that may allow us to tackle physical problems afresh.

[1] See, for instance, McMahon *et al.* [149] and Feist *et al.* [150].

Appendix A

Theory of probabilistic Gaussian quantum optics

This appendix documents the theoretical model used for the experiments from Chapters 7 to 10. Section A.1 is based on notes communicated to me privately by Assad, while the calculations of Section A.2 are that of my own. To my knowledge, most of the content in this section have not been published elsewhere for the reason that they are entirely theoretical in nature.

A.1 Postselection of homodyne measurements

Consider the simplest possible situation where two observables (x_1, x_2) are given, which might, for instance, represent amplitude quadratures from two separate optical modes. The pair share a joint probability distribution $P(x_1, x_2)$ corresponding to homodyne measurements made on these observables, and if the system is Gaussian, then the joint distribution is completely determined by the mean μ and covariance matrix Σ (Eq. 2.18 and 2.19),

$$\mu = \begin{bmatrix} \mu_1 \\ \mu_2 \end{bmatrix}, \ \Sigma = \begin{bmatrix} c_{11} & c_{12} \\ c_{21} & c_{22} \end{bmatrix}. \tag{A.1}$$

Postselecting the outcomes of x_1 with acceptance probability $f(x_1)$ transforms the joint probability distribution by

$$P(x_1, x_2) \to f(x_1)P(x_1, x_2), \tag{A.2}$$

normalised suitably. If the function f is Gaussian, then the resulting probability distribution will also be Gaussian. We shall therefore take the function f to be of Gaussian form,

$$f(x) \propto \exp\left(\frac{x^2}{2}(1 - \frac{1}{g^2})\right), \tag{A.3}$$

parametrised by the free variable g. If we denote the new mean and covariance matrix after postselection by

$$\omega = \begin{bmatrix} \omega_1 \\ \omega_2 \end{bmatrix}, \ \Omega = \begin{bmatrix} o_{11} & o_{12} \\ o_{21} & o_{22} \end{bmatrix}, \tag{A.4}$$

then quantities can be expressed in terms of those prior to postselection, first for the observable that is postselected:

$$\omega_1 = \frac{\mu_1}{c_{11}(1/c_{11} + 1/g^2 - 1)}, \tag{A.5}$$

$$o_{11} = \frac{1}{1/c_{11} + 1/g^2 - 1}, \tag{A.6}$$

and then successively for the other quantities starting with the covariance o_{21},

$$\frac{o_{21}}{o_{11}} = \frac{c_{21}}{c_{11}}, \tag{A.7}$$

then the variance o_{22},

$$o_{22} - \frac{o_{21}}{o_{11}} o_{12} = c_{22} - \frac{c_{21}}{c_{11}} c_{12}, \tag{A.8}$$

and finally the mean value,

$$\omega_2 = \mu_2 + \frac{o_{21}}{o_{11}}(\omega_1 - \mu_1). \tag{A.9}$$

These equations follow by comparing the expression $f(x_1)P(x_1, x_2)$ with the standard normal distribution of two variables and determine completely the state of the system following postselection.

A.2 General case

It is possible to put the results in the previous section into a more compact form that is also more general. Given a joint probability distribution of multiple Gaussian random variables — the amplitude and phase quadratures of arbitrarily many modes $(x_1, p_1, x_2, p_2, ...)$, for instance — we specify a Gaussian filter function,

$$f(x) \propto \exp\left(-\frac{1}{2} x^T S x\right), \tag{A.10}$$

acting on the joint probability distribution in the same manner as in the previous section and parametrised by the matrix

$$S = \begin{bmatrix} 1 & 0 \\ 0 & S_0 \end{bmatrix}. \tag{A.11}$$

The only requirement on S is that the resulting distribution must represent a physical Gaussian state, although this is not a trivial condition and depends not only on the general form of S but also on the precise values. It is assumed without loss of generality that postselection acts only on the batch of modes corresponding to positions occupied by S_0.

As in the previous section, we will associate the initial state and with the mean vector μ and covariance matrix Σ, and the final state with ω and Ω. The analysis will be simplified if we write the covariance matrices also in block form,

$$\Sigma = \begin{bmatrix} \Sigma_{11} & \Sigma_{12} \\ \Sigma_{21} & \Sigma_{22} \end{bmatrix}, \tag{A.12}$$

$$\Omega = \begin{bmatrix} \Omega_{11} & \Omega_{12} \\ \Omega_{21} & \Omega_{22} \end{bmatrix}, \tag{A.13}$$

so that the individual blocks of Ω may then be worked out in succession:

$$\Omega_{22}^{-1} = \Sigma_{22}^{-1} + S_0, \tag{A.14}$$

$$\Omega_{12} = \Sigma_{12}\Sigma_{22}^{-1}\Omega_{22}, \tag{A.15}$$

$$\Omega_{11} = \Sigma_{11} + \Sigma_{12}\Sigma_{22}^{-1}(\Omega_{21} - \Sigma_{21}). \tag{A.16}$$

Once the new covariance matrix is known, the mean can also be determined:

$$\omega = \Omega\Sigma^{-1}\mu. \tag{A.17}$$

These equations therefore provide a method for calculating the transformation of any Gaussian state under Gaussian postselection. For instance, restricting to the case where the vector x is two dimensional (x_1, x_2) and with the postselection matrix

$$S = \begin{bmatrix} 1 & 0 \\ 0 & \frac{1}{g^2} - 1 \end{bmatrix}, \tag{A.18}$$

then the results reduce to that of the previous section (with the order of x_1 and x_2 interchanged).

The description is general in that it can be combined with the usual method of modelling Gaussian systems by matrix multiplications on the mean and covariance matrix, providing a way for simulating the system numerically with software such as Matlab. Effects of optical loss and detector dark noise can be incorporated in a straightforward manner, the former by coupling the system to additional vacuum modes through beam splitters and the latter by simply increasing the relevant variances.

Bibliography

[1] M. Planck, "Ueber das gesetz der energieverteilung im normalspectrum," *Ann. Phys.*, vol. 4, p. 553, 1901.

[2] P. Lenard, "Ueber die lichtelektrische wirkung," *Ann. Phys.*, vol. 5, p. 149, 1902.

[3] A. Einstein, "Ueber einen die erzeugung und verwandlung des lichtes betreffenden heuristischen gesichtspunkt," *Ann. Phys.*, vol. 17, p. 132, 1905.

[4] A. Compton, "A quantum theory of the scattering of x-rays by light elements," *Phys. Rev.*, vol. 21, p. 483, 1923.

[5] P. A. M. Dirac, "The quantum theory of the emission and absorption of radiation," *Proc. R. Soc. Lond. A*, vol. 114, p. 243, 1927.

[6] D. F. Walls and G. J. Milburn, *Quantum optics*. Springer Berlin, Heidelberg, 2008.

[7] M. T. et. al., "Quantum-enhanced advanced ligo detectors in the era of gravitational-wave astronomy," *Phys. Rev. Lett.*, vol. 123, p. 231107, 2019.

[8] A. Einstein, Yu. Podolsky, and N. Rosen, "Can quantum-mechanical description of physical reality be considered complete?," *Phys. Rev.*, vol. 47, p. 777, 1935.

[9] T. C. Zhang, K. W. Goh, C. W. Chou, P. Lodahl, and H. J. Kimble, "Quantum teleportation of light beams," *Phys. Rev. A*, vol. 67, p. 033802, 2003.

[10] A. Ourjoumtsev, R. Tualle-Brouri, J. Laurat, and P. Grangier, "Generating optical schroedinger kittens for quantum information processing," *Science*, vol. 312, p. 83, 2006.

[11] H. Takahashi, J. S. Neergaard-Nielsen, M. Takeuchi, M. Takeoka, K. Hayasaka, and A. Furusawa, "Entanglement distillation from gaussian input states," *Nature Photon*, vol. 4, p. 178, 2010.

[12] S. D. Bartlett, B. C. Sanders, S. L. Braunstein, and K. Nemoto, "Efficient classical simulation of continuous variable quantum information processes," *Phys. Rev. Lett.*, vol. 88, p. 097904, 2002.

[13] J. Niset, J. Fiurasek, and N. J. Cerf, "No-go theorem for gaussian quantum error correction," *Phys. Rev. Lett.*, vol. 102, p. 120501, 2009.

[14] J. Eisert, S. Scheel, and M. B. Plenio, "Distilling gaussian states with gaussian operations is impossible," *Phys. Rev. Lett.*, vol. 89, p. 137903, 2002.

[15] J. Fiurasek, "Gaussian transformations and distillation of entangled gaussian states," *Phys. Rev. Lett.*, vol. 89, p. 137904, 2002.

[16] C. M. Caves, "Quantum limits on noise in linear amplifiers," *Phys. Rev. D*, vol. 26, p. 1817, 1982.

[17] V. Josse, M. Sabuncu, N. J. Cerf, G. Leuchs, and U. L. Andersen, "Universal optical amplification without nonlinearity," *Phys. Rev. Lett.*, vol. 96, p. 163602, 2006.

[18] T. C. Ralph and A. P. Lund, "Nondeterministic noiseless linear amplification of quantum systems," in *Proceedings of the 9th International Conference on Quantum Communication Measurement and Computing* (A. I. Lvovsky, ed.), p. 155, American Institute of Physics, 2009.

[19] G. Y. Xiang, T. C. Ralph, A. P. Lund, N. Walk, and G. J. Pryde, "Heralded noiseless linear amplification and distillation of entanglement," *Nature Photonics*, vol. 4, p. 316, 2010.

[20] F. Ferreyrol, M. Barbieri, R. Blandino, S. Fossier, R. Tualle-Brouri, and P. Grangier, "Implementation of a nondeterministic optical noiseless amplifier," *Phys. Rev. Lett.*, vol. 104, p. 123603, 2010.

[21] A. Zavatta, J. Fiurasek, and M. Bellini, "A high-fidelity noiseless amplifier for quantum light states," *Nature Photonics*, vol. 5, p. 52, 2011.

[22] C. Weedbrook, S. Pirandola, R. García-Patrón, N. J. Cerf, T. C. Ralph, J. H. Shapiro, and S. Lloyd, "Gaussian quantum information," *Rev. Mod. Phys.*, vol. 84, p. 621, 2012.

[23] A. Furusawa and P. van Loock, *Quantum Teleportation and Entanglement: A Hybrid Approach to Optical Quantum Information Processing.* Wiley-VCH, 2011.

[24] P. K. Lam, *Applications of quantum electro-optic control and squeezed light.* Ph.D. thesis, Australian National University, 1998.

[25] M. S. Stefszky, *Generation and detection of low-frequency squeezing for gravitation-wave detection.* Ph.D. thesis, Australian National University, 2012.

[26] H.-A. Bachor and T. C. Ralph, *A Guide to Experiments in Quantum Optics.* Wiley-VCH, 2019.

[27] J. Zhao, *Post-selection-based continuous variable quantum information processing.* Ph.D. thesis, Australian National University, 2019.

[28] X. Jin, J. Su, Y. Zheng, C. Chen, W. Wang, and K. Peng, "Balanced homodyne detection with high common mode rejection ratio based on parameter compensation of two arbitrary photodiodes," *Opt. Express*, vol. 23, p. 23859, 2015.

[29] R. W. P. Drever, J. L. Hall, F. V. Kowalski, J. Hough, G. M. Ford, A. J. Munley, and H. Ward, "Laser phase and frequency stabilization using an optical resonator," *Appl. Phys. B*, vol. 31, p. 97, 1983.

[30] E. D. Black, "An introduction to pound-drever-hall laser frequency stabilization," *Am. J. Phys.*, vol. 69, p. 79, 2001.

[31] D. A. Shaddock, *Advanced Interferometry for Gravitional Wave Detection.* Ph.D. thesis, Australian National University, 2000.

[32] B. M. Sparkes, H. M. Chrzanowski, D. P. Parrain, B. C. Buchler, P. K. Lam, and T. Symul, "A scalable, self-analyzing digital locking system for use on quantum optics experiments," *Rev. Sci. Instrum.*, vol. 82, p. 075113, 2011.

[33] J. Fiurasek and N. J. Cerf, "Gaussian postselection and virtual noiseless amplification in continuous-variable quantum key distribution," *Phys. Rev. A*, vol. 86, p. 060302(R), 2012.

[34] H. M. Chrzanowski, N. Walk, S. M. Assad, J. Janousek, S. Hosseini, T. C. Ralph, T. Symul, and P. K. Lam, "Measurement-based noiseless linear amplification for quantum communication," *Nature Photonics*, vol. 8, p. 333, 2014.

[35] Z. Li, Y. Zhang, X. Wang, B. Xu, X. Peng, and H. Guo, "Non-gaussian postselection and virtual photon subtraction in continuous-variable quantum key distribution," *Phys. Rev. A*, vol. 93, p. 012310, Jan 2016.

[36] P. W. Shor, "Algorithms for quantum computation: discrete logarithms and factoring," in *Proceedings 35th Annual Symposium on Foundations of Computer Science*, p. 124, IEEE, 1994.

[37] S. Aaronson and A. Arkhipov, "The computational complexity of linear optics," in *Proceedings of the forty-third annual ACM symposium on Theory of computing*, p. 333, Association for Computing Machinery, 2011.

[38] C. S. Hamilton, R. Kruse, L. Sansoni, S. Barkhofen, C. Silberhorn, and I. Jex, "Gaussian boson sampling," *Phys. Rev. Lett.*, vol. 119, p. 170501, 2017.

[39] H. Wang, J. Qin, X. Ding, M.-C. Chen, S. Chen, X. You, Y.-M. He, X. Jiang, L. You, Z. Wang, C. Schneider, J. J. Renema, S. Höfling, C.-Y. Lu, and J.-W. Pan, "Boson sampling with 20 input photons and a 60-mode interferometer in a 10^{14}-dimensional hilbert space," *Phys. Rev. Lett.*, vol. 123, p. 250503, Dec 2019.

[40] H.-S. Zhong, H. Wang, Y.-H. Deng, M.-C. Chen, L.-C. Peng, Y.-H. Luo, J. Qin, D. Wu, X. Ding, Y. Hu, P. Hu, X.-Y. Yang, W.-J. Zhang, H. Li, Y. Li, X. Jiang, L. Gan, G. Yang, L. You, Z. Wang, L. Li, N.-L. Liu, C.-Y. Lu, and J.-W. Pan, "Quantum computational advantage using photons," *Science*, vol. 370, p. 1460, 2020.

[41] J. M. Arrazola and T. R. Bromley, "Using gaussian boson sampling to find dense subgraphs," *Phys. Rev. Lett.*, vol. 121, p. 030503, 2018.

[42] J. Huh, G. G. Guerreschi, B. Peropadre, J. R. McClean, and A. Aspuru-Guzik, "Boson sampling for molecular vibronic spectra," *Nat. Photon.*, vol. 9, p. 615, 2015.

[43] A. Marandi, Z. Wang, K. Takata, R. L. Byer, and Y. Yamamoto, "Network of time-multiplexed optical parametric oscillators as a coherent ising machine," *Nat. Photon.*, vol. 8, p. 937, 2014.

[44] Y. Yamamoto, K. Aihara, T. Leleu, K.-I. Kawarabayashi, S. Kako, M. Fejer, K. Inoue, and H. Takesue, "Coherent ising machines— optical neural networks operating at the quantum limit," *npj Quantum Inf*, vol. 3, p. 49, 2017.

[45] D. Deutsch, "Quantum computation networks," *Proc. R. Soc. A*, vol. 425, p. 73, 1989.

[46] A. Barenco, C. H. Bennett, R. Cleve, D. P. DiVincenzo, N. Margolus, P. Shor, T. Sleator, J. A. Smolin, and H. Weinfurtner, "Elementary gates for quantum computation," *Phys. Rev. A*, vol. 52, p. 3457, 1995.

[47] S. Lloyd and S. L. Braunstein, "Quantum computation over continuous variables," *Phys. Rev. Lett.*, vol. 82, p. 1784, 1999.

[48] R. Ukai, S. Yokoyama, J.-I. Yoshikawa, P. van Loock, and A. Furusawa, "Demonstration of a controlled-phase gate for continuous-variable one-way quantum computation," *Phys. Rev. Lett.*, vol. 107, p. 250501, 2011.

[49] P. Marek, R. Filip, and A. Furusawa, "Deterministic implementation of weak quantum cubic nonlinearity," *Phys. Rev. A*, vol. 84, p. 053802, 2011.

[50] F. Arzani, N. Treps, and G. Ferrini, "Polynomial approximation of non-gaussian unitaries by counting one photon at a time," *Phys. Rev. A*, vol. 95, p. 052352, 2017.

[51] K. Marshall, R. Pooser, G. Siopsis, and C. Weedbrook, "Repeat-until-success cubic phase gate for universal continuous-variable quantum computation," *Phys. Rev. A*, vol. 91, p. 032231, 2015.

[52] D. Gottesman, A. Kitaev, and J. Preskill, "Encoding a qubit into an oscillator," *Phys. Rev. A*, vol. 64, p. 012310, 2001.

[53] K. K. Sabapathy and C. Weedbrook, "On states as resource units for universal quantum computation with photonic architectures," *Phys. Rev. A*, vol. 97, p. 062315, 2018.

[54] R. Yanagimoto, T. O. ad E. Ng, L. G. Wright, P. L. McMahon, and H. Mabuchi, "Engineering a kerr-based deterministic cubic phase gate via gaussian operations," *Phys. Rev. Lett.*, vol. 124, p. 240503, 2020.

[55] C. W. S. Chang, C. Sabín, P. Forn-Díaz, F. Quijandría, A. M. Vadiraj, I. Nsanzineza, G. Johansson, and C. M. Wilson, "Observation of three-photon spontaneous parametric down-conversion in a superconducting parametric cavity," *Phys. Rev. X*, vol. 10, p. 011011, 2020.

[56] M. Yukawa, K. Miyata, H. Yonezawa, P. Marek, R. Filip, and A. Furusawa, "Emulating quantum cubic nonlinearity," *Phys. Rev. A*, vol. 88, p. 053816, 2013.

[57] A. I. Lvovsky, "Iterative maximum-likelihood reconstruction in quantum homodyne tomography," *Journal of Optics B: Quantum and Semiclassical Optics*, vol. 6, pp. S556–S559, may 2004.

[58] N. Budinger, A. Furusawa, and P. van Loock, "All-optical quantum computing using cubic phase gates," *arXiv:2211.09060*, Nov 2022.

[59] A. Zavatta, S. Viciani, and M. Bellini, "Quantum-to-classical transition with single-photon-added coherent states of light," *Science*, vol. 306, p. 660, 2004.

[60] A. U. Devi, R. Prabhu, and M. Uma, "Non-classicality of photon added coherent and thermal radiations," *Eur. Phys. J. D*, vol. 40, p. 133, 2006.

[61] H.-J. Briegel, W. Dur, J. I. Cirac, and P. Zoller, "Quantum repeaters: The role of imperfect local operations in quantum communication," *Phys. Rev. Lett.*, vol. 81, p. 5932, 1998.

[62] L.-M. Duan, M. D. Lukin, J. I. Cirac, and P. Zoller, "Long-distance quantum communication with atomic ensembles and linear optics," *Nature*, vol. 414, p. 413, 2001.

[63] R. Alléaume, F. Roueff, E. Diamanti, and N. Lütkenhaus, "Topological optimization of quantum key distribution networks," *New. J. Phys.*, vol. 11, p. 075002, 2009.

[64] C. Elliott and H. Yeh, "Darpa quantum network testbed," tech. rep., BBN Technologies, Cambridge, MA, July 2007.

[65] M. Peev, C. Pacher, R. Alléaume, C. Barreiro, J. Bouda, W. Boxleitner, T. Debuisschert, E. Diamanti, M. Dianati, J. F. Dynes, S. Fasel, S. Fossier, M. Fürst, J.-D. Gautier, O. Gay, N. Gisin, P. Grangier, A. Happe, Y. Hasani, M. Hentschel, H. Hübel, G. Humer, T. Länger, M. Legré, R. Lieger, J. Lodewyck, T. Lorünser, N. Lütkenhaus, A. Marhold, T. Matyus, O. Maurhart, L. Monat, S. Nauerth, J.-B. Page, A. Poppe, E. Querasser, G. Ribordy, S. Robyr, L. Salvail, A. W. Sharpe, A. J. Shields, D. Stucki, M. Suda, C. Tamas, T. Themel, R. T. Thew, Y. Thoma, A. Treiber, P. Trinkler, R. Tualle-Brouri, F. Vannel, N. Walenta, H. Weier, H. Weinfurter, I. Wimberger, Z. L. Yuan, H. Zbinden, and A. Zeilinger, "The secoqc quantum key distribution network in vienna," *New. J. Phys.*, vol. 11, p. 075001, 2009.

[66] D. Stucki, M. Legré, F. Buntschu, B. Clausen, N. Felber, N. Gisin, L. Henzen, P. Junod, G. Litzistorf, P. Monbaron, L. Monat, J.-B. Page, D. Perroud, G. Ribordy, A. Rochas, S. Robyr, J. Tavares, R. Thew, P. Trinkler, S. Ventura, R. Voirol, N. Walenta, and H. Zbinden, "Long-term performance of the SwissQuantum quantum key distribution network in a field environment," *New Journal of Physics*, vol. 13, no. 12, p. 123001, 2011.

[67] M. Sasaki, M. Fujiwara, H. Ishizuka, W. Klaus, K. Wakui, M. Takeoka, S. Miki, T. Yamashita, Z. Wang, A. Tanaka, K. Yoshino, Y. Nambu, S. Takahashi, A. Tajima, A. Tomita, T. Domeki, T. Hasegawa, Y. Sakai, H. Kobayashi, T. Asai, K. Shimizu, T. Tokura, T. Tsurumaru, M. Matsui, T. Honjo, K. Tamaki, H. Takesue, Y. Tokura, J. F. Dynes, A. R. Dixon, A. W. Sharpe, Z. L. Yuan, A. J. Shields, S. Uchikoga, M. Legré, S. Robyr, P. Trinkler, L. Monat, J.-B. Page, G. Ribordy, A. Poppe, A. Allacher, O. Maurhart, T. Länger, M. Peev, and A. Zeilinger, "Field test of quantum key distribution in the tokyo qkd network," *Opt. Express*, vol. 19, pp. 10387–10409, May 2011.

[68] S. Wang, W. Chen, Z.-Q. Yin, Y. Zhang, T. Zhang, H.-W. Li, F.-X. Xu, Z. Zhou, Y. Yang, D.-J. Huang, L.-J. Zhang, F.-Y. Li, D. Liu, Y.-G. Wang, G.-C. Guo, and Z.-F. Han, "Field test of wavelength-saving quantum key distribution network," *Opt. Lett.*, vol. 35, pp. 2454–2456, Jul 2010.

[69] S. Muralidharan, L. Li, J. Kim, N. Lütkenhaus, M. D. Lukin, and L. Jiang, "Optimal architectures for long distance quantum communication," *Sci. Rep.*, vol. 6, p. 20463, 2016.

[70] J. Dias and T. C. Ralph, "Quantum repeaters using continuous-variable teleportation," *Phys. Rev. A*, vol. 95, p. 022312, Feb 2017.

[71] C. Navarrete-Benlloch, R. García-Patrón, J. H. Shapiro, and N. J. Cerf, "Enhancing quantum entanglement by photon addition and subtraction," *Phys. Rev. A*, vol. 86, p. 012328, Jul 2012.

[72] Y. Huang, "Computing quantum discord is np-complete," *New J. Phys.*, vol. 16, p. 033027, 2014.

[73] M. M. Wolf, G. Giedke, and J. I. Cirac, "Extremality of gaussian quantum states," *Phys. Rev. Lett.*, vol. 96, p. 080502, Mar 2006.

[74] Y. Kurochkin, A. S. Prasad, and A. I. Lvovsky, "Distillation of the two-mode squeezed state," *Phys. Rev. Lett.*, vol. 112, p. 070402, Feb 2014.

[75] A. E. Ulanov, I. A. Fedorov, A. A. Pushkina, Y. V. Kurochkin, T. C. Ralph, and A. I. Lvovsky, "Undoing the effect of loss on quantum entanglement," *Nature Photon.*, vol. 9, p. 764, 2015.

[76] G. Giedke and J. I. Cirac, "Characterization of gaussian operations and distillation of gaussian states," *Phys. Rev. A*, vol. 66, p. 032316, 2002.

[77] R. Garcia-Patron, *Quantum information with optical continuous variables.* Ph.D. thesis, Université Libre de Bruxelles, 2007.

[78] A. Einstein, "Die plancksche theorie der strahlung und die theorie der spezifischen wärme," *Annalen der Physik*, vol. 327, no. 1, pp. 180–190, 1907.

[79] G. E. Uhlenbeck and S. Goudsmit, "Ersetzung der hypothese vom unmechanischen zwang durch eine forderung bezüglich des inneren verhaltens jedes einzelnen elektrons," *Naturwissenschaften*, vol. 47, p. 953, 1925.

[80] R. Bach, D. Pope, S.-H. Liou, and H. Batelann, "Controlled double-slit electron diffraction," *New J. Phys.*, vol. 15, p. 033018, 2013.

[81] A. Aspect, J. Dalibard, and G. Roger, "Experimental test of bell's inequalities using time-varying analyzers," *Phys. Rev. Lett.*, vol. 49, p. 1804, 1982.

[82] G. V. Avosopiants, K. G. Katamadze, Y. I. Bogdanov, B. I. Bantysh, and S. P. Kulik, "Non-gaussianity of multiple photon-subtracted thermal states in terms of compound-poisson photon number distribution parameters: theory and experiment," *Laser Physics Letters*, vol. 15, p. 075205, may 2018.

[83] V. Parigi, A. Zavatta, M. Kim, and M. Bellini, "Probing quantum commutation rules by addition and subtraction of single photons to/from a light field," *Science*, vol. 317, no. 5846, pp. 1890–1893, 2007.

[84] S. M. Barnett, G. Ferenczi, C. R. Gilson, and F. C. Speirits, "Statistics of photon-subtracted and photon-added states," *Phys. Rev. A*, vol. 98, p. 013809, Jul 2018.

[85] A. Zavatta, V. Parigi, M. S. Kim, and M. Bellini, "Subtracting photons from arbitrary light fields: experimental test of coherent state invariance by single-photon annihilation," *New Journal of Physics*, vol. 10, p. 123006, dec 2008.

[86] H. Jeng, S. Tserkis, J. Y. Haw, H. M. Chrzanowski, J. Janousek, T. C. Ralph, P. K. Lam, and S. M. Assad, "Entanglement properties of a measurement-based entanglement distillation experiment," *Phys. Rev. A*, vol. 99, p. 042304, April 2019.

[87] C. H. Bennett, H. J. Bernstein, S. Popescu, and B. Schumacher, "Concentrating partial entanglement by local operations," *Phys. Rev. A*, vol. 53, p. 2046, 1996.

[88] R. Horodecki, P. Horodecki, M. Horodecki, and K. Horodecki, "Quantum entanglement," *Rev. Mod. Phys.*, vol. 81, p. 865, 2009.

[89] C. H. Bennett, D. P. DiVincenzo, J. A. Smolin, and W. K. Wootters, "Mixed-state entanglement and quantum error correction," *Phys. Rev. A*, vol. 54, p. 3824, 1996.

[90] G. Vidal and R. F. Werner, "Computable measure of entanglement," *Phys. Rev. A*, vol. 65, p. 032314, 2002.

[91] V. Vedral, M. B. Plenio, M. A. Rippin, and P. L. Knight, "Quantifying entanglement," *Phys. Rev. Lett.*, vol. 78, p. 2275, 1997.

[92] S. Scheel and D.-G. Welsch, "Entanglement generation and degradation by passive optical devices," *Phys. Rev. A*, vol. 64, p. 063811, 2001.

[93] M. Christandl and A. Winter, "Squashed entanglement: An additive entanglement measure," *J. Math. Phys.*, vol. 45, p. 829, 2004.

[94] R. Simon, "Peres-horodecki separability criterion for continuous variable systems," *Phys. Rev. Lett.*, vol. 84, p. 2726, 2000.

[95] M. D. Reid, "Demonstration of the einstein-podolsky-rosen paradox using nondegenerate parametric amplification," *Phys. Rev. A*, vol. 40, p. 913, 1989.

[96] B. Schumacher and M. A. Nielsen, "Quantum data processing and error correction," *Phys. Rev. A*, vol. 54, p. 2629, 1996.

[97] R. Garcia-Patrón, S. Pirandol, S. Lloyd, and J. H. Shapiro, "Reverse coherent information," *Phys. Rev. Lett.*, vol. 102, p. 210501, 2009.

[98] S. Tserkis and T. C. Ralph, "Quantifying entanglement in two-mode gaussian states," *Phys. Rev. A*, vol. 96, p. 062338, 2017.

[99] K. Goodenough, D. Elkouss, and S. Wehner, "Assessing the performance of quantum repeaters for all phase-insensitive gaussian bosonic channels," *New J. Phys.*, vol. 18, p. 2016, 2016.

[100] Y. Zinchenko, S. Friedland, and G. Gour, "Numerical estimation of the relative entropy of entanglement," *Phys. Rev. A*, vol. 82, p. 052336, 2010.

[101] P. M. Hayden, M. Horodecki, and B. M. Terhal, "The asymptotic entanglement cost of preparing a quantum state," *J. Phys. A: MAth. Gen.*, vol. 34, p. 6891, 2001.

[102] H. Araki and E. H. Lieb, "Entropy inequalities," *Comm. Math. Phys.*, vol. 18, p. 160, 1970.

[103] V. Vedral and M. B. Plenio, "Entanglement measures and purifiation procedures," *Phys. Rev. A*, vol. 57, p. 1619, 1998.

[104] I. Devetak and A. Winter, "Distillation of secret key and entanglement from quantum states," *Proc. R. Soc. A*, vol. 461, p. 207, 2005.

[105] L.-M. Duan, G. Giedke, J. I. Cirac, and P. Zoller, "Inseparability criterion for continuous variable systems," *Phys. Rev. Lett.*, vol. 84, pp. 2722–2725, Mar 2000.

[106] S. Pirandola, R. Laurenza, C. Ottaviani, and L. Banchi, "Fundamental limits of repeaterless quantum communications," *Nature Comm.*, vol. 8, p. 15043, 2017.

[107] E. M. Rains, "Bound on distillable entanglement," *Phys. Rev. A*, vol. 60, pp. 179–184, Jul 1999.

[108] R. Dong, M. Lassen, J. Heersink, C. Marquardt, R. Filip, and G. Leuchs, "Continuous-variable entanglement distillation of non-gaussian mixed states," *Phys. Rev. A*, vol. 82, p. 012312, 2010.

[109] R. Dong, M. Lassen, J. Heersink, C. Marquardt, R. Filip, and G. Leuchs, "Experimental entanglement distillation of mesoscopic quantum states," *Nature Phys.*, vol. 4, p. 919, 2008.

[110] J.-I. Yoshikawa, T. Hayashi, T. Akiyama, N. Takei, A. Huck, U. L. Andersen, and A. Furusawa, "Demonstration of deterministic and high fidelity squeezing of quantum information," *Phys. Rev. A*, vol. 76, p. 060301, 2007.

[111] H. Valbruch, M. Mehmet, K. Danzmann, and R. Schnabel, "Detection of 15 db squeezed states of light and their application for the absolute calibration of photoelectric quantum efficiency," *Phys. Rev. Lett.*, vol. 117, p. 110801, 2016.

[112] J. Zhao, K. Liu, H. Jeng, M. Gu, J. Thompson, P. K. Lam, and S. M. Assad, "A high-fidelity heralded quantum squeezing gate," *Nature Photonics*, vol. 14, p. 306, 2020.

[113] K. Miyata, H. Ogawa, P. Marek, R. Filip, H. Yonezawa, J.-I. Yoshikawa, and A. Furusawa, "Implementation of a quantum cubic gate by an adaptive non-gaussian measurement," *Phys. Rev. A*, vol. 93, p. 022301, 2016.

[114] C. H. Bennett, G. Brassard, C. Crepeau, R. Josza, A. Peres, and W. K. Wootters, "Teleporting an unknown quantum state via dual classical and einstein-podolsky-rosen channels," *Phys. Rev. Lett.*, vol. 70, p. 1895, 1993.

[115] D. Bouwmeester, J.-W. Pan, K. Mattle, M. Eibl, H. Weinfurtner, and A. Zeilinger, "Experimental quantum teleportation," *Nature*, vol. 390, p. 575, 1997.

[116] M. Riebe, H. Haffer, C. F. Roos, W. Hansel, J. Benhelm, G. P. T. Lancaster, T. W. Korber, C. Becher, F. Schmidt-Kaler, D. F. V. James, and R. Blatt, "Deterministic quantum teleportation with atoms," *Nature*, vol. 429, p. 734, 2004.

[117] M. D. Barrett, J. Chiaverini, T. Schaetz, J. Britton, W. M. Itano, J. D. Jost, E. Knill, C. Langer, D. Leibfried, R. Ozeri, and D. J. Wineland, "Deterministic quantum teleportation of atomic qubits," *Nature*, vol. 429, p. 737, 2004.

[118] C. Nölleke, A. Neuzner, A. Reiserer, C. Hahn, G. Rempe, and S. Ritter, "Efficient teleportation between remote single-atom quantum memories," *Phys. Rev. Lett.*, vol. 110, p. 140403, Apr 2013.

[119] M. A. Nielsen, E. Knill, and R. Laflamme, "Complete quantum teleportation using nuclear magnetic resonance," *Nature*, vol. 396, p. 52, 1998.

[120] L. Steffen, Y. Salathe, M. Oppliger, P. Kurpiers, M. Baur, C. Lang, C. Eichler, G. Puebla-Hellmann, A. Fedorov, and A. Wallraff, "Deterministic quantum teleportation with feed-forward in a solid state system," *Nature*, vol. 500, p. 319, 2013.

[121] W. Pfaff, B. J. Hensen, H. Bernien, S. B. van Dam, M. S. Blok, T. H. Taminiau, M. J. Tiggelman, R. N. Schouten, M. Markham, D. J. Twitchen, and R. Hanson, "Unconditional quantum teleportation between distant solid-state quantum bits," *Science*, vol. 345, p. 532, 2014.

[122] Q. Zhang, A. Goebel, C. Wagenknecht, Y.-A. Chen, B. Zhao, T. Yang, A. Mair, J. Schmiedmayer, and J.-W. Pan, "Experimental quantum teleportation of a two-qubit composite system," *Nature Physics*, vol. 2, p. 678, 2006.

[123] X.-L. Wang, X.-D. Cai, Z.-E. Su, M.-C. Chen, D. Wu, L. Li, N.-L. Liu, C.-Y. Lu, and J.-W. Pan, "Quantum teleportation of multiple degrees of freedom of a single photon," *Nature*, vol. 518, p. 516, 2015.

[124] S. L. Braunstein and H. J. Kimble, "Teleportation of continuous quantum variables," *Phys. Rev. Lett.*, vol. 80, p. 869, 1998.

[125] A. Furusawa, J. L. Sorensen, S. L. Braunstein, C. A. Fuchs, H. J. Kimble, and E. S. Polzik, "Unconditional quantum teleportation," *Science*, vol. 282, p. 706, 1998.

[126] M. Yukawa, H. Benichi, and A. Furusawa, "High-fidelity continuous-variable quantum teleportation toward multistep quantum operations," *Phys. Rev. A*, vol. 77, p. 022314, 2008.

[127] H. Krauter, D. Salart, C. A. Muschik, J. M. Petersen, H. Shen, T. Fernholz, and E. S. Polzik, "Quantum teleportation between distant atomic objects," *Nature Physics*, vol. 9, p. 400, 2013.

[128] J. F. Sherson, H. Krauter, R. K. Olsson, B. Julsgaard, K. Hammerer, I. Cirac, and E. S. Polzik, "Quantum teleportation between light and matter," *Nature*, vol. 443, p. 557, 2006.

[129] K. G. Fedorov, M. Renger, S. Pogorzalek, R. D. Candia, Q. Chen, Y. Nojiri, K. Inomata, Y. Nakamura, M. Partanen, A. Marx, R. Gross, and F. Deppe, "Experimental quantum teleportation of propagating microwaves," *Science Advances*, vol. 7, no. 52, p. eabk0891, 2021.

[130] T. C. Ralph, P. K. Lam, and R. E. S. Polkinghorne, "Characterizing teleportation in optics," *J. Opt. B: Quantum Semiclass. Opt.*, vol. 1, p. 483, 1999.

[131] M. Fuwa, S. Toba, S. Takeda, P. Marek, L. Mista, and R. Filip, "Noiseless conditional teleportation of a single photon," *Phys. Rev. Lett.*, vol. 113, p. 223602, 2014.

[132] J. Zhao, J. Y. Haw, T. Symul, P. K. Lam, and S. M. Assad, "Characterization of a measurement-based noiseless linear amplifier and its applications," *Phys. Rev. A*, vol. 96, p. 012319, 2017.

[133] F. Grosshans and P. Grangier, "Quantum cloning and teleportation criteria for continuous quantum variables," *Phys. Rev. A*, vol. 64, p. 010301, Jun 2001.

[134] R. Blandino, N. Walk, A. P. Lund, and T. C. Ralph, "Channel purification via continuous-variable quantum teleportation with gaussian postselection," *Phys. Rev. A*, vol. 93, p. 012326, 2016.

[135] T. C. Ralph and P. K. Lam, "Teleportation with bright squeezed light," *Phys. Rev. Lett.*, vol. 81, pp. 5668–5671, Dec 1998.

[136] T. Ralph, R. Polkinghorne, and P. Lam, "Characterization of teleportation in optics," in *Quantum Electronics and Laser Science Conference*, p. QWA5, Optica Publishing Group, 1999.

[137] S. Tserkis, J. Dias, and T. C. Ralph, "Simulation of gaussian channels via teleportation and error correction of gaussian states," *Phys. Rev. A*, vol. 98, p. 052335, Nov 2018.

[138] R. Raussendorf, "A one-way quantum computer," *Phys. Rev. Lett.*, vol. 86, p. 5188, 2001.

[139] E. Knill, "Quantum computing with realistically noisy devices," *Nature*, vol. 434, p. 39, 2005.

[140] E. Knill, "Scalable quantum computing in the presence of large detected-error rates," *Phys. Rev. A*, vol. 71, p. 042322, Apr 2005.

[141] Y.-H. Luo, M.-C. Chen, M. Erhard, H.-S. Zhong, D. Wu, H.-Y. Tang, Q. Zhao, X.-L. Wang, K. Fujii, L. Li, N.-L. Liu, K. Nemoto, W. J. Munro, C.-Y. Lu, A. Zeilinger, and J.-W. Pan, "Quantum teleportation of physical qubits into logical code spaces," *Proceedings of the National Academy of Sciences*, vol. 118, no. 36, p. e2026250118, 2021.

[142] K. Noh, S. M. Girvin, and L. Jiang, "Encoding an oscillator into many oscillators," *Phys. Rev. Lett.*, vol. 125, p. 080503, 2020.

[143] C. Flühmann, T. L. Nguyen, M. Marinelli, V. Negnevitsky, K. Mehta, and J. P. Home, "Encoding a qubit in a trapped-ion mechanical oscillator," *Nature*, vol. 556, p. 513, 2019.

[144] P. Campagne-Ibarcq, A. Eickbusch, S. Touzard, E. Zalys-Geller, N. E. Frattini, V. V. Sivak, P. Reinhold, S. Puri, S. Shankar, R. J. Schoelkopf, M. Mirrahimi, and M. H. Dovoret, "Quantum error correction of a qubit encoded in grid states of an oscillator," *Nature*, vol. 584, p. 368, 2020.

[145] U. L. Andersen, R. Filip, J. Fiurasek, V. Josse, and G. Leuchs, "Experimental purification of coherent states," *Phys. Rev. A*, vol. 72, p. 060301(R), 2005.

[146] N. J. Cerf, M. Levy, , and G. V. Assche, "Quantum distribution of gaussian keys using squeezed states," *Phys. Rev. A*, vol. 63, p. 052311, 2001.

[147] W. K. Wootters and W. H. Zurek, "A single quantum cannot be cloned," *Nature*, vol. 299, p. 1982, 1982.

[148] M. Usuga, C. Müller, C. Wittmann, P. Marek, R. Filip, C. Marquardt, G. Leuchs, and U. L. Andersen, "Noise-powered probabilistic concentration of phase information," *Nature Phys.*, vol. 6, p. 767, 2010.

[149] N. A. McMahon, A. P. Lund, and T. C. Ralph, "Optimal architecture for a nondeterministic noiseless linear amplifier," *Phys. Rev. A*, vol. 89, p. 023846, 2014.

[150] A. Feist, K. E. Echternkamp, J. Schauss, S. V. Yalunin, S. Schaefer, and C. Ropers, "Quantum coherent optical phase modulation in an ultrafast transmission electron microscope," *Nature*, vol. 521, p. 200, May 2015.